Elucidating the Role of Iron-Handling Macrophages in Adipose Tissue

By

Merla Johanna Hubler

Dissertation

Submitted to the Faculty of the

Graduate School of Vanderbilt University

in partial fulfillment of the requirements

for the degree of

DOCTOR of PHILOSOPHY

in

Molecular Physiology and Biophysics

August 10, 2018

Nashville, Tennessee

Approved:

David H. Wasserman, Ph.D.

Eric P. Skaar, Ph.D.

Wenbiao Chen, Ph.D.

Volker Haase, M.D., Dr. med.

Pampee Young, M.D., Ph.D.

Alyssa Hasty, Ph.D.

DEDICATION

This dissertation is dedicated to my parents.

Mami – You are not only my mother but one of my dearest friends. You have always been an unwavering source of support through all of my endeavors.

Papi – I know I can give you no greater gift than my own success. You were the spark that ignited my love for science and you taught me the definition of persistence. I wish I had even one more day with you, and that it were the day of my PhD defense.

ACKNOWLEDGEMENTS

Acknowledgement of Dr. Alyssa Hasty:

I joined Alyssa's lab because I recognized she possesses traits that I hoped to learn. Some of these traits include: optimistic persistence to complement her passion for her science, self-awareness, continual personal and career aspirations, and an uncommon balance of humility and self-assuredness that reflects real strength. I admire her ability to have unlimited goals for own success, while also recognizing and enabling the success in those around her.

Alyssa brings great scientific mentorship and dedication to every student's project. She always makes time for weekly meetings, critically discusses experimental plans, and helps analyze and formulate results in constructive ways.

I have also experienced personal mentorship from Alyssa over these years, during times of failure and success. I remember a time when my experiments were not succeeding, and I felt at odds with my progress. My normal ambition and focus were compromised and I consequently made absent-minded mistakes. Alyssa recognized this and approached me about it. She did not shame me, but she suggested how I could realign myself with success – in my mindset and my daily research practices. I internalized this advice and consciously altered my approach over the next weeks. This was a moment of growth for me and an example of true mentorship. Complementing these more trying times, I also experienced a mentor and friend in Alyssa during times of success. For example, she called me and sent enthusiastic messages when my manuscript was favorably reviewed.

Lastly, Alyssa genuinely goes above and beyond to show her appreciation for everyone in the group, including myself. When I came to the lab for a week with a cold, she left a box of Kleenex on my desk with a note: "Happy noses make for happy students!" These small kindnesses make an impact on the daily lives of her students. Indeed, I have deep appreciation for Alyssa's flexibility and acceptance as I dealt with the loss of my father during this last year.

These are just a glimpse of many similar moments of struggle, success, and kindness I have experienced with Alyssa over the course of my doctoral training. Of one thing I am certain – I am eternally grateful for both the difficult and good times because they have helped me grow as a person and scientist. I will keep this gratitude towards Alyssa in my heart through all of my future endeavors.

Acknowledgement of my dissertation committee:

I would like to thank my dissertation committee: Drs. David Wasserman, Wenbiao Chen, Eric Skaar, Pampee Young, and Volker Haase. This committee has guided me through the trenches of my successes and failures to be able to produce this final dissertation. I thank them for taking the time to meet with me, even outside of our planned committee meetings, to discuss experimental ideas. Their time and insights have propelled my doctoral studies to the finish line.

Acknowledgement of my coworkers:

I would be remiss not to acknowledge my fellow labmates. I thank Marnie Gruen for being a consistent source of logistical and emotional support through the years. I thank Dr. Arion Kennedy for her friendship, for helping me keep perspective, and most importantly, for her critical scientific insight when I needed it. I have no doubt that Arion will make an amazing mentor to all her future students. Dr. Andrea McAlester, Dr. Reid Bolus, Dr. Magda Ameka, Kristin Peterson, and Matthew Cottam were companions on this journey: from drawn-out conversations about life and the world during mouse sacrifices, to planning experimental designs, to fun adventures at conferences. I hope to always maintain contact with these great people and wish the best for them in their future endeavors.

Acknowledgement of the MSTP and funding sources:

I thank the Vanderbilt MSTP for supporting me personally and financially through this training.

Myself and my research were supported by the following funding sources: an F30 fellowship (DK103438) awarded through the NIH, and MSTP support through NIGMS of the NIH (T32GM007347).

TABLE OF CONTENTS

LIST OF FIGURES

Figure Page

LIST OF ABBREVIATIONS

AAS: atomic absorption spectrometry

AT: adipose tissue

ATM: adipose tissue macrophage

Akt: protein kinase B

BMDM: bone marrow derived macrophage

BMP6: bone morphogenic protein 6

CAT1: cationic acid transporter 2

CD: cluster of differentiation

CD163lipo: PEGylated liposome coated with anti-CD163 antibody

CD163lipo/calcein: CD163lipo loaded with calcein

CD163lipo/dox: CD163lipo loaded with doxorubicin

CD206: mannose receptor

$Cy5^{+}$dsDNA: Cy5-conjugated double stranded DNA

DC: dendritic cell

DIOS: dysmetabolic iron overload syndrome

DMT-1: divalent metal transporter 1

Dox: doxorubicin

eAT: epididymal adipose tissue

FACS: flow-assisted cell sorting

Ft: ferritin

FtH: ferritin heavy chain

FtL: ferritin light chain

Fpn1: ferroportin 1

GLUT-4: glucose receptor 4

HDL: high-density lipoprotein

HFD: high fat diet

Hmox1: heme oxygenase 1

ICP-MS: inductively coupled plasma mass spectrometry

IL: interleukin

INFγ: interferon γ

iNOS/Nos2: nitric oxide synthase 2

IP: intraperitoneal

IR: insulin resistance

IRE: iron response element

IRP: iron response protein

IRS1:insulin receptor substrate 1

JNK1: c-Jun N-terminal kinase 1

LDL: low-density lipoprotein

LFD: low fat diet

LIP: labile iron pool

LysM: lysozyme M

MFe^{hi}: paramagnetic adipose tissue macrophage

MFe^{lo}: non-paramagnetic adipose tissue macrophage

Mhem / M(Hb): high-iron macrophages in atherosclerotic plaques

Mme: metabolically activated macrophages

MnNP: mannosylated nanoparticle

NO: nitric oxide

PEG: polyethyleneglycol

pAkt: phospho-Akt

RES: reticuloendothelial system

ROS: reactive oxygen species

SFA: saturated fatty acid

siRNA: small inhibitory RNA

SREBP1c: sterol regulatory element binding protein 1c

SVF: stromal vascular fraction

TAM: tumor-associated macrophage

Tf: transferrin

TfR1: transferrin receptor 1

TIBC: total iron binding capacity

TG: triglyceride

TLR4: toll-like receptor 4

TNFα: tumor necrosis factor α

UTR: untranslated region

CHAPTER I

INTRODUCTION

Portions of this Introduction have been published in a review article in *Trends in Endocrinology & Metabolism,* by Hubler, Peterson, and Hasty[2].

Obesity epidemic and type 2 diabetes

The obesity epidemic: Obesity is defined as a body mass index greater than 30. This weight-to-height ratio is an indicator of excess adipose tissue. Adipose tissue hypertrophy is an important functional adaptation for survival through times of low food availability in most mammals. However, just like many physiologic systems, lipid storage in adipose tissue has a maximum healthy capacity. With changes in cultural eating habits, reduced physical demands, and the ready availability of palatable foods, humans are exceeding their natural adaptation to store fat. In the United States, the prevalence of obesity is 30% in adults and 17% in children[3]. In 2008, the CDC attributed an extra annual medical cost of $1,429 to obesity in patients[3]. This disparity can be explained in large part by obesity-associated metabolic conditions – including the triad of the metabolic syndrome: hypertension, hyperglycemia, and hyperlipidemia. Unfortunately, obesity is a risk factor for cardiovascular disease, type 2 diabetes, and even cancers and asthma.

Diabetes: Diabetes occurs when the body is unable to sufficiently regulate serum glucose levels, leading to hyperglycemia. High levels of serum glucose cause to vascular endothelial damage from to excess intracellular glucose and aberrant protein glycation[4]. The resulting vascular and neurological damage can lead to organ dysfunction in the eye, kidneys, pancreas, and heart. Serum glucose is regulated by insulin, a hormone secreted by beta cells of the pancreas. Insulin induces glucose uptake into tissues and reduces glucose production. Diabetes has been classified into two types, with deficits in insulin common to both. Type 1 diabetes presents early in life and is associated with auto-immune destruction of insulin-secreting beta cells[5]. The etiology of type 1 diabetes is thought to be an autoimmune response to an environmental stimulus in genetically predisposed individuals. In contrast, type 2 diabetes is closely associated with obesity. Disordered energy utilization and storage, and subsequent inflammatory responses, lead to progressive tissue insulin resistance (IR)[6]. Eventually insulin demand exceeds the functional capacity of the pancreas, causing beta cell death and insulin deficiency.

Insulin resistance, pre-diabetes, and type 2 diabetes lay on a continuum of disorder that reflects the tissues resistance to insulin signals, and the ability of beta cells to compensate. Over time, beta cells are unable to contend with insulin demand, leading to beta cell failure. In the liver, normal insulin signaling allows for glucose uptake and maintains gluconeogenesis and glycolysis appropriately. In AT and muscle, insulin signaling is primarily responsible for glucose disposal[7]. Insulin acts on these tissues by binding the insulin receptor, thereby activating insulin receptor substrate 1 (IRS1). Through a cascade of signaling molecules, protein kinase B (Akt2) is activated. This can

directly lead to translocation of the glucose receptor 4 (GLUT-4) to the cell surface, and can stimulate glycogen synthase. In the liver and AT, insulin signaling also activates *de novo* lipogenesis through sterol regulatory element-binding protein c (SREBP1c). The pathogenesis of insulin resistance in AT is complex, involving ectopic lipid deposition, adipokines/cytokines, and inflammatory stimuli, all acting on the insulin signaling cascade. For example, lipids like diacylglycerol can act through PKCs to inhibit IRS1, and inflammatory cytokines like tumor necrosis factor α (TNFα) can act through c-Jun N-terminal kinase 1 (JNK1) to inhibit IRS1[7]. Adipokines, cytokines, and inflammatory signals involved in AT insulin resistance are outlined in the next sections.

AT endocrine function and inflammation

AT secretes cytokines, chemokines, adipokines, and other proteins that act locally and systemically to control lipid, glucose, and energy homeostasis[8]. Furthermore, in obesity, a pro-inflammatory milieu of immune cells within the AT alters its ability to maintain these homeostatic controls. Interestingly, almost all cells of the innate and adaptive immune system have been found in both lean and obese AT, with their proportions changing to promote inflammation and IR in obesity[9]. Recognizing the endocrine function and inflammatory responses of AT is a major step in understanding why AT malfunction is associated with systemic changes in metabolic health.

Chemokines, cytokines and adipokines: Unhealthy expansion of AT is associated with increased levels of the inflammatory cytokine, tumor necrosis factor α (TNFα). The discovery of TNFα expression in obese AT was foundational to the field of immunometabolism nearly two decades ago[10], because adipose-tissue macrophages

(ATMs) have been shown to be the primary source of TNFα in obese AT[10]. Interleukin-6 (IL-6) is also highly expressed in AT and correlates with obesity, but its exact role in obesity is contended; while IL-6 deficient mice show metabolic dysfunction, administration of intravenous IL-6 also leads to insulin resistance[11]. Adipocytes treated with TNFα produce 34 different chemokines associated with monocyte recruitment[12]. Therefore, elevated TNFα when ATMs infiltrate can feed-forward to amplify further recruitment.

Adipokines are hormones produced by AT to communicate with other organs and systems in the body. The discovery of these molecules changed the appreciation of AT from an inert lipid depot, to an actively signaling organ. Two major adipokines – leptin and adiponectin – play a role in feeding and energy expenditure through the central nervous system[13], and directly impact AT inflammation. Leptin deficiency is associated with hyperphagia. However, obese humans and mice have higher levels of serum leptin, indicating a state of central leptin resistance, possibly mediated through inflammatory signals[14]. Leptin also activates ATMs to produce pro-inflammatory cytokines[15]. In contrast, adiponectin is considered an anti-inflammatory adipokine, and its expression is suppressed by inflammatory cytokines, as well as oxidative stress[16], and iron overload (discussed below)[17]. Adiponectin acts through AMPK to increase glucose uptake and fatty acid oxidation, and to reduce liver gluconeogenesis[18]. Studies in mice with adiponectin excess or deficiency support its role in insulin sensitization[19, 20].

Inflammatory cells in AT: Macrophages are the most common immune cell in AT. ATMs are localized in interstitial spaces suggesting communication between the two cell types, and a role for macrophages in AT homeostasis. Over the last decade[21], ATMs have been proposed to be involved in AT development, expansion[22, 23], antigen presentation[24], and catecholamine synthesis[25]. In obesity, there is a large influx of macrophages from the monocyte pool, such that up to 40% of cells in obese AT are macrophages[26]. These ATMs accumulate in crown-like structures around dead adipocytes[27, 28] and have a gene expression profile reflective of a more classically activated, M1-like phenotype[29]. Inflammatory ATMs are thought to contribute to IR in AT by secretion of inflammatory cytokines, such as TNFα and IL-1β. However, recent studies have demonstrated that even though inflammatory ATMs from obese AT express many inflammatory cytokines, they have a phenotype that is distinct from infection-associated inflammatory macrophages; Kratz *et al.* used proteomics and functional studies to identify the "metabolically activated" (Mme) phenotype[30]. Mme ATMs exist in obese AT and have a balance of pro-inflammatory and anti-inflammatory signaling pathways that keep them in a state of unresolving inflammation. They are activated by glucose, insulin, and palmitate, through toll-like receptor 4 (TLR4), and have unique cell surface expression of CD36, PLIN2, and ABCA1. They have low expression of classic M1 markers, but also M2 markers, e.g. cluster of differentiation (CD) 163 and CD206. This finding further emphasizes that macrophages may take on tissue-specific phenotypes in response to their local environment. Furthermore, Mme polarization of *in vitro* macrophages, using glucose, palmitate and insulin, can now be implemented as a more representative model of inflammatory ATMs.

DCs in AT are predominantly conventional $CD11b^+$ DCs, and their numbers increase in obesity[31]. AT DCs can be distinguished from ATMs because they are negative for CD64 but commonly express CD11c. Like ATMs, they can stimulate the proliferation of $CD4^+$ T cells.

Neutrophils are commonly first-responders in the innate immune system. Studies have shown that a neutrophil influx occurs early in obesity, indicating that neutrophils may be involved in initial recruitment of immune cells. However, neutrophils are not common in lean AT, and neutrophil accumulation in AT in obesity is 30-fold lower than macrophages[32].

Eosinophils were first described in AT by Wu *et al*[33]. They were found to be more abundant in lean AT than obese AT, and their presence correlated with M2-like polarization of ATMs. Using both a eosinophil-deficient model (dblGATA) and eosinophilia model (IL-5 transgenic) the authors concluded that eosinophils protected AT from metabolic dysfunction[33]. However, our lab recently published a model using chronic IL-5 injections to induce AT eosinophilia in diet-induced obesity[34]. These studies showed that eosinophils are not sufficient to protect AT from metabolic dysfunction in obesity[34].

Mast cells are generically associated with allergic responses, but their counts are also increased in obese AT[35]. In fact, genetic mast cell knockout studies have shown that their deficiency reduces weight gain, and possibly ATM accumulation[35]. Basophils are similar to mast cells, but no specific role for this cell type has been delineated in AT, and their lineage marker is not highly expressed[36].

Both Th_1 and Th_2 T lymphocytes cells are present in AT. Total T-cell knockout mice have worsened metabolic profiles and weight gain. This may be because some $CD4^+$ T cells, such as regulatory T cells, have also been shown to be protective against metabolic function[37, 38]. In contrast, studies have shown that $CD3^+$ Th_1 T cells increase with obesity, and their expression of the cytokine INFγ may exacerbate insulin resistance in the tissue[39]. When CD3-neutralizing antibodies were administered to mice, a phenotypic switch was observed in ATMs from M1 to M2[40].

Association of obesity and metabolic syndrome with iron

The role of chemokines, cytokines and inflammatory cells in metabolic dysfunction in AT has been revealed over the course of the last decade. However, it is only now coming to light that iron overload of adipocytes also contributes to local and systemic IR[17]. The association between obesity, inflammation, and adipocyte iron overload is an area of new interest outlined in the sections below, and fundamentally underlies the goals of research efforts outlined in Chapters III-V.

In humans, elevated body iron stores have repeatedly been linked to factors comprising the metabolic syndrome, including obesity, dyslipidemia, hypertension, fasting hyperglycemia, and diabetes[41-48]. An analysis of four different studies on the link between iron and diabetes demonstrated that men and women in the highest quintile of serum ferritin (Ft) levels – the primary intracellular iron-storage protein that can be released in overload situations – had a relative risk of greater than 3.5 for developing diabetes[49]. In fact, this condition is now called dysmetabolic iron overload syndrome (DIOS)[50] and it has even been suggested that serum Ft may serve as a surrogate

marker for insulin resistance[51]. Although inflammatory cytokines can influence iron storage in various cell types, studies have shown that the link between elevated iron and obesity/diabetes is independent of inflammation[41, 43]. It is also not associated with dietary iron intake or absorption[52] or to beta cell function[53]. Further supporting the relationship between iron and metabolic disease, a recent 7-year prospective study found that serum Ft was positively associated with the clinical indicator of IR, HOMA2-IR, and both hepatic and adipocyte IR[54]. This aligns well with the finding that IR is associated with changes in iron-handling proteins in AT[55]. Furthermore, iron depletion by phlebotomy, even in healthy subjects, has been shown to improve insulin sensitivity[56]. Although extensive research efforts have been focused on understanding the association between obesity and the metabolic syndrome, mechanisms for impact of iron on metabolic health have not been well elucidated.

Despite the link between iron-overload and obesity mentioned above, inflammation in obesity also leads to iron-deficient anemia[57]. Linking obesity with both tissue iron overload and iron deficient anemia may seem counterintuitive. However, this occurs because macrophages sequester iron during chronic inflammation. The mechanism underlying this phenomenon can be understood by parsing out systemic and cell autonomous regulation of iron storage, as detailed below.

Systemic and cellular iron cycles

Systemic iron handling: Iron is absorbed from the diet through apical transporters on duodenal enterocytes. It is released basally from enterocytes through the only known mammalian iron exporter, ferroportin 1 (Fpn1). In serum, iron is found in three main forms: Fe^{3+} bound to transferrin (Tf), heme bound to hemopexin, or hemoglobin bound to haptoglobin. In bone marrow erythroblasts, iron is used to form hemoglobin for incorporation into nascent erythrocytes. Senescent erythrocytes are phagocytized by splenic macrophages and the iron is recycled back to the erythroblasts. The development of these splenic red pulp macrophages is dependent on the expression of SpiC (gene *SpiC*)[58]. Overall, ten times more iron is recycled by macrophages than is even absorbed through the duodenum[59]. Resident macrophages are responsible for iron-cycling in many tissues, including bone marrow, spleen[60], liver[61], and lung[62]. Macrophages also express receptors for all three types of iron that are present in serum; transferrin receptor (TfR1) binds Fe^{3+}-Tf, CD91 binds heme-hemopexin, and CD163 binds haptoglobin-hemoglobin (Hp-Hb).

Regulation of systemic iron: The systemic uptake and release of iron is regulated through the acute phase reactant protein hepcidin, which is secreted by hepatocytes. Hepcidin induces Fpn1 endocytosis and degradation[63] and therefore regulates the primary control points of plasma iron: absorption of iron from the intestine, release of stored iron from hepatocytes, and recycling of iron by macrophages. This is also the primary pathway for regulated iron clearance: hepcidin reduces Fpn1 on enterocytes, leading to the sequestration of iron in cells that will be sloughed off and excreted[64]. In acute infection, hepcidin-induced iron sequestration results in dramatic

reductions in plasma iron as a bacteriostatic mechanism. Hepcidin is also synthesized by adipocytes[65] and macrophages[66]. Under homeostatic conditions, hepcidin production is induced through signaling of the bone morphogenetic protein 6 (BMP6)/Smad pathway with a co-receptor for BMP6, hemojuvelin. During inflammation, this is accomplished via the IL-6/STAT3 pathway[67].

Effects of obesity on systemic iron concentrations: Inflammatory signaling, often associated with chronic diseases such as obesity, is associated with increased expression of hepcidin, via IL-6 induction, and can lead to anemia of chronic disease – a disease in which tissue iron overload and anemia occur concomitantly. Increased circulating hepcidin can explain this apparent conundrum. Cells such as macrophages, enterocytes, and hepatocytes have high iron uptake and depend on Fpn1 for iron release[68]. Therefore, when hepcidin is up-regulated, Fpn1 is down-regulated and iron is sequestered, reducing its availability in plasma. A consequence of decreased plasma iron levels is reduced availability for erythrocytosis, thereby leading to anemia. Thus, in the case of chronic inflammation-induced hepcidin expression, increased serum Ft is reflective of tissue iron overload that occurs concomitantly with anemia.

Obesity has also been directly linked to changes in iron storage. For example, in the liver, high-fat/high-sucrose diet induces hepatic iron storage[69]. However, these findings are still conflicted, as some studies have shown a decrease in liver iron in obese mice[70, 71]. It is thought that iron accumulation in certain cells not only alters iron-handling genes but also changes inflammatory cytokine expression. These conflicting studies demonstrate that there is still much to be learned regarding the reciprocal regulation of iron and inflammation in obesity.

Regulation of the cellular iron cycle: Cellular iron regulation is important because excess free iron in a cell can readily cause oxidative damage. Following endocytosis via one of the iron receptors, iron is released from is carrier proteins by acidification of the endosome, and transported across the endosomal membrane by divalent metal transporter 1 (DMT-1) to be bound by Ft, or incorporated into iron-containing proteins. The proteins involved in cellular iron handling are translationally controlled in response to intracellular iron concentrations[72]. This occurs through iron-response proteins (IRPs) that can bind iron-response elements (IREs) to either stabilize or de-stabilize mRNAs for iron-related transcripts. In iron-deplete cells, IRP1 and IRP2 bind IREs in the 3' untranslated region (UTR) of *Tfrc* (gene for TfR1) and *Slc11a2* (gene for DMT-1) and in the 5' region of *Fth1* and *Ftl1* (FtH, FtL, respectively) and *Slc40a1* (gene for Fpn1). Binding in the 3' UTR stabilizes the mRNA for TfR1 and Slc11a2, whereas binding in the 5' UTR inhibits translation of Fth1 and Slc40a1. Ultimately, protein levels of TfR1 and DMT-1 are elevated, while levels of Ft and Fpn1 are reduced. The overall effect is that more iron is imported into the cell, less is bound by Ft, and less is exported. Effectively, active IRPs increase the cell's labile iron pool (LIP) - the transitory, chelatable, and redox-active iron pool in a cell. When the cell becomes iron-replete, IRP1 is bound by an iron-sulfur cluster to form c-aconitase, and IRP2 is ubiquitinated and degraded. Ft levels increase and Ft is released at concentrations proportional to its expression in the cells. Due to this fine-tuned regulation, Ft is commonly used as a surrogate measure of body iron stores in humans[51].

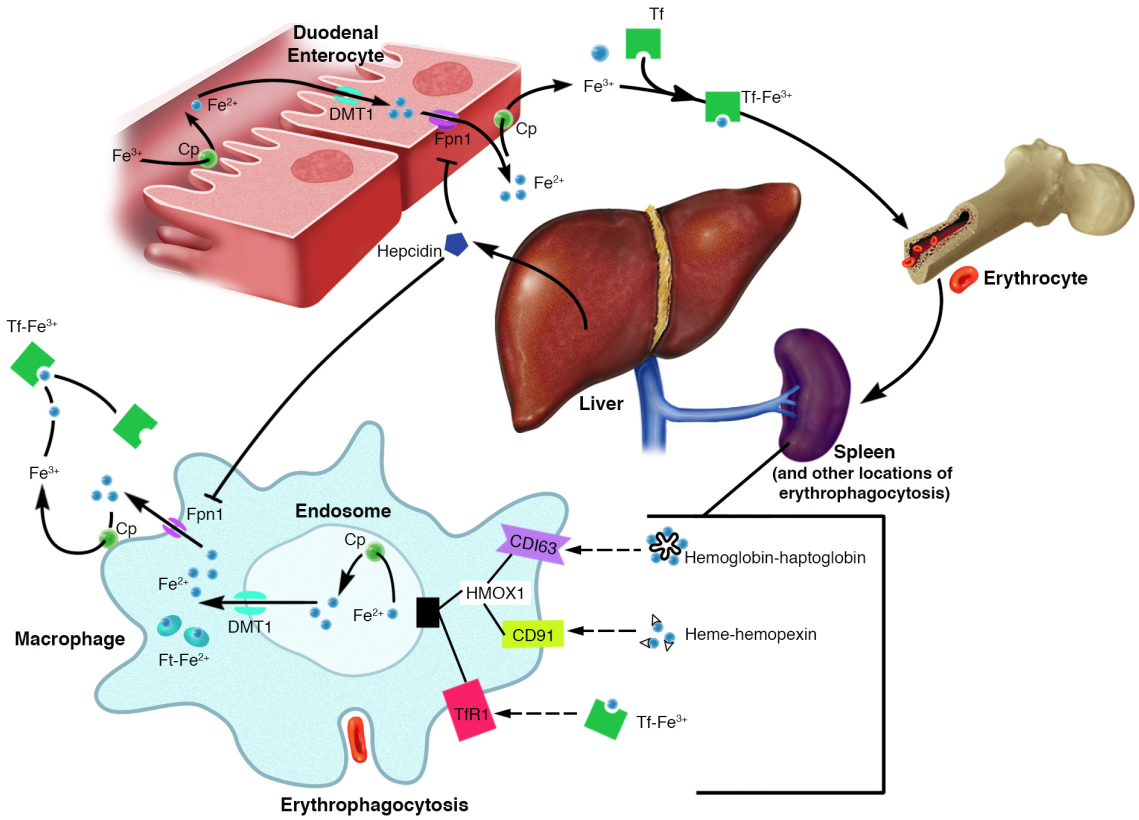

Figure 1.1. **Schematic of systemic and cellular iron handling**. Dietary iron is taken up via DMT-1 on enterocytes. It is transferred into the plasma through Fpn1, where it is again oxidized and binds Tf. Thereafter, it is primarily transported to bone marrow to produce heme for erythrocyte formation. In the spleen, most of the iron taken up by macrophages derives from phagocytosis of senescent red blood cells. However, systemic macrophages can also reabsorb iron through three primary receptors: CD163 binds hemoglobin-haptoglobin complexes, CD91 binds heme-hemopexin complexes, and TfR1 binds Tf-Fe^{3+}. Once bound, the receptor is endocytosed and a change in pH induces the reduction of iron and its release into the cytoplasm. In the cytoplasm, iron exists in three forms; bound by Ft, incorporated into proteins, or retained as part of the unbound LIP. Iron is released from cells through Fpn1, again to be bound by Tf. Hepcidin is secreted from the liver in response to acute and chronic inflammatory stimuli and functions to degrade Fpn1, primarily on enterocytes and macrophages. [**Cp**: ceruloplasmin; **DMT-1**: divalent metal transporter 1; **Fpn1**: ferroportin 1; **Tf**: transferrin; **TfR1**: transferrin receptor 1; **Hmox1**: Heme oxygenase 1; **Ft**: ferritin].

Genetic iron overload disorders

The relationship between obesity and cellular iron overload contrasts with findings in genetic forms of iron overload, such as hereditary hemochromatosis. Genetic causes of iron overload are most commonly caused by defects in hepcidin leading to inappropriately high Fpn1 on the cell surface[73]. With constitutively elevated Fpn1, enterocytes continually import dietary iron into serum, and excess iron is stored in tissues such as the liver, heart, and endocrine organs that have naturally lower Fpn1 levels, thereby lower iron export. Iron is initially not deposited in macrophages and enterocytes because they can upregulate Fpn1 to export the excess iron; however, in later stages of this disease, even macrophages can become iron-loaded. These disorders are associated with an increased prevalence of diabetes, likely due to iron-mediated toxicity to the pancreas[74]. While it is not considered a genetic disorder, it has also been shown that genetic variants in iron-related genes, such as *HFE*, *Slc40a1*, and even beta-globin genes, can impact the pathogenesis of DIOS[75, 76].

Adipocytes and iron

Based on multiple studies correlating obesity and metabolic syndrome to iron overload, it is of no surprise that scientific attention has recently turned to iron in AT. *In vitro* and *in vivo* studies by several different groups have begun to elucidate the role of iron in lipid handling, mitochondrial biogenesis, and other adipocyte functions.

Iron and adipocyte lipid handling: Iron can impact adipocyte lipid handling in several ways, including lipid accumulation in adipogenesis, lipid release in lipolysis, and lipid peroxidation. As shown by *in vitro* 3T3-L1 differentiation models, adipocytes require

iron for adipogenesis[77]. Conversely, knockdown of Tf or Ft light chain (FtL), as well as iron chelation, result in iron depletion and antiadipogenic effects in human AT explants[77]. Iron also alters adipocyte lipolysis and lipid peroxidation. For example, iron treatment of primary adipocytes is sufficient to reversibly increase lipolysis[78] and reduce insulin-mediated glucose uptake[79]. The mechanism underlying this iron-induced lipolysis is not through canonical lipolysis regulatory pathways (such as cAMP, MAP kinase, protein kinase C, or phosphatidylinositol 3-kinase). Rather, iron-induced lipolysis can be inhibited by a free-radical scavenger, and can be mimicked by 4-hydroxy-2-nonenal (4-HNE), a by-product of lipid peroxidation[78, 80]. Lipid peroxidation is an end product of excess reactive oxygen species (ROS) in adipocytes, and increases with increased iron. Therefore, iron likely induces lipolysis through a pro-oxidant mechanism. These studies suggest that regulation of adipocyte iron exposure in a temporal and concentration dependent manner is a priority for maintaining healthy AT expansion.

Iron, mitochondrial function and biogenesis: Mitochondria depend on iron for many functions, including regulation of cellular redox potential, regulation of apoptotic cell death, and production of iron-sulfur clusters, steroids, and heme[81]. Adipocyte iron depletion decreases expression of the mitochondrial transcription factor, Tfam, indicating decreased mitochondrial transcription and replication. Conversely, mitochondrial biogenesis is upregulated during adipogenesis. Iron and IRPs have been shown to reversibly stimulate mitochondrial biogenesis and activity[77], which is also a primary mechanism for the efficacy of pharmaceutical agonists of peroxisome proliferator-activated receptor gamma commonly used to treat diabetic patients[82]. Therefore, adipocyte iron concentrations must be maintained within a proper range to

allow for proper mitochondrial biogenesis and function, without being so high that oxidative stress occurs.

Iron overload in adipocytes: Several recent studies have explored the impact on iron overload on adipocyte function. In a study by Dongionvanni *et al.*, mice fed a high-iron diet developed IR in visceral AT[50]. In contrast, a low-iron diet has been associated with improved insulin sensitivity in genetically obese leptin deficient ob/ob mice[83]. Furthermore, in mice, high dietary iron was associated with a decrease in the insulin-sensitizing adipokine, adiponectin[17], as well as an increase in the insulin-resistance inducing adipokine, resistin[50], despite a decrease in fat mass. In two separate studies adipocyte-specific Fpn1 knockout mouse models were used to induce adipocyte iron accumulation[17, 84]. Britton *et al*. did not observe adipocyte iron accumulation in Fpn1 knockout mice[84], however, Gabrielsen *et al.* quantified an increase in adipocyte Ft in their model[17]. Their Fpn1 knockout mice also demonstrated decreased systemic glucose tolerance in a mechanism driven by reduced serum adiponectin. These findings complement studies in humans showing that serum Ft is the strongest predictor of low serum adiponectin[17, 54, 85]. High serum Ft is also associated with adipocyte-specific IR, even after controlling for a host of covariates[54].

Adipocyte dysfunction with high iron: There is no known single mechanism to explain the impact of iron on adipocytes; however, iron may impact adipocytes' mitochondrial function and adiponectin production, as mentioned above. What is known about adipocyte function and iron is shown diagrammatically in Figure 1.2. Excess free intracellular iron leads to amplified production of ROS. These increased ROS alter mitochondrial function in adipocytes, contributing to IR[86]. In fact, oxidative stress from

ROS appeared to impair mitochondrial function in adipocytes through FOXO1[87], and FOXO1 activation inhibited adipocyte differentiation[29]. Interestingly, altered FOXO1 activation also seemed to underlie the association between adipocyte iron overload and reduced adiponectin expression – but by FOXO1 deacetylation, rather than dephosphorylation[17]. These findings suggest that multiple mechanisms for altering adipogenesis and adipocyte function converge on the transcription factor FOXO1, and that iron-induced oxidative stress and adiponectin can be added to the list. Despite this extensive background outlining the impact of iron on adipocyte function, little is understood about how iron availability is regulated in AT.

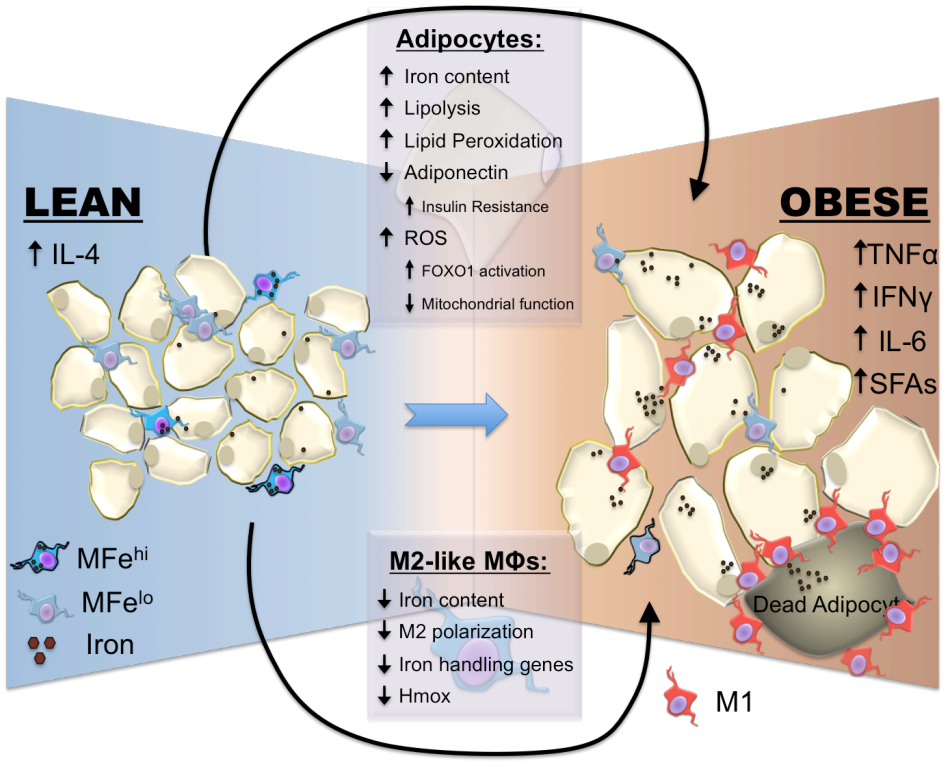

Figure 1.2. Mechanisms by which iron alters adipocyte functions. In normal AT, iron concentrations are controlled such that adipogenesis, mitochondrial function, and adipokine secretion are properly regulated. When adipocyte iron concentrations are elevated, such as in obesity, dietary iron excess, and in iron-related diseases, an increase in ROS can lead to FOXO1 activation which can result in decreased adipogenesis, decreased mitochondrial function, and decreased adiponectin secretion. In addition, ROS promote lipid peroxidation that can lead to uncontrolled lipolysis. [**AT**: adipose tissue; **ROS**: reactive oxygen species; **FOXO1**: Forkhead box protein O1]

Iron handling by resident AT macrophages

Macrophages are responsible for iron handling in most tissues, especially during resolution of inflammatory processes and wound healing. In some cases, iron uptake by macrophages appears to promote restoration of tissue homeostasis, but macrophage iron overload can also contribute to disease processes, with a few examples described below.

Hemorrhagic plaques*:* Alternatively activated (M2-like) macrophages have increased iron content and atheroprotective effects during atherosclerotic plaque rupture. These M2-like macrophages, termed "Mhem", and "M(Hb)"[88-90] were shown to take up iron from the local milieu in hemorrhagic plaques. Concomitantly, Mhem/M(Hb) macrophages appeared to upregulate lipid export genes. Functionally, this would protect the cells from lipid peroxidation that occurs if cellular iron and lipid concentrations are elevated simultaneously.

Wound healing: Although M1-like macrophages fight infection acutely, anti-inflammatory M2-like macrophages contribute to resolution of inflammation during wound healing. A recent study in chronic venous leg ulcers added even more complexity to this model: iron-overloaded macrophages had an unrestrained M1-like, pro-inflammatory phenotype, while still expressing high levels of the M2 markers, CD163 and CD206[91].

Cancer: Alternatively activated macrophages in the tumor microenvironment, or tumor-associated macrophages (TAMs) are associated with increased iron release, which correlates with tumor cell proliferation. In this system, M2-like TAMs promote

angiogenesis, while M1-like cells tend to sequester iron and decrease tumor development[92].

Multiple Sclerosis lesions: M1-like macrophages on the edges of demyelinated lesions have increased depositions of iron. Interestingly, these macrophages tend to be myelin-deplete, while myelin-laden "foamy" macrophages do not contain iron and resemble an M2 phenotype[93]. Furthermore, the count of M2-like iron-laden macrophages is higher in patients with active relapsing multiple sclerosis.

These examples demonstrate that the polarization of macrophages, their iron content, and their ability to recycle iron, contribute to the overall outcome of disease processes and resolution of inflammation. Much remains to be understood about how macrophages respond to environmental cues in specific tissues to adapt their iron handling status.

Iron handling by MFe^{hi} macrophages in AT

Macrophages are the most abundant immune cell in AT. In lean AT, these macrophages have a gene expression profile most similar to an anti-inflammatory, M2-like phenotype[94]. Considering macrophages play a prominent role in iron metabolism in other tissues, it is possible M2-like ATMs contribute to the local control of iron metabolism in AT. In a 2016 publication by Orr *et al*, the Hasty lab demonstrated that 25% of macrophages in lean AT have a 2-fold increase in intracellular iron stores, allowing them to be isolated based upon their ferromagnetic properties[71]. While all ATMs present in the lean mice were M2-like, the paramagnetic ATMs were referred to as "MFe^{hi}" and the remaining ATMs as "MFe^{lo}" (Fig. 1.3A). Compared to MFe^{lo} cells,

MFe^{hi} cells had a 2-fold elevation in all iron metabolism-related genes quantified, including *Cd163*, *Tfr1*, *Hmox1*, *Fth*, *Ftl*, and *Slc40a1*, which was dubbed as a "iron-cycling" phenotype (Fig. 1.3B). Furthermore, MFe^{hi} ATMs had even greater expression of M2-associated genes, and a reduction in M1 genes (Fig 1.3C).

The increase in all iron-related genes suggested a role for these macrophages in iron-recycling rather than iron-storage. Furthermore, in diet-induced obesity, newly recruited macrophages did not take on a role in iron handling, and the MFe^{hi} cells become more inflammatory and appeared to lose their iron-cycling gene profile[71]. Importantly, this change in MFe^{hi} cells with regards to iron handling in obesity occurred concomitantly with adipocyte iron overload and reduced adipocyte adiponectin expression[71]. Taken together, these studies suggested that MFe^{hi} cells are a unique population of macrophages that regulate iron homeostasis in AT.

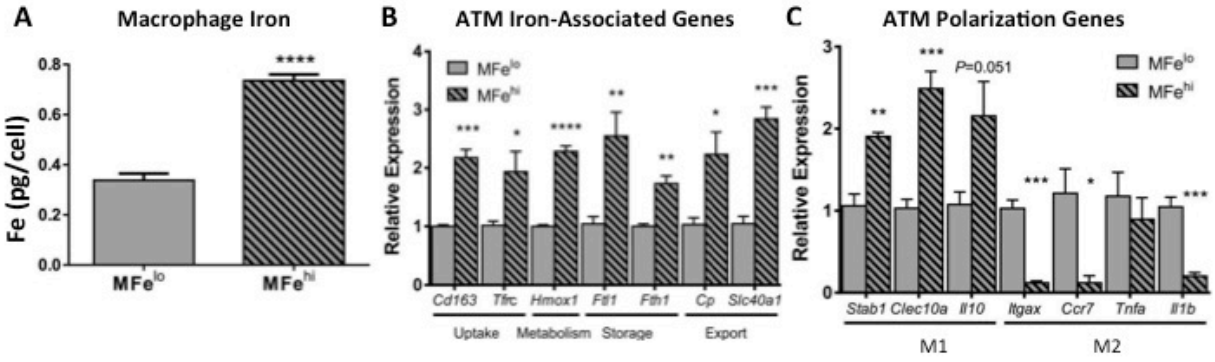

Figure 1.3. [**Adapted from Orr *et al*. 2013 [73]**] **Profile of high-iron "MFe^{hi}" adipose tissue macrophages.** (**A**) Iron quantification of magnetically sorted macrophages. (**B**) Iron-associated gene expression in MFe^{lo} and MFe^{hi} ATMs. (**C**) Polarization gene expression in MFe^{lo} and MFe^{hi} ATMs. *p<0.05, **p<0.01, ***p<0.001, ****p<0.0001

Macrophage polarization and iron

A long-standing dogma in the field of immunology is the association between M1-polarized macrophages and increased intracellular iron. This view is grounded in the observation that iron is sequestered by M1-polarized macrophages in serum following spikes in hepcidin during acute inflammation[95]. In addition, this view holds that patterns of gene expression in macrophages either favor iron storage (increased import and storage genes) or iron release (decreased storage and increased export genes). The study of MFe^{hi} cells discussed above contradicts these dogma, showing that MFe^{hi} ATMs are highly M2-polarized, have increased iron content, and also have high expression of all iron-related genes, i.e. iron uptake, storage, and release[71] (Fig. 1.3A). This could be a phenomenon unique to MFe^{hi} cells in AT; however, other studies support the observation that M2-polarized macrophages have an iron-cycling phenotype[96, 97]. When these *in vitro* studies compare M2-polarized to M1-polarized macrophages, TfR1 and Fpn1 proteins were both up-regulated in M2 macrophages, while Ft was down-regulated. M2 macrophages also had enhanced binding of IRPs to IREs, corresponding to an increased LIP and a more flexible iron-cycling phenotype. Characterization of *in vitro* polarized macrophages to *in vivo* macrophages, like MFe^{hi}, leaves many questions concerning the mechanisms by which macrophage polarization and iron handling are linked.

Obesity and the MFe^{hi} phenotype

In obese mice, MFe^{hi} ATMs had decreased iron content as well as decreased expression of iron uptake and release genes[71]. Cytokines such as TNFα, IL-6, IL-1β, and saturated fatty acids (SFAs), are important modulators of inflammation in obese AT. This can be correlated to *in vitro* findings; exposure of primary peritoneal macrophages to SFAs to induce inflammation reduces expression of iron metabolism genes[71]. Figure 1.4 depicts a schematic to summarize our current understanding of the intersection of inflammation and iron content in macrophages *in vivo* and *in vitro*.

Other inflammatory molecules have not been studied extensively in the context of iron handling in ATMs; however, in one recent report, high-iron macrophages in the spinal cord were shown to be uniquely susceptible to M1 polarization by TNFα[98]. Thus, the inflammatory milieu of obese AT may explain why MFe^{hi} ATMs take on a more M1-like phenotype. The susceptibility of MFe^{hi} ATMs to inflammatory polarization relative to the other ATMs has not been explored, but may partially explain increased adipocyte dysfunction in iron-overloaded humans. Obesity is associated with an increase in the cytokine IL-6. In fact, 30% of serum IL-6 is thought to come from visceral AT, and is attributed to macrophages, not adipocytes[99]. IL-6 directly induces the production of hepcidin[100]. Interestingly, in obesity, hepcidin can be secreted by visceral AT, and like IL-6, it is produced mainly from macrophages[101]. Whether hepcidin can be expressed in MFe^{hi} cells specifically is not known. The production of hepcidin by ATMs could indicate that they are responsible for sensing and responding to changes in local iron concentrations, causing reduced iron cycling by macrophages and iron retention in adipocytes. Differences in IL-6 expression in obesity could also explain changes in

hepcidin and iron content between tissues in obesity. For example, hepcidin did not increase in the liver in obesity, possibly explaining why elevated iron content was seen more in AT than in the liver in obesity[71].

IL-4 is a potent T helper type 2 cytokine whose expression is reduced in AT in obesity. IL-4 has been shown to induce M2-like macrophage polarization; it also inhibits NO-induced IRP activation by reducing binding of IRP1 and IRP2 to RNA[102], thereby decreasing the LIP. Furthermore, IL-4 enhances production of TfR1 mRNA through a non-IRP dependent pathway. Thus, IL-4 may serve as a node of control for both macrophage polarization and iron handling.

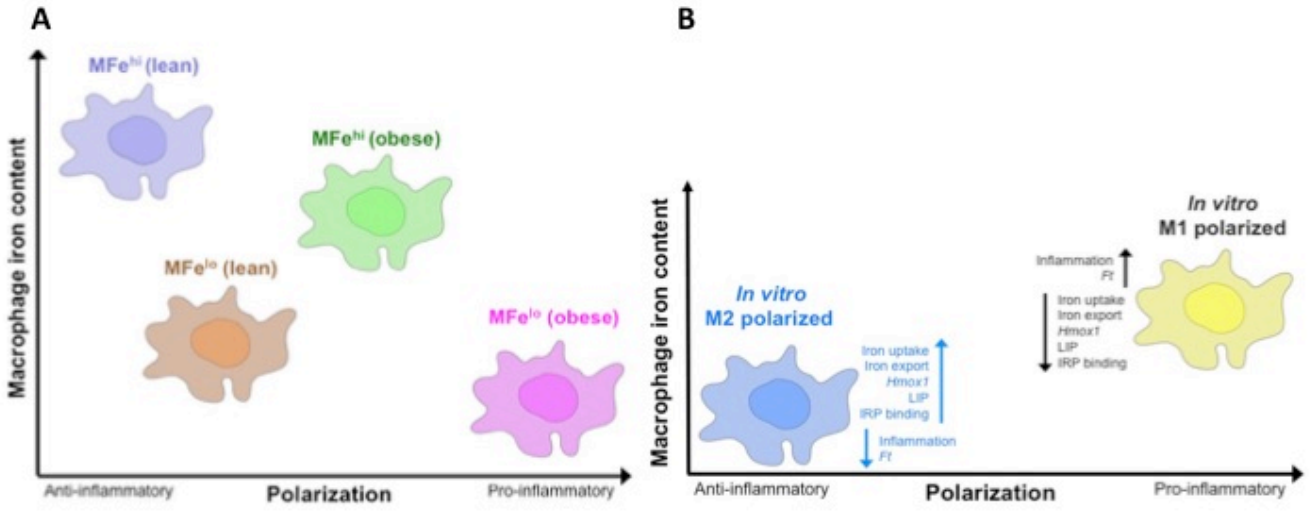

Figure 1.4. Inflammation and iron content of macrophages. (**A**) ATMs can be magnetically isolated based upon natural paramagnetic properties due to increased iron stores. MFe^{hi} macrophages have elevated iron concentrations compared to MFe^{lo} macrophages. In both lean and obese mice, MFe^{hi} macrophages have increased expression of M2-like anti-inflammatory genes and decreased expression of M1-like pro-inflammatory genes, as compared to MFe^{lo} macrophages from the same animals. It is known that obesity induces a pro-inflammatory phenotype in AT macrophages. In high fat diet-induced obesity, MFe^{hi} macrophages become more inflammatory compared to MFe^{hi} macrophages from lean mice, but do not exhibit the extent of M1-like inflammatory properties observed in MFe^{lo} macrophages from obese animals. (**B**) *In vitro* polarized M1 and M2 macrophages have unique properties regarding iron handling. M1 macrophages have decreased iron uptake and export, and a smaller LIP while M2 macrophages have an iron recycling phenotype. [**LIP**: labile iron pool; ***Ft***: gene for ferritin; ***Hmox1***: gene for heme oxygenase 1; **IRP**: iron response protein].

Heme oxygenase 1 and macrophage iron handling

Heme oxygenase 1 (Hmox1, gene *Hmox1*) is an enzyme that metabolizes heme into iron, bilirubin and CO. It is part of the cellular defense against oxidative stress and has largely been considered protective against cellular dysfunction. For example, peritoneal macrophages from Hmox1 knockout mice have increased ROS and the inflammatory cytokine MCP-1[103]. However, the cellular role of Hmox1 may be much more context-dependent than previously appreciated. In a recent study, macrophage-specific Hmox1 knockout mice on a high fat diet had decreased AT inflammation and a dramatic improvement in nearly every metabolic parameter compared to controls[104]. These findings not only contradict the dogmatic "anti-inflammatory" categorization of Hmox1, but also obfuscate the finding that Hmox1 is one of the genes most highly up-regulated in MFe^{hi} ATMs, which are very polarized to the M2-like phenotype. However, iron content of macrophages could be very important in determining the impact of Hmox1 on cellular function. For example, splenic macrophages are absent in Hmox1-deficient mice and humans[105]. Splenic macrophages have high iron content due to persistent heme recycling, and their absence in Hmox1-deficient mice indicates that Hmox1 may be required for the viability of macrophages with high heme or iron content. Interestingly, *Hmox1* expression in MFe^{hi} ATMs is reduced in obese mice (Fig. 1.3A & 1.4). Paralleling this, Hmox1 in human M2-polarized macrophages is decreased by the inflammatory cytokine IFNγ and increased by IL-4[106]. Figure 1.5 depicts a schematic to summarize our current understanding of the impact of obesity-associated inflammation on macrophage iron handling.

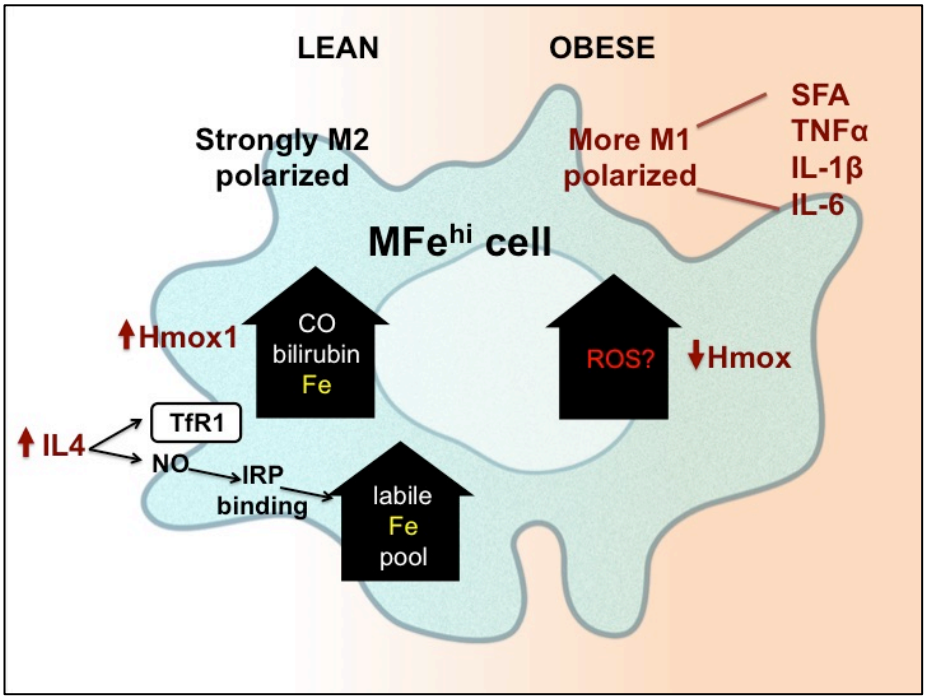

Figure 1.5. Proposed mechanisms by which obesity could impact MFe^{hi} cells. In lean AT, MFe^{hi} ATMs are highly M2-polarized and express elevated levels of Hmox1 and thereby could breakdown heme into CO, bilirubin, and iron in an anti-inflammatory process. In addition, they are exposed to elevated levels of IL-4, which could increase TfR1 and NO. An increase in NO has been shown to increase IRP binding and therefore the labile iron pool in other settings. In obesity, the MFe^{hi} ATMs become more M1-like, likely due to the milieu of SFA and inflammatory cytokines such as TNFα and IL-1β. A decrease in Hmox1 could result in increased ROS. In vitro studies with cultured macrophages have shown similar mechanisms to occur; however, these have yet to be tested in MFe^{hi} ATMs. [**AT**: adipose tissue; Hmox: heme oxygenase 1; **TfR1**: transferrin receptor; **NO**: nitric oxide; **ROS**: reactive oxygen species; **SFA**: saturated fatty acid; **TNFα**: tumor necrosis factor α; **IL-1β**: interleukin 1β].

Summary and significance

The impact of the obesity epidemic and its associated metabolic diseases makes it imperative that we better understand the intricate relationships between adipocytes and the immune system. While much attention has been paid to the function of ATMs in obesity, much less is known about the fundamental homeostatic functions of ATMs in AT. The literature described suggests a strong association between iron storage and metabolic regulation. In AT, iron levels must be sufficiently high to facilitate adipogenesis, while not so high that they induce IR. In addition, the gene expression profile of MFe^{hi} ATMs suggested that they are M2 polarized and have an iron recycling phenotype. This M2-associated "iron-cycling" phenotype has been substantiated by *in vitro* studies published by other groups.

As depicted in Figure 1.6, Chapter III delves into functional questions presented by the discovery of MFe^{hi}, i.e. Can MFe^{hi} ATMs contribute to local control of AT iron concentrations, perhaps acting as "ferrostats"? It is yet to be determined how the presence of MFe^{hi} may protect adipocyte function. Chapter IV outlines studies to address the impact of obesity on this hypothesized ferrostatic function of MFe^{hi}. Lastly, Chapter V outlines methodological attempts to target MFe^{hi} in AT.

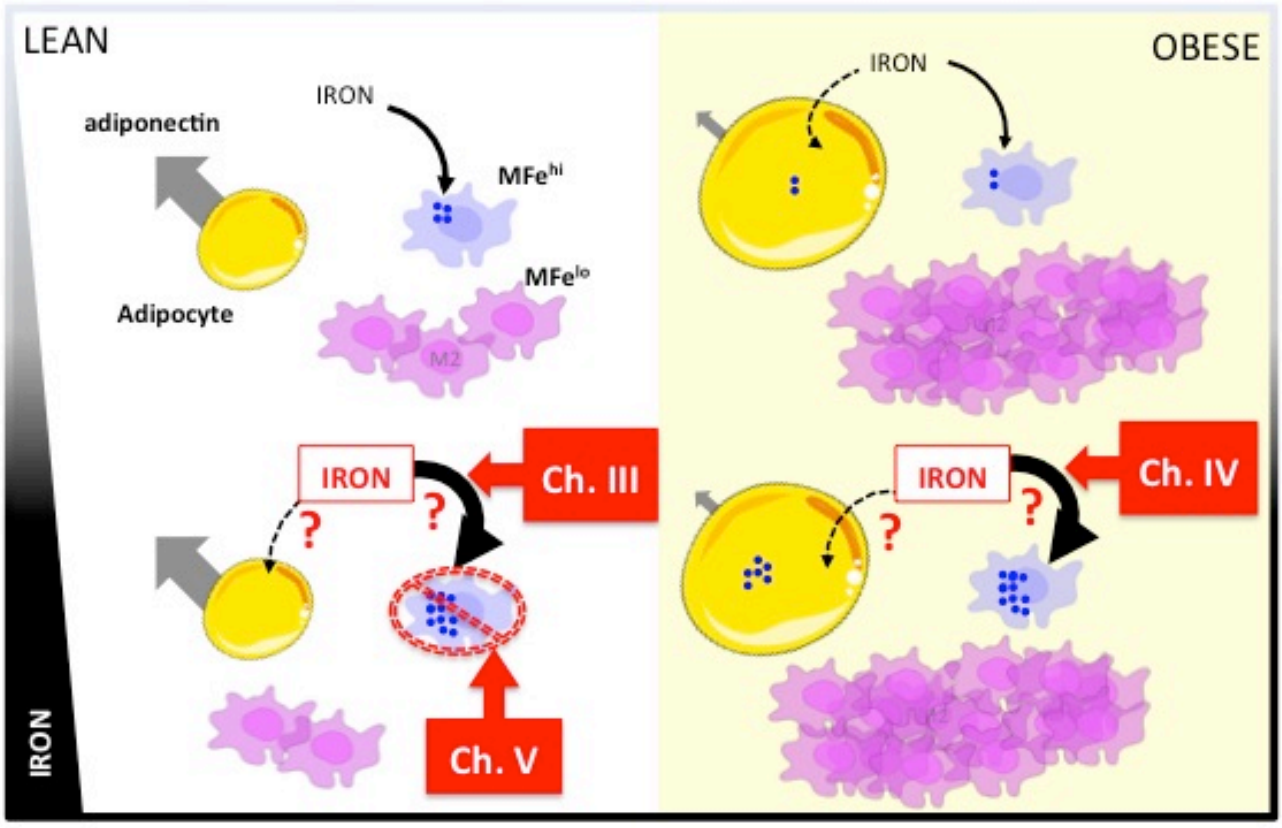

Figure 1.6. **Model representing an overview of experimental questions in Chapters III-V.** Previous studies by our lab demonstrated that MFe^{hi} ATMs have increased intracellular iron content. In obesity, the iron content of MFe^{hi} ATMs is decreased but adipocyte iron increases. Chapter III will aim to understand if MFe^{hi} ATMs take up exogenous iron, preventing adipocyte iron uptake. Based on the described changes in adipocyte iron content in obesity, Chapter IV will provide excess iron in obesity to explore if can still serve as an iron-sink. Chapter V explores methods of interfering with MFe^{hi} ATM uptake of iron through cellular depletion or gene knockdown.

CHAPTER II

MATERIALS AND METHODS

Animal care and usage

Animal care and procedures described in this chapter were performed with approval from the Institutional Animal Care and Usage Committee at Vanderbilt University. Experiments used male C57BL/6J mice from The Jackson Laboratory (Bar Harbor, ME).

Animal diets

Unless specified otherwise, mice were provided standard rodent chow diet (LabDiet 5001) with a kcal composition of 12% fat, 28% protein, and 60% carbohydrates. All mice were given free access to water.

Iron diets: For iron diet studies, mice were fed macronutrient-matched iron diets that contained low iron levels (35ppm iron, cat. no. TD-10211; Envigo), average iron (500ppm, cat. no. TD-10212; Envigo) or high iron (2000ppm, cat. no. TD-10324; Envigo) for 8 weeks starting at 8 weeks of age. These dietary iron levels were selected because dietary iron as low as 25ppm supports hematopoiesis in C57BL/6J mice, while around approximately 250ppm is commonly found in chow diet[107, 108]. Body weight and dietary intake were tracked and mice were provided water and food *ad libitum* for the course of the studies.

Diet induced obesity: In high fat diet (HFD), studies mice were provided diet *ad libitum* consisting of 60% kcal from fat (Research Diets, D12492) for 16-20 weeks. Control groups received low fat diet (LFD) consisting of 10% kcal from fat (Research Diets, D12450B).

Tissue digestion for SVF and adipocyte isolation

Mice were euthanized by isoflurane overdose and cervical dislocation, then perfused with 20 ml PBS through the left ventricle. Unless otherwise specified, ATMs were collected from eAT. The eAT fat pads were collected, minced, and digested in 6 ml of 2 mg/ml type II collagenase (cat. no. C6885; Sigma) for 40 min at 37°C. The stromal vascular fraction (SVF) was separated from adipocytes by centrifugation followed by erythrocyte lysis with Ack buffer, as previously described[71]. The top adipocyte layer was transferred to a new vial and washed, then pelleted and stored at -80^{o}C for either iron quantification or gene expression analysis.

Cell staining with fluorescent antibodies

The SVF was treated with Fc block (BD) for 10 min and then stained with an appropriate combination of fluorophore-conjugated antibodies against cell-surface markers for 30 min at 4°C; F4/80-APC (eBioscience), F4/80-BV785 (BioLegend), CD11b-FITC (eBioscience), CD11b-APC/Cy7 (BD), CD45-BV605 (BioLegend), CD45-PE (eBioscience), or CD163-CF594 (Antibody kindly provided by Dr. Soren Moestrup, Aarhus University; conjugated using the Mix-n-Stain CF594 kit; Biotium). Cells were washed in fluorescence-assisted cell sorter (FACS) buffer and filtered through filter-top FACS tubes to make a single-cell suspension.

Magnetic sorting with AutoMACS

Following staining and single-cell suspension (see **Cell staining with fluorescent antibodies**), cells were sorted by their ferromagnetic qualities through the sensitive positive selection (possel_s) program on the AutoMACS magnetic activated cells-sorting system (Milltenyl Biotech). After separation, the magnetic and non-magnetic fractions were centrifuged at 500 g for 10 min at 4 °C.

Flow cytometry and flow assisted cell sorting *(FACS)*

Cell stained with fluorescent antibodies were resuspended with a live/dead marker (DAPI or propridium iodide) and spiked with 50µl of CountBright counting beads (ThermoFischer Life Science). The samples were then analyzed in the Vanderbilt Flow Cytometry Shared Resource with either the LSRFortessa flow cytometer (BD Bioscience) or sorted with the FACSAria III cell sorter (BD Biosciences) with appropriate compensation controls and fluorescence minus one controls. Results were analyzed using FlowJo software v.10 (BD Biosciences), using gating previously published by our lab in the visual methods journal Jove[109]. The general gating scheme was: singlet cells → $CD45^+$ → live (PE or DAPI negative) → $F4/80^+CD11b^+$ → M1 or M2 markers.

Iron injections

Mice were intraperitoneally injected with 5mg/kg Iron-100 (dextran conjugated solution, Durvet), diluted in 0.9% bacteriostatic sodium chloride solution (Hospira). Control groups received only intraperitoneal (IP) injection of the sodium chloride solution.

PKH26 cell stain

The PKH26 Red Fluorescent Cell Linker (Sigma) is selectively phagocytized by macrophages and neutrophils when they ingest the dye aggregate. The dye is resistant to metabolism and sustained *in vivo* for multiple weeks. This method can be used to stain all cells at a given time point. Following a wash-out period, any non-PKH cells are considered to be recruited after the time of injection. Twelve-week old mice were IP-injected with 1ml of 5uM PKH26. Control groups were injected with an equal volume of the diluent. Following a 2-day wash-out period, mice were injected with either saline or iron (described in **Iron injections**).

Iron staining with Prussian blue

Iron was visualized in section of paraffin-embedded eAT using the Perls' Prussian blue staining method. The tissue was sectioned to 10μm onto glass slides, cleared, hydrated and stained with microwave-heated Prussian blue staining solution (10% hydrochloric acid, 10% Prussian blue) for 20 min, then counterstained with nuclear fast red for 5 min.

Gene expression by quantitative real-time PCR *(RT-PCR)*

Macrophages were collected via FACS, as described above, pelleted and resuspended in RLT buffer to allow for RNA extraction with the RNeasy Micro RNA kit (Qiagen), according to the manufacturers instructions. Adipocytes were collected as described above, but the final pellet was collected in TRIzol reagent (Invitrogen) and isolated with the Direct-zol RNA MiniPrep kit (Genesee). For both macrophage and

adipocytes, cDNA was synthesized with the iScript cDNA synthesis kit (BioRad) and quantitative RT-PCR was performed with the Taqman assay system (Applied Biosystems) on a CFX96 cycler (BioRad). Gene expression was normalized to glyceraldehyde-3-phosphate dehydrogenase, and the control group, using the $2^{-\Delta\Delta Ct}$ method.

Glucose tolerance tests

Lean body mass of mice in the study was quantified using body composition values from the Minispec Model mq7.5 (Bruker). Glucose tolerance was determined by IP injection of dextrose at 2mg/kg lean mass. Blood glucose was subsequently tested at 15-30 minutes intervals over two hours, using tail-vein blood and a handheld glucometer (ACCU-CHEK, Aviva Plus, Roche).

Insulin injections

Insulin signaling was assessed by IP injection of 0.5U/kg of insulin or saline control 15 minutes prior to sacrifice. Tissues were flash-frozen to assess insulin-response by Western blot quantification (see **Western blot of AT and liver proteins**).

Serum iron and hormone parameters

Iron, Tf, Ft and total iron-binding capacity (TIBC) were quantified from serum using the ACE Alera clinical chemistry system (Alfa Wasserman). Adiponectin was quantified in plasma with the Milliplex MAP Mouse Adiponectin Magnetic Single Plex Kit (Millipore).

Cell iron quantification

Macrophages: Iron was quantified in ATMs with double-focusing sector field high-resolution inductively-coupled mass spectrometry (ICP-MS; ELEMENT II; Thermo Fischer Scientific, Bremen, Germany) equipped with ESI auto sampler, in the Vanderbilt Mass Spectrometry Core.

Adipocytes: The adipocyte fraction was collected and pelleted, as described above. For atomic absorption spectrometry (AAS), samples were homogenized in 100µl radioimmunoprecipitation assay buffer for bicinchoninic assay protein analysis, digested in 1:2 v/v ultra-pure HNO3, and further diluted in 2% nitric acid. Internal standardization was performed with bovine liver (184 µg Fe/g; National Bureau of Standards, Standard Reference Material, United States Department of Commerce, Washington, DC). To perform ICP-MS, samples were homogenized in 2% SDS RIPA buffer and an aliquot was collected to quantify protein concentration by BCA assay. The remaining sample was digest in ultra-pure HNO3 (1:3 v/v dilution) for 12 hours at 60^{o}F, then diluted with milliQ water for ICP-MS quantification at the Vanderbilt Mass Spectrometry Core. Quantification of adipocyte iron was compared between ICP-MS and AAS, with no significant difference found between the two methods (data not shown).

Western blot of AT and liver proteins

Western blotting was used to quantify protein expression in liver and eAT. 0.1g of tissue was digested in 500ul of 2% RIPA lysis buffer [50mM Tris-HCl pH 7.4, 150mM NaCl, 1% Triton-X, 2% SDS, 1mM EDTA, 10mM NaF, Na deoxycholate, 1mM PMSF, 1mM Na orthovandate]. The sample was homogenized, and the supernatant collected.

Total protein concentrations were determined with BCA assay, and concentrations were standardized and stored in NuPAGE LDS Sample Buffer (Invitrogen). For denaturation, samples were incubated for 30 minutes at 60^{o}C, then cooled. Gel electrophoresis was performed with the NuPAGE Western Blot System with 4-12% Bis-Tris Gels (Invitrogen). Protein was transferred from the gel to 0.45um nitrocellulose blotting membrane (Amersham Protran, GE). The membrane was blocked with Odyssey Blocking Buffer. Primary antibodies were applied overnight at 4^{o}C. Primary antibodies used in these studies were: Beta-actin mouse anti-mouse mAb (Cell Signaling 3700S), rabbit anti-mouse phosphorylated Akt (pAkt) (Cell Signaling 4060S), and rabbit anti-mouse Akt (Cell Signaling 9272S). Secondary antibodies were applied for 1hr at RT, and included: 800CW goat anti-rabbit IgG and 680RD goat anti-mouse IgG (Licor). The blots were imaged on a Li-Cor Odyssey Infrared Imaging System and band intensities were quantified using Image Studio Lite software.

Adipose tissue explants

Mice were sacrificed and eAT fat pads were collected and cut into 50-60mg pieces. Each piece was placed into a 48-well tissue-culture plate with 300µl of DMEM and 5% fetal bovine serum, at 37^{o}C for the time specified in the experiment. For subsequent RNA analysis, explant pieces were collected and digested in TRIZol Reagent (described in **Gene expression by quantitative real-time PCR**). Otherwise, samples were digested with type II collagenase and analyzed by flow cytometry (described previously in this chapter).

Live animal hepatic fat quantification

Hydrogen MR spectroscopy was performed by the Center for Small Animal Imaging (Vanderbilt) using the 4.7T (31cm bore) Agilent (Varian). MR spectroscopy was used to quantify liver fat at 5 locations in mice under 0.5% isofluorane anesthesia.

Triglyceride quantification

The left lateral liver lobe was flash-frozen at sacrifice. 60mg of tissue was digested in 3M KOH in 65% EtOH and incubated at 70^{o}C for 1hr, and at RT overnight. After samples were diluted with 2M Tris-HCl pH 7.5, the Infinity Triglycerides Liquid Stable Reagent (Thermo Scientific) was added at 2:3 ratio for colorimetric quantification of total triglycerides at 500nm.

Metabolomics

Single-cell samples from AT or from spleen were magnetically sorted and then macrophages were collected using FACS (methods previously described in this chapter). The cell pellet was flash frozen and provided to Metabolon (NC, USA) for analysis. Metabolon provided metabolic pathway and subpathway analysis.

Bone marrow derived macrophage** (BMDM) **differentiation and polarization

L929 media: L929 media is collected from serum-starved L929 cells because it is able to provide GM-CSF and other growth products to induce the differentiation of macrophages from bone marrow cells. This media is produced by growing up L929 cells into large flasks with 10% DMEM over a course of 14 days. The serum is collected twice, at confluency and 3 days later. These two serum collections are mixed 1:1 and frozen at -20^{o}C for use in BMDM differentiation, as described.

Bone marrow collection: BMDMs were produced by collecting bone marrow from female C57BL/6J mice. Briefly, mice are sacrificed by isofluorane exposure and cervical dislocation. Long bones of the lower extremity are cleaned off and flushed with DMEM with 10% fetal bovine serum, 1% HEPES, and 1% penicillin-streptomycin (10% FBS DMEM). Following red blood cell lysis with Ack buffer, the cells are filtered through a 100um filter. The bone marrow is plated in tissue-culture treated plates for 6-8 days in 10% FBS DMEM spiked with 14% of L929 media. The media is changed every 2-3 days and differentiation can be observed visually. At full differentiation and 70-80% confluence, BMDMs are dislodged and plated into experimental wells for polarization.

BMDM polarization: BMDMs are plated at 1 million cells/ml in 14% L929, 10% DMEM. For M2 polarization, the media is spiked with 10ng/ml IL-4 (R&D Systems) and 10ng/ml IL-13 (R&D Systems) for four days. For M1 polarization, the media is spiked with 10 ng/ml LPS (Sigma) and 100ng/ml IFNγ (R&D Systems) for 24 hours. For Mme polarization, the media is spiked with 30mM glucose, 0.4mM palmitic acid (Nu-check Prep, Inc.), and 10nM of insulin (Novolin R, Novo Nordisk) for 24 hours.

CD163 liposome treatments

Liposomes were produced by our collaborators Dr. Anders Etzerodt and Dr. Soren Moestrup (Aarhaus University, Denmark), as previously described[110]. These liposomes (CD163lipos) are polyethylene glycol (PEG)-coated long-circulating liposomes adapted to target CD163 via surface attachment of rat anti-mouse CD163 antibody (E10B10, Cytoguide Aps, Denmark). CD163lipos were either loaded with calcein disodium salt (Sigma Aldrich), a fluorescent protein, or with the cytotoxin doxorubicin (dox). For calcein studies, 12-week old mice were injected one time with calcein-loaded CD163lipos (CD163lipo/calcein), or empty controls (CD163lipo/empty). After 24 hours, mice were sacrificed and their tissues were imaged using the Xenogen IVIS 200 bioluminescent and fluorescent imaging system (Vanderbilt University Institute of Imaging). Autofluorescent background signal from lipids was subtracted, to provide a final image of true calcein fluorescent signal.

For depletion studies, mice were injected twice over a 10 day time period with dox-loaded CD163lipos (CD163lipo/dox) or empty controls (CD163lipo/empty). Both liposome solutions were brought to a 0.67mM lipid concentration with sterile PBS and warmed to room temperature. Every third day, for four total injections, 26.7ul of the liposome solution per gram body weight was injected IP using a 22G single-use needle. In studies combining CD163lipo with iron injections, the iron-dextran was injected (as described above), three days following the first liposomes injection. As in the previous studies, this iron injection occurred one week prior to sacrifice and was flanked by CD163lipo injections in order to maintain depletion.

Mannosylated nanoparticle** (MnNP) **treatments

MnNPs were provided to us by Dr. Giorgio (Vanderbilt). For a technical explanation of the production of mannosylated micelles, refer to their publication[111] Briefly, micelles are composed of multifunctional polymers with three main parts: a hydrophobic / pH-sensitive part, a siRNA condensing part, and a section that allows for addition of mannose to the end of polymer. The micelle is coated with mannose to be recognized by the mannose receptor (CD206) on phagocytic cells, initiating endocytosis.

siRNA and $Cy5^+$ dsDNA: Dicer-substrate small inhibitory RNAs (siRNAs) (IDT 146862759, 146862762, 146862765, 146862768, 146862771) or the negative scrambled control (51011908) were resuspended at 50nM in sterile-filtered TE buffer and frozen in aliquots at -20^{o}C. For $Cy5^+$ double-stranded (dsDNA) studies, a $Cy5^+$ antisense strand (IDT, 151568383) was annealed to complementary DNA sense strand (IDT, 12213382) for 5 minutes at 95^{o}C, then cooled for 1 hour.

MnNP preparation: 5mg of dry MnNP polymer was resuspended in EtOH to make a 3 mg/ml micelle stock. The required amount of stock was diluted with citric acid buffer (pH 4). The diluted micelle solution was sterile-filtered through 0.45μm filter and incubated with the correct ratio of siRNA at room temperature for 30 minutes. The ratio of siRNA or dsDNA to micelles was determined by the charge of the nucleotide chains. The micelle-siRNA mixture was diluted with 10mM sodium phosphate buffer (pH 8). siRNA-loaded MnNPs were directly added to BMDMs in culture for up to 48 hours.

Statistical analysis

All graphical data are presented as mean ± SEM. Statistical tests were performed using GraphPad Prism (La Jolla, CA) by two-tailed unpaired *t* tests and one-way ANOVA with the Tukey correction for multiple comparisons, when appropriate. In experiments with a 2 x 2 design, two-way ANOVA's were applied to determine significant variables and the impact of each factor.

CHAPTER III

MFe^{hi} ATMs COMPENSATE FOR TISSUE IRON PERTURBATIONS

This chapter represents work that has been accepted for publication in the *American Journal of Physiology – Cell Physiology,* by Hubler, Erikson, Kennedy, and Hasty[112].

Introduction

In order to respond to metabolic demand appropriately, adipocytes are in reciprocal communication with other tissues via systemic hormones (*e.g.* insulin, leptin, adiponectin). Under normal conditions, adipocytes are able to metabolize, store, and synthesize lipids without lipotoxicity[80]. Within the last decade, interest in AT has expanded as it becomes clear that local adipocyte physiology, such as oxidative stress or inflammation levels, can have beneficial or detrimental effects systemically.

ATMs are intercalated throughout the tissue matrix in close contact with individual adipocytes. ATMs were first identified in the context of obese AT, where metabolically-inflamed ATMs (Mme, described by Kratz[30]) accumulate and induce chronic inflammation [26, 94, 113]. However, resident ATMs are also present in lean AT and fall on the anti-inflammatory (M2-like) end of the polarization spectrum. Understanding the homeostatic functions of resident M2-like ATMs in lean AT may provide a mechanism by which to influence the adipocyte microenvironment, supporting healthy AT expansion.

To briefly review, macrophages are the primary cell responsible for handling iron in the body. Due to its scarcity, iron is recycled, primarily through the erythrocyte hemoglobin cycle[114]. Senescent erythrocytes are phagocytized and their heme-associated iron is released as transferrin-bound iron. In fact, the transferrin-iron pool turns over several times daily in humans. Kupffer cells and splenic macrophages are primarily responsible for this turnover, which is regulated by hepcidin[114]. M1-like inflammatory macrophages have an important iron-sequestration role during infection. However, the field has expanded its understanding of macrophages in iron homeostasis beyond just M1-like macrophages in blood, to include resident M2-like macrophages in tissues. Iron is now thought to be spatially regulated on a microenvironmental scale in muscle, spinal cord, and vasculature, and even regulated in a time-dependent manner during wound repair[90, 98, 115]. In these studies, resident M2-like macrophages are responsible for fine-tuned iron uptake and release. Similarly, regulated control of iron homeostasis is important in AT because AT requires iron availability for healthy adipogenesis[17] and because excess fatty acids in AT can react with free iron to facilitate a lipid peroxidation chain reaction[116]. Studies have shown that iron overload, specifically in adipocytes, can reduce systemic insulin sensitivity through a reduction in adiponectin[17, 117]. This emphasizes the importance of tight regulation of iron in AT – providing the impetus to assess the role of macrophages in this process.

As described in the Chapter I, "MFe^{hi}" ATMs were discovered by our lab as resident macrophages of the AT that have innate ferromagnetism due to high intracellular iron content[71]. Like all macrophages in lean AT[118], their cell surface protein profile is representative of an M2-like, alternatively activated macrophage[71]. This is in

contrast to M1 classically activated inflammatory macrophages, or Mme, the metabolically activated macrophages, that infiltrate AT in obesity. Macrophage polarization is useful for generic classification but, *in vivo*, macrophages span a spectrum of activation states[119]. Studies have shown that macrophage polarization strongly influences their iron handling – broadly, M2 macrophages have an iron-cycling phenotype, preferring iron uptake and release over inert storage[96, 97, 106, 120]. Although all ATMs in lean AT are M2-like, when they are sorted out by ferromagnetic qualities, MFe^{hi} ATMs were found to have an even stronger M2 expression pattern relative to other resident M2 "MFe^{lo}" ATMs. Reflecting this iron-cycling phenotype, MFe^{hi} have increased expression of iron-uptake associated genes. However, unlike M2 macrophages polarized *in vitro*, MFe^{hi} ATMs have higher cellular iron content. Therefore, even though MFe^{hi} ATMs have an M2-like iron-cycling phenotype based on their gene expression, their increased iron content is more reflective of M1-like ATMs. This contrast presents an opportunity to better understand the specific functional role for MFe^{hi} ATMs in regulating adipose tissue iron[2]. We hypothesized that MFe^{hi} cells respond to iron perturbations in AT by regulating their intracellular iron pool in response to iron in the microenvironment, and that this function is necessary to prevent adipocyte iron-loading when excess iron is present.

To test this hypothesis we looked at the response of MFe^{hi} ATMs, MFe^{lo} ATMs and adipocytes in the context of two conditions of high iron: dietary iron and iron injection. Our studies demonstrated that MFe^{hi} ATMs increase their intracellular iron content, upregulate iron-handling genes, and recruit macrophages, both from the MFe^{lo} population and from the circulation, as a compensatory response to excess iron.

Results

MFe^{hi} ATMs accumulate iron with high-iron diet

Based on the described MFe^{hi} ATM iron-cycling phenotype, we hypothesized that MFe^{hi} ATMs would respond to changes in iron concentrations in the AT environment. We sought to determine if MFe^{hi} ATMs would respond to systemic changes in iron through a high-iron diet. After 8 weeks on low-, average-, or high-iron diet, we noted systemic iron overload with increased serum iron and Tf saturation (Fig 3.1A & B, $p<0.0001$), but no change in hematocrit (Fig. 3.1C). Dietary iron caused no changes in weight gain, body composition, or glucose tolerance (Fig. 3.1D - F). Iron-laden cells were seen by Prussian-blue staining (Fig. 3.2A). Using ICP-MS quantification, iron content per cell positively correlated with dietary iron (Fig. 3.2B; $p<0.01$ 35ppm vs. 2000ppm; $p<0.05$ 500ppm vs. 2000ppm). There was also a significant increase in the count of MFe^{hi} ATMs from low-to-average-to-high iron, with 7.6×10^4, 1.1×10^5, 1.5×10^5 per gram tissue, respectively (Fig. 3.2C; $p<0.05$ 35ppm vs. 500ppm; $p<0.05$ 500ppm vs. 2000ppm; $p<0.001$ 35ppm vs. 2000ppm). Neither MFe^{lo} ATMs nor adipocytes had an increase in iron content (Fig. 3.2C & D). Adipocyte iron was quantified using both AAS and ICP-MS methods to ensure rigor and reproducibility of this finding, with no significant differences between the two methods (data not shown). The size of the adipocytes was 1017±103, 1004±22, and 946±97 μm^2, low-to-high iron respectively, with no significant difference between the groups.

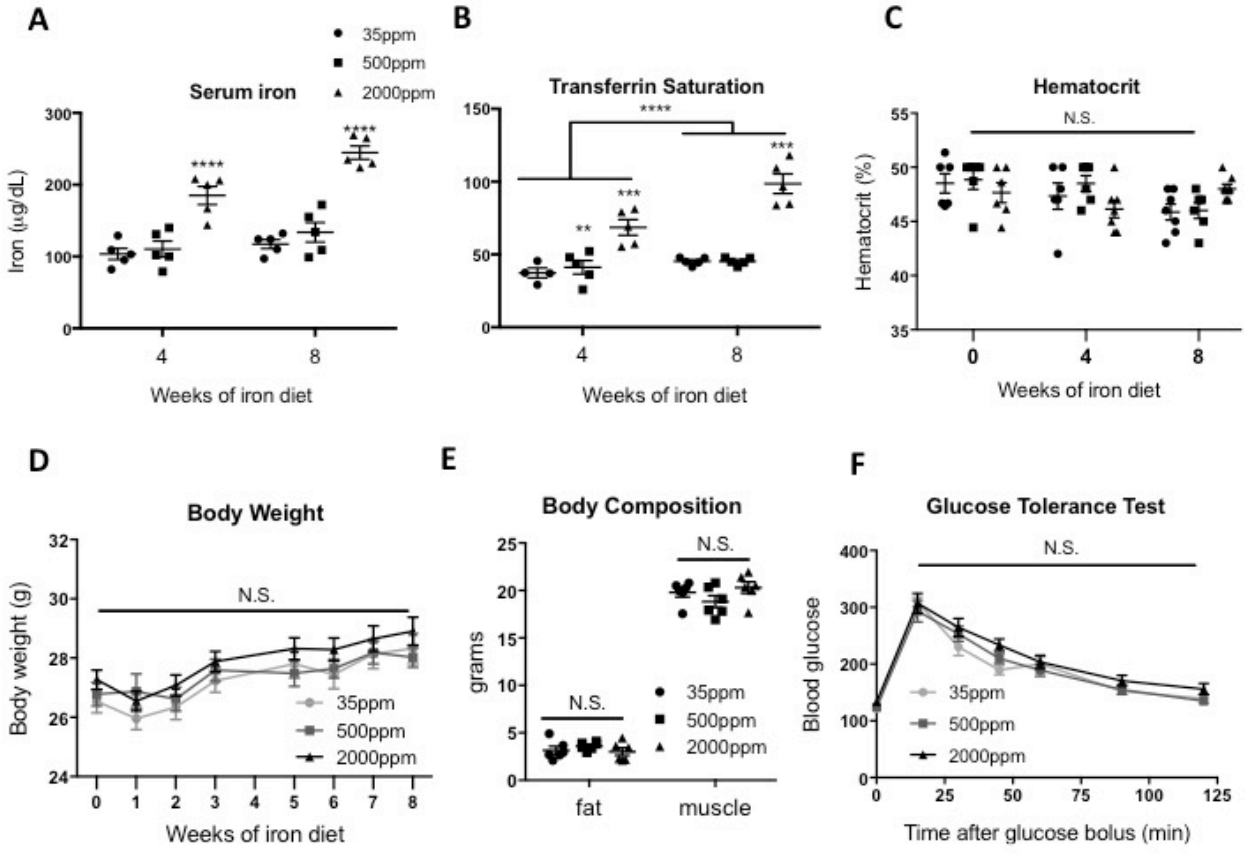

Figure 3.1. Physiological and serum iron parameters from mice on iron diets. C57BL/6J mice were given 8 weeks of low (35ppm), average (500ppm), and high (2000ppm) iron diets. Serum iron parameters such as (A) serum iron (N=5), (B) transferrin saturation calculated as % iron/TIBC (N=4-6), and (C) hematocrit (N=6) were quantified. (D) Body weight was recorded over the study course (N=18-22). (E) Body composition (N=6) and (F) glucose tolerance tests were performed after 8 weeks on diet (N=6). For all studies, significant differences were identified using ANOVA and t-test, with the following p-value indicators: ***p<0.001, ***p<0.0001.

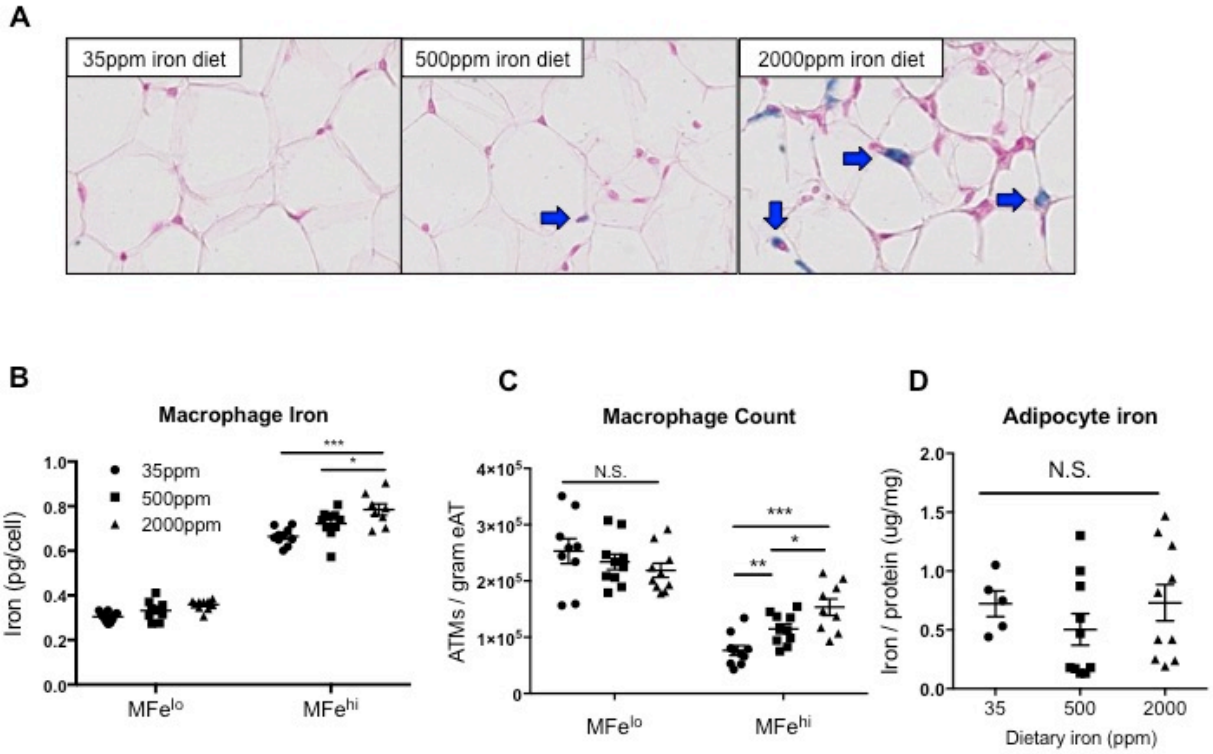

Figure 3.2. Effect of 8 weeks of iron diet feeding on ATM and adipocyte iron content. C57BL/6J mice were on 8 weeks of low (35ppm), average (500ppm), and high (2000ppm) iron diet. (A) Whole AT was fixed and sectioned, then stained with Prussian blue to visualize iron and counter-stained with nuclear fast red. Cells were sorted in order to quantify (B) iron content per ATM (N=8-10), (C) ATMs per gram of tissue, and (D) adipocyte iron content (N=8-10). For all studies, significant differences were identified using ANOVA and t-test, with the following p-value indicators: *p<0.05, **p<0.01, ***p<0.001.

MFe^{hi} respond to high dietary iron by upregulating iron-storage genes

MFe^{hi}, MFe^{lo}, and adipocytes were collected for gene expression from mice fed varying levels of dietary iron to assess the cells' response to iron availability. Expression of iron uptake genes *Cd163* and *Tfrc*, iron processing *Hmox1*, and iron export, *Slc40a1*, were greater in MFe^{hi} ATMs compared to MFe^{lo} ATMs across all concentrations of dietary iron (Fig. 3.3). Furthermore, MFe^{hi} were generally more M2-polarized, with less expression of *Itgax* and *Nos2* compared to MFe^{lo}. In response to excess dietary iron, the MFe^{hi} population had an increase in expression of iron storage-associated genes *Ftl1* and *Fth1*, significant by 2-way ANOVA with a $p<0.01$ between cell types, and $p<0.05$ between diets (Fig. 3.3). Lastly, in response to high dietary iron, the MFe^{hi} population expressed higher levels of *Spic*, the transcription factor required for the development of iron-handling macrophages in the spleen and bone marrow[60]. In contrast, MFe^{lo} ATMs had no change in iron-handling gene expression levels due to increased iron (Fig. 3.3A - J). Similarly, there was no difference in adipocyte iron-handling genes upon dietary iron challenge, although a trend for an increase in *Ftl1, Fth1, and Il6* was noted (Fig. 3.4A - F). Importantly, *Adipoq* expression was not different between groups (Fig. 3.4G).

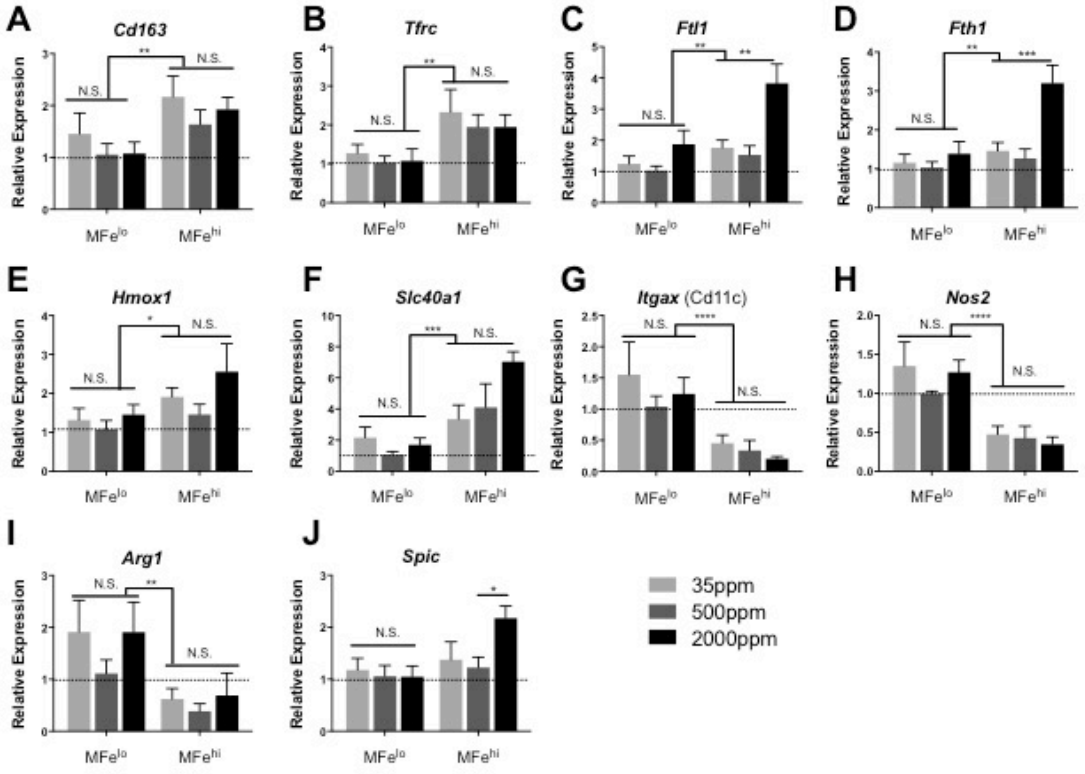

Figure 3.3. Effect of 8 weeks of iron diet feeding on ATM gene expression. C57BL/6J mice were on 8 weeks of low (35ppm), average (500ppm), and high (2000ppm) iron diet. Iron-handling genes were quantified by RT-PCR for MFe^{lo} and MFe^{hi} ATMs (N=4-5). Results are normalized to MFe^{lo} expression in the average (500ppm) iron diet. For all studies, significant differences were identified using ANOVA and t-test, with the following p-value indicators: *p<0.05, **p<0.01, ***p<0.001, ****p<0.0001.

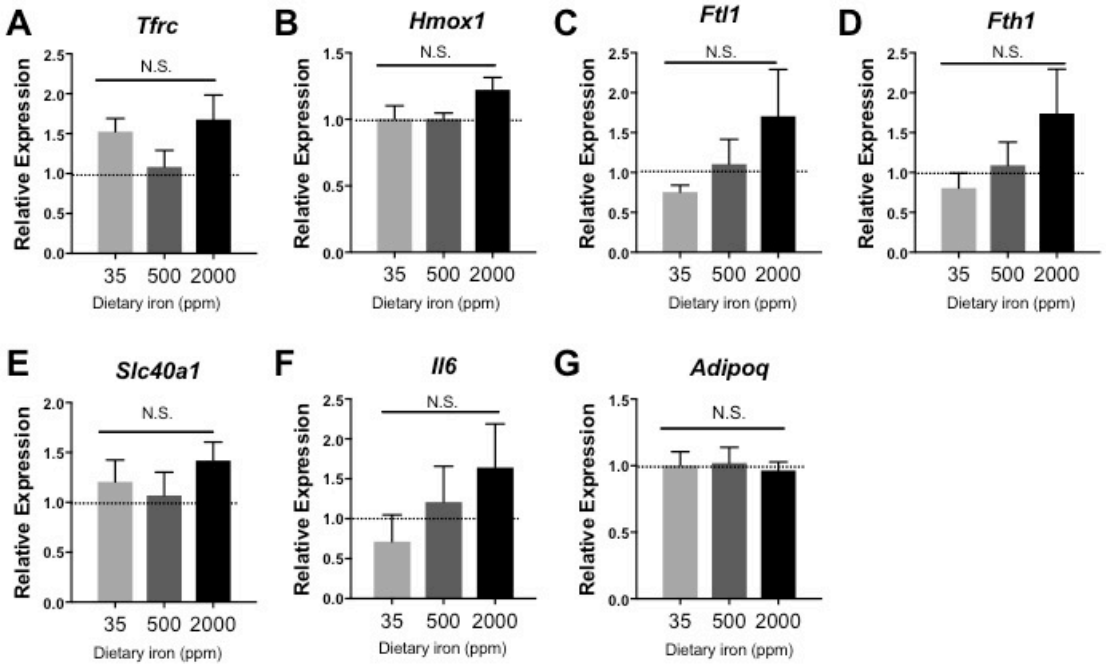

Figure 3.4. Adipocyte gene expression after 8 weeks on iron diets. C57BL/6J mice were on 8 weeks of low (35ppm), average (500ppm), and high (2000ppm) iron diet. Iron-handling genes were quantified by RT-PCR (N=4-5). For all studies, significant differences were identified using ANOVA and t-test.

Excess peritoneal iron is taken up by ATMs, not by adipocytes

Iron absorption is regulated through the intestinal tract, so diet-mediate iron overload is somewhat limited by a feedback-regulated maximum absorptive capacity. IP iron administration provides a direct way to provide higher iron levels to the peritoneum. This method was used to demonstrate the proof-of-concept that ATMs compensate for excess iron, as IP iron administration circumvents some of the systemic and absorption limitations of iron-diet models. In iron-injected mice, there was a visible increase in SVF iron content by Prussian blue staining (Fig. 3.5A). MFe^{hi} had a significant increase in intracellular iron content ($p<0.01$), while MFe^{lo} ATM iron content did not change (Fig. 3.5B). Interestingly, the number of MFe^{lo} cells per gram eAT was decreased (by $6.7x10^4$; $p<0.02$), while conversely, the number of MFe^{hi} cells per gram eAT was increased (by $1.3x10^5$; $p<0.0001$; Fig. 3.5C). Most importantly, adipocyte intracellular iron, quantified by both AAS and ICP-MS, was not altered by the acute high-dose injection of iron (Fig. 3.5D).

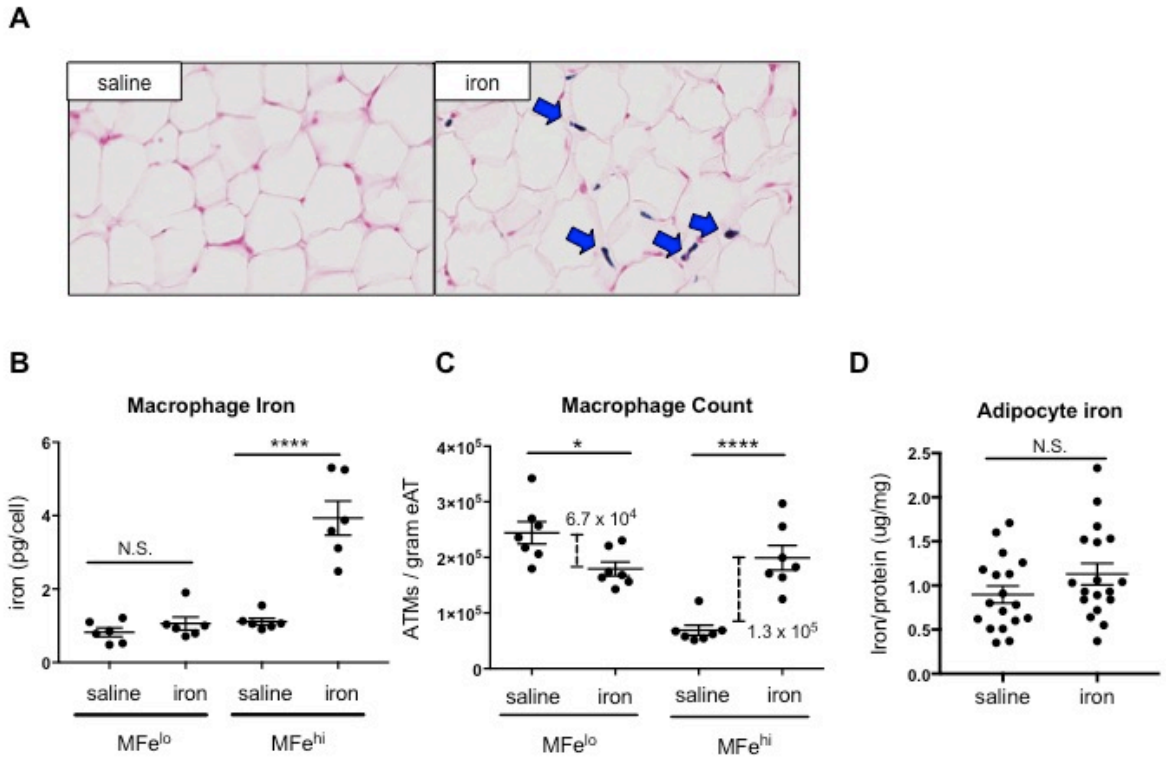

Figure 3.5. Effect of iron injection on ATM and adipocyte iron content. C57BL/6J mice were given an IP injection of 5 mg/kg iron dextran 1 week prior to sacrifice. (A) Whole AT was fixed and sectioned, then stained with Prussian blue to visualize iron and counter-stained with nuclear red. Cells were sorted in order to quantify (B) iron content per ATM (N=6), (C) ATMs per gram of tissue (N=7), and (D) adipocyte iron content (N=18). For all studies, significant differences were identified using ANOVA and t-test, with the following p-value indicators: *p<0.05, ****p<0.0001.

MFe^{hi} ATMs respond to acute high iron with alterations in iron-handling genes

The MFe^{hi} ATMs demonstrate changes in their iron-related gene expression in response to excess iron. Iron-import genes, *Cd163* (p=0.01) and *Tfrc* (p=0.001) decreased, while the iron-storage gene *Fth1* (p=0.01), iron-metabolism gene *Hmox1* (p=0.01), and the iron-export gene *Slc40a1* (p<0.0001) were all increased (Fig. 3.6A - F). Interestingly, in ANOVA analysis comparing the effect or the iron injection to the cell type, the iron effect drove the significant difference for all genes except *Fth1.* This is in contrast to MFe^{lo}, which showed no significant difference in any of the iron-handling genes in response to IP iron (Fig. 3.6A - F). Adipocytes did not have significant changes in the iron handling genes *Fth1* or *Ftl1* (although there was a trend toward an increase), reflecting their unaltered iron content (Fig. 3.7C - D). But adipocytes did have an elevation of *Hmox1* (p=0.01) and *Slc40a1* (p<0.01) (Fig. 3.7B, E). Importantly, *Adipoq* and *Il6,* indicators of inflammation and dysfunction in adipocytes, were unchanged (Fig. F & H).

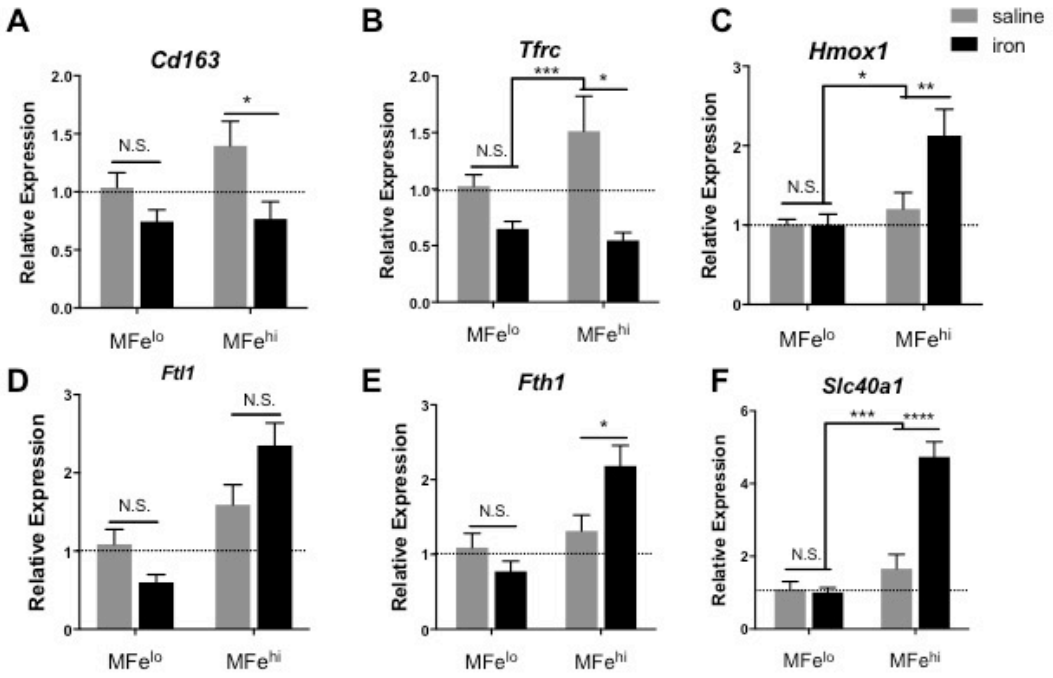

Figure 3.6. Effect of iron injection on ATM gene expression. C57BL/6J mice were given an IP injection of 5 mg/kg iron dextran 1 week prior to sacrifice. Iron-handling genes were quantified by RT-PCR for MFe^{lo} and MFe^{hi} ATMs (N=6). For all studies, significant differences were identified using ANOVA and t-test, with the following p-value indicators: *p<0.05, **p<0.01, ***p<0.001, ****p<0.0001.

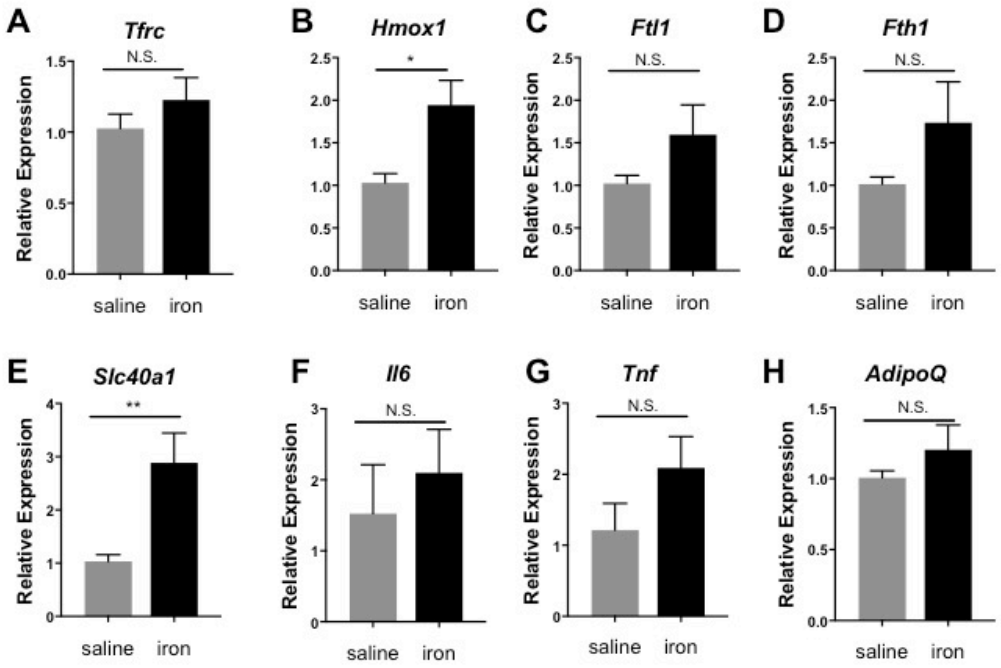

Figure 3.7. Effect of iron injection on adipocyte gene expression. C57BL/6J mice were given an IP injection of 5 mg/kg iron 1 week prior to sacrifice. Adipocytes were isolated, RNA prepared, and iron-handling genes quantified by RT-PCR (N=6). For all studies, significant differences were identified using ANOVA and t-test, with the following p-value indicators: *p<0.05, **p<0.01.

Addressing increased MFe^{hi} counts following iron injection

Increased MFe^{hi} counts can be explained by three mechanisms: (1) Monocytes are recruited and become MFe^{hi} ATMs, (2) MFe^{lo} ATMs take up enough excess iron to essentially convert into MFe^{hi} cells, or (3) MFe^{hi} ATMs undergo cellular proliferation. We used the cell tracer PKH26 to address the first two possibilities. PKH26 is readily taken up by phagocytic cells and can be used to mark resident macrophages. Any PKH26-stained (PKH^{+}) cells detected at the end of the study must have been present at the time of PKH26 injection. In contrast, an increase in PKH26-negative (PKH^{-}) cells represents monocyte-derived macrophages recruited after the time of PKH26 injection. Reciprocal changes in counts of PKH^{+} MFe^{hi} or MFe^{lo} ATMs could indicate a shift between the two populations. We combined PKH26-mediated cell tracing with the 1-week iron injection model to understand whether changes in the ATM cell counts were due to shifts in iron-containing populations or due to monocyte recruitment. At 1 week post iron-injection, 78% of all macrophages were PKH^{+}. The count of resident PKH^{+} MFe^{lo} ATMs decreased by 7.1×10^{4} cells/gram tissue and PKH^{+} MFe^{hi} ATMs increased by 1.1×10^{5} cells per gram tissue (Fig. 3.8A). This shift accounted for 83% of the total difference in MFe^{hi} (Fig. 3.5C). Of the recruited PKH^{-} ATMs, there was no difference in MFe^{lo} ATMs. Interestingly, almost no MFe^{hi} macrophages were recruited in the absence of iron injection; however, 2.0×10^{4} PKH^{-} MFe^{hi} ATMs/gram tissue were recruited upon iron injection (Fig. 3.8B, $p<0.01$). Based on these results, monocyte recruitment accounts for 17% of the increase in MFe^{hi} in response to iron injections. Thus, our PKH studies reveal that shifts in ATM populations from MFe^{lo} to MFe^{hi} ATMs and monocyte recruitment fully account for the increase in MFe^{hi} following iron injection.

Iron uptake by ATMs is associated with M2-polarization

MFe^{lo} incorporation into the ferromagnetic fraction accounts for the majority of the increase in MFe^{hi} population following iron injection. Because the MFe^{lo} have reduced M2-like phenotype compared to MFe^{hi}, we hypothesized that their incorporation into the MFe^{hi} pool would shift the overall polarization state of the MFe^{hi} population to lower relative expression of M2-associated proteins. However, the opposite was true; in iron-injected mice, the MFe^{hi} ATMs had a decrease in cells positive for inflammation-associated surface markers (CCR2*,* CD11c) and an increased in cells with M2-associated marker*,* CD206 (Fig. 3.8E). In contrast, there was a decrease in the count of MFe^{lo} ATMs positive for CCR2 and CD11c, and no change in CD206 (Fig. 3.8C-E). The findings indicate that iron uptake does not drive an inflammatory profile in macrophages MFe^{hi} cells, while it does in MFe^{lo}. Thus, even with MFe^{lo} incorporation into the MFe^{hi} population, the MFe^{hi} profile is even more M2-like post iron-injection.

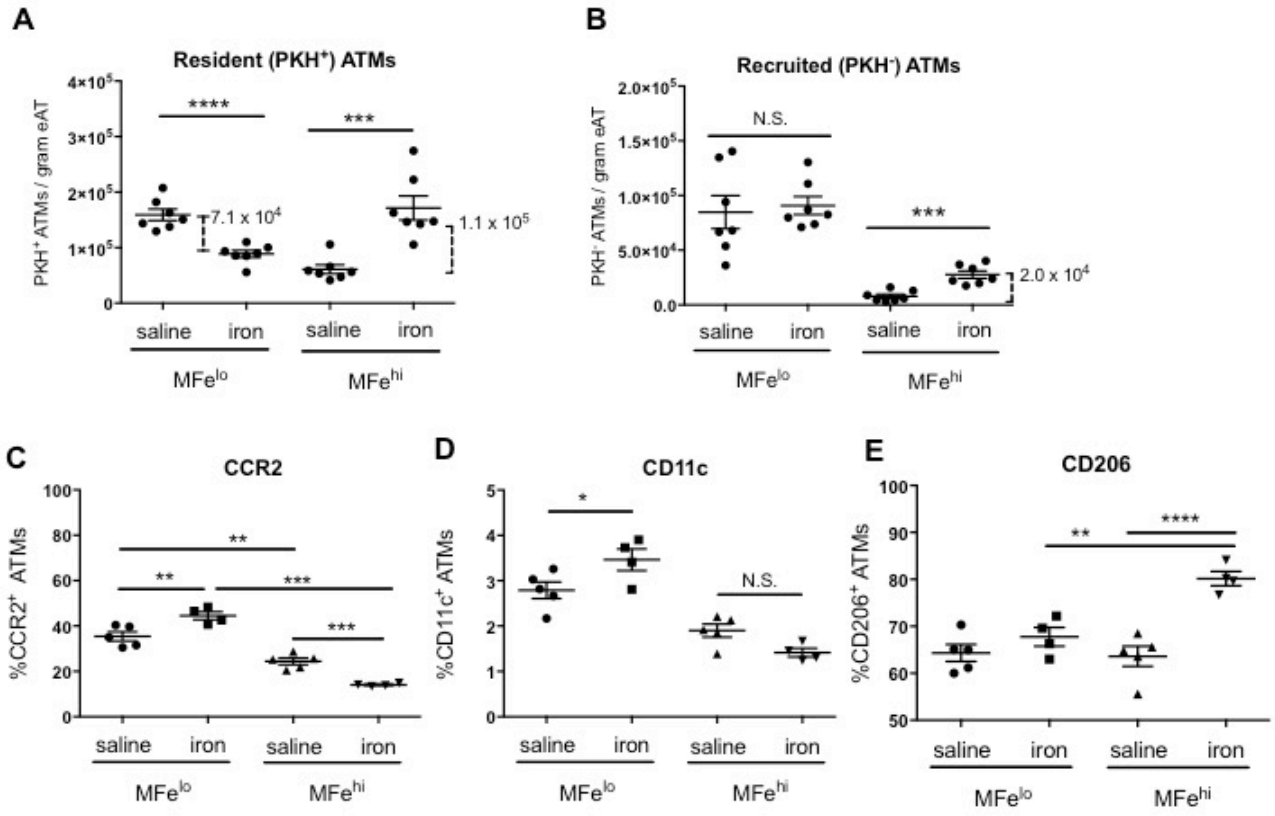

Figure 3.8. Effect of iron injection on ATM inflammatory markers and recruitment. ATMs were marked with PKH26 prior to iron injection to assess for population shifts as quantified by the (A) resident PKH^+ ATMs, and monocyte recruitment as quantified by (B) PKH^- ATMs (N=7). MFe^{hi} and MFe^{lo} polarization response to iron injection was quantified by cell surface inflammatory markers, including M1-associated (C) CCR2 and (D) CD11c, as well as M2-associated (E) CD206 (N=4-6). For all studies, significant differences were identified using ANOVA and t-test, with the following p-value indicators: *p<0.05, **p<0.01, ***p<0.001, ****p<0.0001.

Discussion

Reflecting the field's current interest in macrophage polarization and iron handling by tissue-associated macrophages, we challenged MFe^{hi} ATMs with excess iron to investigate their functional role in maintaining AT iron levels. We approached this by supplying iron through a dietary route as well as direct IP injection. Dietary iron provision has commonly been used in other studies, often over a course of 8 weeks, and with non-heme sources of iron, because mice cannot absorb heme iron[121]. While systemic iron loading does occur consistently in dietary iron studies, the metabolic impact has been variable. McClain *et al*. provided high-, normal- and low-iron diets (20,000 mg/kg, 330 mg/kg, and 7 mg/kg carbonyl iron, respectively) to C57BL/6 mice for 8 weeks and observed a 40% decrease in *Tfrc* in adipocytes, 30% decrease in *Adipoq,* and an overall decrease in fat mass and increase in lean mass. These changes were associated with increased oxygen consumption by high-iron diet mice, and were adiponectin-dependent. However, in our studies, we so no impact of dietary iron on body weight or fat mass. We also noted no impact on glucose tolerance or difference in adipocyte gene expression. The most likely explanation for this difference is that our high-iron diet model had 10-fold lower iron than the McClain study. To confirm iron loading, we quantified serum iron and Tf saturation. The increased iron levels were supported by the increased iron content in MFe^{hi} ATMs themselves. We recognized that the adipocyte iron content had high variability. This may be due to the need to standardize the iron quantification to cellular protein. Furthermore, variability in adipocyte iron content appears to be a common finding in this type of study[84]. A second concern with this technique is the possibility that high-iron adipocytes are lost during the

adipocyte collection process, selecting for adipocytes that are not iron loaded. However, at this time, there are no alternative methodologies for collecting adipocytes. Even given these limitations, our studies highlight the fact that MFe^{hi} macrophages in AT appear to serve as an iron-sink during chronic iron exposure.

We were interested in the proof-of-concept that MFe^{hi} ATMs accommodate for excess iron. Therefore, we gave iron-dextran at supra-physiological doses. Even as a model of excess iron, iron-dextran injection is medically relevant, as both iron-dextran and superparmagnetic iron oxide nanoparticles have been commonly used in humans to treat anemia, and interestingly, accumulate in AT[122, 123]. Iron-dextran is processed in a similar manner to hemoglobin iron, and has not been associated with cardiac dysfunction in C57BL/6 mice, presumably because they are able to excrete some of the excess iron in the feces[124]. The type of iron processed by macrophages also influences their phenotype and could explain some of the contradictions between studies describing “iron-cycling” macrophages *in vitro* and *in vivo*. In tissues closely associated with the reticular system such as spleen, vasculature, and muscle, heme-associated iron is abundantly recycled by macrophages. Heme uptake liberates ferrous iron, and M2 macrophages respond by enhancing their oxidative stress pathways, Hmox1, and Fpn[125]. In fact, $CD163^{hi}$ macrophages (Mhem) have been described as being protected from oxidative stress and less prone to lipid accumulation[126]. In these systems, the recycling of iron from heme can be provisional to red blood cell production or wound healing and the degradation process is inherently anti-inflammatory. However, most *in vitro* studies of macrophage iron handling have been performed with sources of ferric iron or Tf-bound iron. AT is known to have very low levels of hemolysis. Therefore, we

postulated that Tf-bound iron is the primary source of iron for macrophages - whether from serum or adjacent cells - but this area warrants further analysis.

Macrophages have been coopted by many tissues to perform homeostatic functions outside of their typical immunological role. What is especially unique about these functions is that they allow for fine-tuned hemostatic regulation in tissues, often uncoupled from systemic physiology. For example, Corna *et al.* used a macrophage-specific Fpn1-knockdown model in muscle damage[115]. Even though the macrophages became iron-loaded, they still accumulated at the site of damage and did not become oxidatively stressed. Importantly, in this model of impaired macrophage iron export, myofiber regeneration was limited[115]. Furthermore, changes in expression levels of iron-associated genes in the muscle were not associated with changes in systemic iron homeostasis, indicating that there was an independent micro-environmental homeostasis between the tissue and resident macrophages. Similarly, in human atherosclerotic plaques, M2 macrophages process the iron released from hemolysis[90]. Our results indicate that ATMs respond to excess iron, preventing iron overload in adipocytes. Even though adipocytes had increased expression of *Slc40a1*, the gene for the iron exporter Fpn1, and trends in *Fth*/*Ftl*, they had no increase in intracellular iron or inflammatory markers. So, even if the adipocytes did uptake iron, they were able to release this iron, likely to be taken up by MFe^{hi}. Interestingly, with acute iron injection the MFe^{hi} had an M2-like iron cycling phenotype (i.e. increased *Tfrc*, *Slc40a1*) (Fig. 3.6), whereas, in the chronic iron diet studies, MFe^{hi} mainly had increased expression of M1-like iron-storage genes *Fth1/Ftl1* (Fig. 3.3). However, in both contexts, MFe^{hi} ATMs

accrued higher levels of iron. This may indicate a temporality to the response of these ATMs to take up and store iron effectively.

The functional adaptability of macrophages has been linked to their phenotypic flexibility. Generally, the polarization state of macrophages is associated with different responses to iron – M1 macrophages dogmatically sequester iron as a bacteriostatic mechanism, and M2 macrophages take up and release iron quickly. Studies have demonstrated that iron handling by macrophages can be impacted simply by altering their polarization stimuli[96, 97]. However, there is a complex and reciprocal relationship between the phenotype of macrophages and their response to iron. For example, when macrophages are iron-loaded due to Fpn1 deficiency, they respond to inflammatory stimulation with increased inflammatory cytokine expression[127]. This effect is iron-dependent, as it can be ameliorated in the presence of an iron chelator[127]. In contrast, iron-loaded M2-polarized macrophages have high expression of iron uptake and iron export genes, even in the presence of excess iron[96]. The shift in iron handling gene expression can be tied back to a change in the binding of IRPs in response to iron levels[113]. In human M2-polarized macrophages, simply chelating intracellular iron can shift M2 macrophages from an iron-cycling phenotype (higher import/export genes) to an iron-storage phenotype (higher *Ft*)[120].

Some of these differences are also seen *in vivo.* For example*,* the M2-polarized macrophages seen in atherosclerotic plaques have an iron-cycling profile, and they are quick to release iron rather than accrue it[90]. The “iron-cycling” phenotype has been shown to play an important role in certain tissues because the macrophages can take up and release iron as needed. Considering these findings, it is surprising that the iron-

storing MFe^{hi} ATM population is not only very strongly M2-polarized, but also maintains this polarization even while accumulating iron. We noted that MFe^{hi} ATMs were able to take up and sequester the excess iron provided through diet or injection, in line with the macrophage response in muscle damage, in which Fpn knockout macrophages load iron, even without oxidative stress[115]. In fact, the M2 macrophage phenotype in tissues may be more complex than the stereotypical iron-handling dichotomy described for M1 and M2. We observed an increase in *Fth* in response to iron injection, reflecting a protective response by MFe^{hi} ATMs. Furthermore, even with iron loading, MFe^{hi} ATMs did not take on a more inflammatory profile. This contrasts studies in liver and alveolar macrophages, where iron loading of macrophages is associated with increased inflammation [128].

Indeed, comparing resident macrophages from different tissues highlights the adaptability and specification of macrophages. Our understanding of the iron-cycling phenotype of the MFe^{hi} ATMs is limited by our inability to assess iron-related proteins specifically in these cells due to their low numbers. This restricts us to the use of flow cytometry and gene expression to assess the phenotype of the cells, rather than Western blot. In future studies, it would be ideal to develop a method for assessing iron-response protein levels because a cell's iron response is primarily driven through the iron-response protein system, such that levels of these proteins is the most sensitive and accurate way of determining the iron status of a cell. Despite this limitation, the observation that MFe^{hi} take up excess iron and yet remain M2 polarized suggests a specialized function for this unique cell population.

Following iron injection, there was an increase in MFe^{hi} per gram of tissue, with a reciprocal decrease in MFe^{lo}. Increased MFe^{hi} were also observed with iron diets, but the effect was more subtle. In fact, PKH26 staining of resident macrophages allowed us to deduce that the enlarged MFe^{hi} population was likely due to MFe^{lo} cell "conversion" to MFe^{hi}. The MFe^{hi} population is defined by positive magnetic sorting, but relative to MFe^{lo}, MFe^{hi} were also found to have extreme M2-polarization by gene expression and flow cytometry[71]. With more cells adhering to the magnet, we cannot conclude if the uptake of iron by MFe^{lo} represents a conversion in ATM subtypes, or simply acquired paramagnetic qualities of MFe^{lo} who have taken up excess iron.

There are no known methods that would allow us to trace MFe^{hi} versus MFe^{lo}. However, we would predict that if the MFe^{hi} population became enriched with MFe^{lo}, the average polarization profile would shift away from the extreme M2-polarization. MFe^{hi} are on average more M2-polarized with iron uptake – even with newly incorporated MFe^{lo} cells. This suggests that the MFe^{lo} cells incorporated into the MFe^{hi} pool are not simply paramagnetic but may be changing their actual phenotype and function. This contradicts other studies that show inflammatory polarization of macrophages with iron treatment. Therefore, we hypothesize that a unique conversion of macrophages may be occurring with excess iron in adipose tissue. Interestingly, we noted an increase in the expression of the developmental transcription factor *Spic* in MFe^{hi} in our iron diet studies. This may demonstrate a mechanism by which either MFe^{lo} ATMs or recruited monocytes are converting to the MFe^{hi} phenotype.

Our studies further explore a role for a subtype of ATMs in taking up and processing iron to protect adipocytes from iron overload. Using dietary and IP iron

overload we demonstrated that MFe^{hi} ATMs are able to fully compensate for excess iron in the AT. As part of this response, the MFe^{hi} pool expands to include iron-loaded MFe^{lo} that have shifted to a stronger M2-phenotype. Furthermore, circulating monocytes are also recruited to the MFe^{hi} pool. These findings expand our understanding of iron-handling by macrophages beyond the classic M1/M2 paradigm. In conjunction with other studies in the field, this further demonstrates the importance of fine-tuned iron regulation for adipocytes, and the intimate homeostatic relationship between macrophages and adipocytes. It is thought that iron release by M2 macrophages allows for cellular proliferation. For example, in co-culture studies, media from human M2-polarized cells supported cancerous growth, and this effect was reversible with iron chelation[97]. Similarly, studies have shown that iron is necessary for adipogenesis[77]. Therefore, future studies in this area will look at the interaction of resident macrophages in AT and their role in iron homeostasis in the context of adipogenesis.

CHAPTER IV

MFe^{hi} IRON HANDLING AND THE DIET-INDUCED OBESITY MODEL

Introduction

Feeding HFD to C57BL/6J mice is a common and useful model of obesity because the mice respond to the excess dietary fat with weight gain, hyperinsulinemia, hyperglycemia, and hypertension[129]. Hyperglycemia occurs within four weeks of HFD, and adipocyte hypertrophy and hyperplasia continue up to 16 weeks of diet[28]. Strissel *et al.* studied AT over a course of 20 weeks in C57BL/6J mice on 60% HFD. They noted that adipocyte death correlated with AT expansion and M1-like polarization of ATMs, in conjunction with matrix deposition and adiponeogenesis[28]. Considering that adipogenesis is also a time of high iron-need by adipocytes, it is of interest to understand how MFe^{hi} macrophages may be playing a role in the timing of AT remodeling. In Strissel's paper, AT remodeling at 18 weeks of HFD in C57BL/6J mice occurred only in eAT, not subcutaneous AT (Fig. 4.1). While adipocyte death increased progressively up to 20% at 14 weeks of diet, at 16 weeks, dying adipocytes jumped up to nearly 80%, then dropped down to 20% again at 20 weeks of diet[28] (Fig. 4.1A). Furthermore, the loss of eAT mass starting at 16 weeks of diet was associated with an increase in liver hepatosteatosis[28]. Others in the field have postulated a connection between hepatic iron and lipid metabolism[130]. For example, iron deficiency in rats was associated with increased hepatic triglyceride (TG) accumulation[131]. While lipid storage

changes over time on HFD in AT and liver, no studies have been conducted to associate the lipid storage over time with iron content in both of these tissues.

Just as macrophages have homeostatic functions in lean AT, they play an important role in AT remodeling in obesity. In obesity, ATMs are found around necrotic adipocytes in formations called crown-like structures, forming a syncytia that develops into a multinucleated giant cells, a classic indication of chronic inflammation[27].

Considering the impact of obesity on nearly every aspect of AT function, it is natural to suspect that the ferrostatic function of MFe^{hi} ATMs, described in Chapter III, may be impacted by obesity. Changes in iron handling by ATMs in obesity would be especially significant in relation to DIOS. DIOS is based on studies in humans correlating high ferritin levels, a marker for iron load, with metabolic syndrome[47]. Considering that adipocytes are already oxidatively stressed with excess lipids in obesity, altered iron availability could have an additive detrimental effect on adipocytes. This was evident in the adipocyte-specific iron overload model in mice, that led to systemic metabolic dysfunction, due to reduced adiponectin release[17].

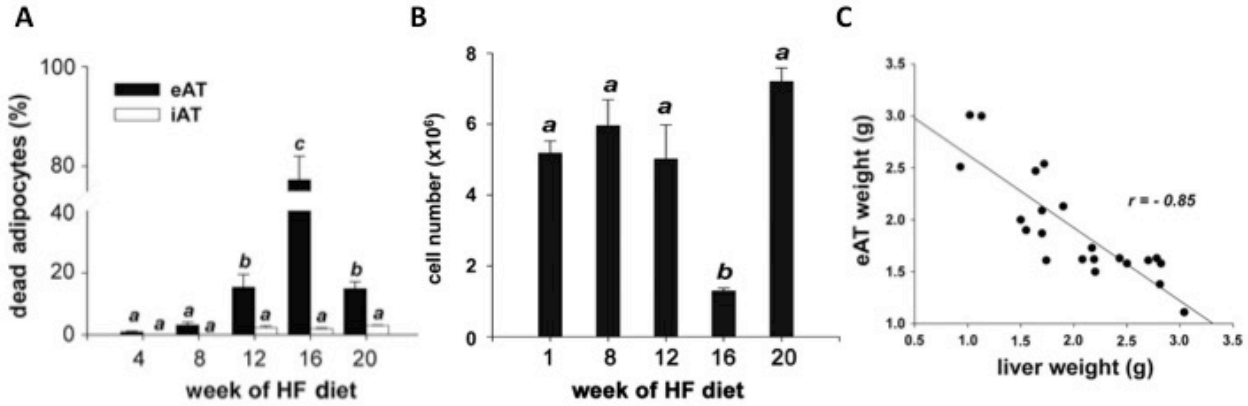

Figure 4.1. [**Adapted from Strissel *et al.* 2007**[28]] **Adipose tissue remodeling over 20 weeks of HFD in C57BL/6J mice**. (**A**) Dead adipocytes in visceral AT (eAT) and subcutaneous AT (iAT). (**B**) Adipocyte cell numbers over 1-20 weeks of HFD. (**C**) There exists an inverse correlation between eAT weight and liver weight.

Adipocytes have a four-fold increase in adipocyte iron content in 16 week HFD-induced obese mice[71] (Fig. 4.2A). In contrast, in the liver, there is a 50% reduction in iron. Adipocytes also had altered gene expression that corresponded with iron-storage: decreased *Tfrc*, increased *Hmox1, Fth1, Ftl1*, and a trend toward decreased *Slc40a1*, in conjunction with decreased *Adipoq* (adiponectin) expression (Fig. 4.2C). In contrast to adipocytes, MFe^{hi} ATMs had reduced intracellular iron content in obesity. Their gene expression profile was more reminiscent of a M1-like macrophage, with higher levels of Ft, and decreased iron-uptake and release genes (Fig. 4.2). Orr *et al*. also demonstrated that monocytes recruited during HFD-induced obesity were incorporated into the MFe^{lo} population, and the MFe^{hi} population remained the same size[71].

The observed changes in tissue iron in response to diet-induced obesity aligns with the theory of DIOS in humans. Furthermore, alterations in MFe^{hi} iron suggest that MFe^{hi} function may be impaired in obesity, which could underlie the observed increases in adipocyte iron. To address this hypothesis, we applied the same IP iron injection model as in Chapter III, but in diet-induced obese mice. The combination of iron injections and obesity allowed us to probe the ability of MFe^{hi} ATMs to compensate for excess iron in the inflammatory state of obesity.

Specifically, we hypothesized that obesity would impair iron uptake by MFe^{hi} ATMs, thereby leading to adipocyte iron loading and reduced adiponectin expression. We explored possible mechanisms underlying this effect, including arginine metabolism and oxidative stress. Studies from our lab have shown that some of the major metabolite profiles differentiating MFe^{hi} from MFe^{lo} could be traced back to the arginine metabolism pathway (Fig. 4.3). Therefore, when considering the impact of HFD-

associated inflammation on MFe^{hi} ATMs, arginine metabolism is of particular interest. Arginine catabolism has been shown to play a defining role in M1/M2 polarization of macrophages in general[132]. Under Th1 stimulation, arginine is metabolized by inducible nitric oxide synthase (Nos2) to make nitric oxide (NO). Under Th2 stimulation, arginine is metabolized by arginase to make urea and ornithine. This system is regulated by arginine availability through the cationic amino acid transporter (CAT2). Furthermore, arginine deficiency in either context could lead to production of superoxide radicals, which would be an especially potent oxidative stressor in the presence of iron[133, 134].

Oxidative stress is thought to play a role in macrophage polarization in obesity[135, 136]. Furthermore, inappropriate iron handling by cells can lead to oxidative damage. This motivated us to explore markers for antioxidant response in MFe^{hi} and MFe^{lo} in response to diet and iron injections. Nrf2 (*Nfe2l2*) is a transcription factor that regulates the expression of many antioxidant proteins[137]. In its inactive form, it stays in the cytoplasm, bound by Keap1 (*Keap1*), and its levels are regulated by ubiquitination and degradation[138]. Therefore, while gene expression levels of *Nfe2l2* may not reflect the oxidative state of a cell, *Keap1* levels can reflect regulation of the cell's antioxidant response[137].

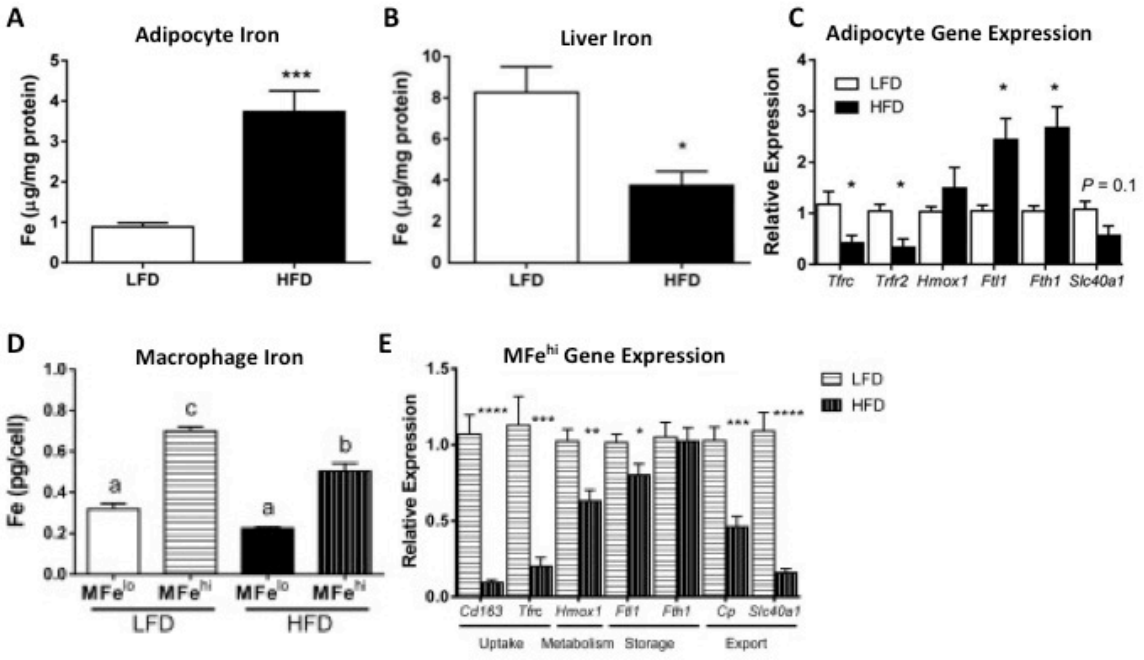

Figure 4.2. **[Adapted from Orr *et al*. 2013[73]] Adipocyte liver and ATM response to 16 weeks of HFD.** (A) Adipocyte iron content was quantified with AAS. (B) Liver iron content quantified by AAS. (C) Adipocyte iron-handling gene expression, from LFD-fed and HFD-fed mice. (D) Iron quantified by ICP-MS in ATMs from lean and obese mice. (E) Iron-handling gene expression in MFe^{hi} from lean or obese mice. *p<0.05, **p<0.01, ***p<0.001, ****p<0.0001

A

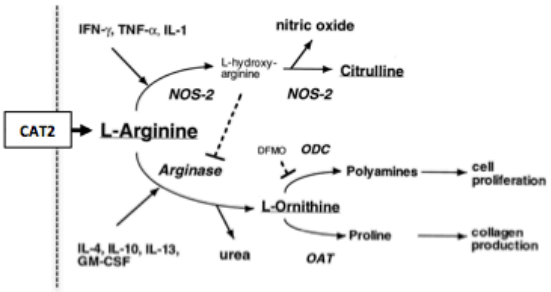

B

		RATIO: MFelo / MFehi				RATIO: HFD/LFD			
		LFD		HFD		MFelo		MFehi	
Pathway	Biochemical	ratio	p-value	ratio	p-value	ratio	p-value	ratio	p-value
Arginine metabolism	arginine	6.59	0.76	0.16	0.02	0.09	0.2	3.8	0.1
	urea	0.83	0.66	0.03	0.0003	0.19	0.04	5.31	0.03
	proline	1.33	0.97	0.15	.0.1	0.37	0.18	3.49	0.03
	dimethylarginine	1.07	0.59	0.08	0.001	0.29	0.33	3.78	0.02

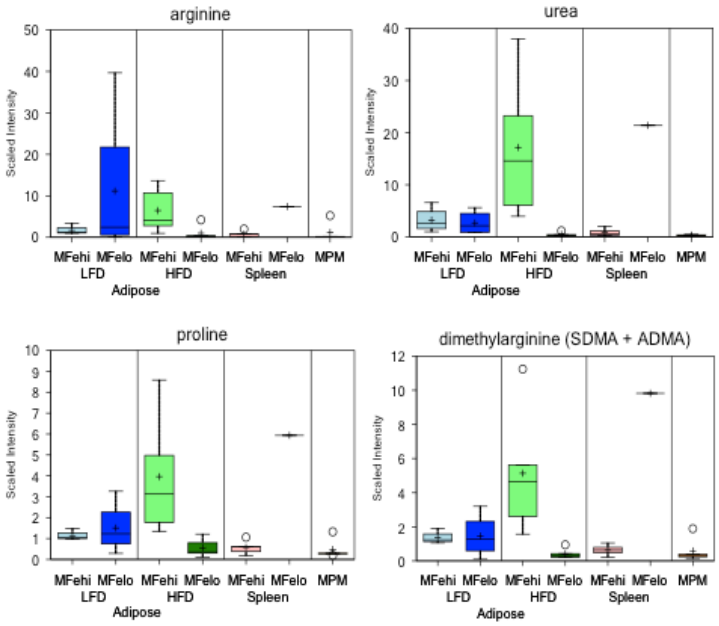

Figure 4.3. **Arginine catabolism in the context of MFe^{hi} and MFe^{lo}.** (**A**) [Adapted from Hesse *et al.* 2001[1]] Schematic of Th1 and Th2 stimuli impacting arginine catabolism pathways, (**B**) Model of hypothesized arginase metabolism between MFe^{lo} and MFe^{hi}, based on results of (**C**) metabolomics studies comparing MFe^{lo} and MFe^{hi} from lean and obese mice, as well as high- and low-iron cells from the spleen.

In the following studies we aimed to understand the impact of obesity on iron-handling by MFe^{hi} ATMs. We found that obesity does not impact the ability of MFe^{hi} to take up iron, but the "iron-cycling" phenotype is blunted. We also – unexpectedly – observed no increase in adipocyte iron content in obesity. This lead to further set of studies investigating the time course of AT and liver lipid and iron storage over 20 weeks of HFD. However, no significant differences were observed. Even with unexpected results in these specific studies, the methodologies outlined in the following studies set the stage for further evaluation of MFe^{hi} function in obese AT.

Results

Iron is taken up by MFe^{hi} in obesity

C57BL/6J mice were placed on 10% LFD or 60% HFD for 16 weeks, with a final weight difference of 20g (Fig. 4.4). One week prior to sacrifice, both groups were split in a weight-matched subgroups and injected once with iron-dextran.

AT sections stained with Prussian blue demonstrate iron uptake in cells intercalated between adipocytes, in both diet groups (Fig. 4.5A). The SVF was extracted and, following magnetic sorting, MFe^{hi} and MFe^{lo} were sorted out using macrophage markers by FACS. The MFe^{lo} population increased in cell count (Fig. 4.5B $p<0.01$). This response could be tied to the known obesity-associated influx of monocytes. As previously described by Orr *et al*, all recruited monocytes in obesity were MFe^{lo}, and there was no increase in MFe^{hi} ATMs in response to obesity[71]. Comparing saline to iron groups in both HFD and LFD, there was an upward trend in MFe^{hi} in response to iron injections, as had also been seen in chow iron-injection studies (Fig. 3.5A)[112]. Mass spectrometry quantification of whole tissue showed that, in obesity, total ATMs only had 1/3 as much iron per cell in response to the iron injection (Fig. 4.5C, $p<0.0001$). The change in macrophage iron was parsed out by sorting MFe^{hi} and MFe^{lo}. Unexpectedly, MFe^{hi} from obese AT appeared to take up the same amount of intracellular iron in HFD as in LFD mice (Fig. 4.5 D, $p<0.0001$). This effect was further confirmed by calculating the total iron in all MFe^{hi} and MFe^{lo}, multiplying total cells by iron content per cell. Again, there was no change in the total MFe^{hi} iron pool (Fig. 4.5E). While there was an increase in iron in the MFe^{lo} ATM pool in HFD mice, this increase was driven only by increased cell counts (Fig. 4.5E, $p<0.0001$).

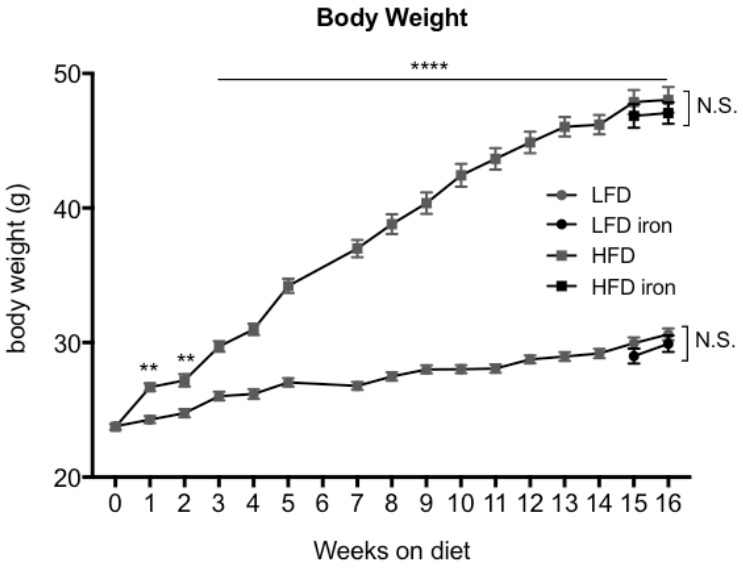

Figure 4.4. **Body weight of C57BL/6J mice over 16 weeks of diet**. At 1 week prior to sacrifice, weight-matched groups were separated for iron injection sub-groups. Significant differences were identified using ANOVA and t-test, with the following p-value indicator: ****p<0.0001.

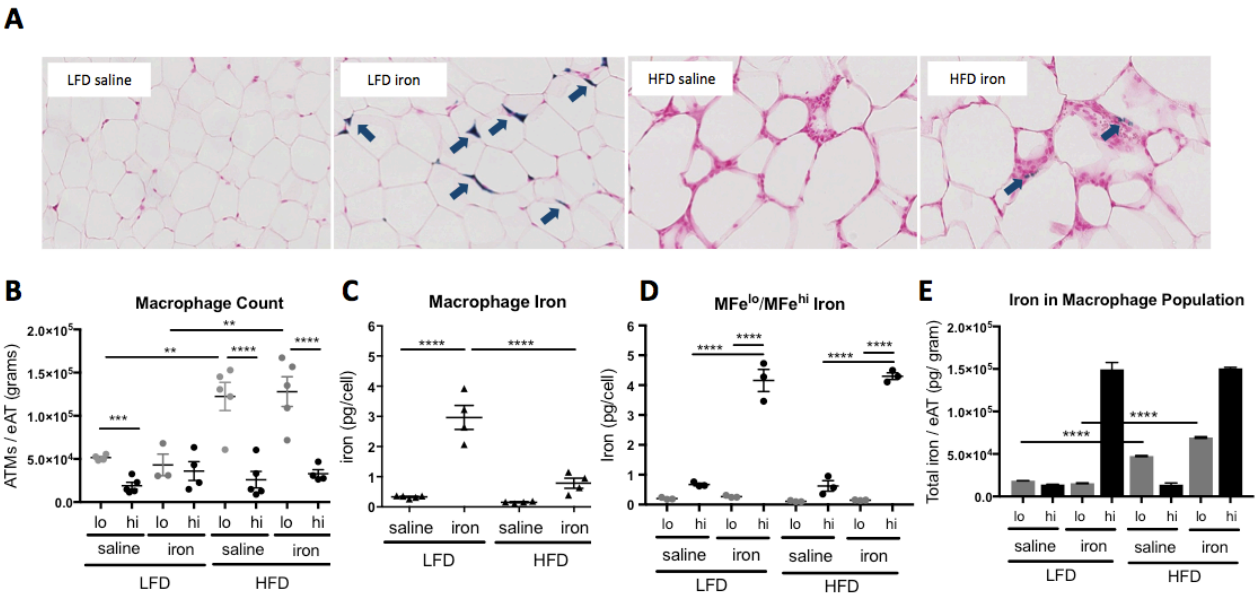

Figure 4.5. **Effect of obesity on iron uptake by ATMs.** C57BL/6J mice on 16 weeks of LFD or HFD were given a IP injection of 5mg/kg iron-100 1 week prior to sacrifice. (A) Whole AT was fixed and sectioned, then stained with Prussian blue to visualize iron and counter-stained with nuclear red. Cells were sorted in order to quantify (B) ATMs per gram of tissue (N=3-5), (C) iron content per ATM (N=4-5), and (D) iron content in MFe^{lo} and MFe^{hi} (N=3-5). (E) Total population iron was calculated by multiplying the iron/cell in each cell type by the total cell counts. For all studies, significant differences were identified using ANOVA and t-test, with the following p-value indicators: **p<0.01, ***p<0.001 ***p<0.0001.

Obesity ameliorates the MFe^{hi} genetic response to iron uptake

Macrophages respond to altered iron availability through IRPs that directly impact transcription of iron-related genes. Therefore, gene expression of iron-related genes is one way to investigate a macrophage's iron state. Sorted MFe^{hi} and MFe^{lo} were collected to determine their response to iron injections, specifically to compare LFD and HFD. As in the previous study, there were 4 study groups: LFD with saline or iron injection, and HFD with saline or iron injection. The observed increases in iron-associated gene expression comparing MFe^{hi} to MFe^{lo} in saline groups were reminiscent of the iron-cycling phenotype, as previously described[71] (Fig. 4.6A - F) MFe^{hi} from LFD-fed mice also responded to iron injections just like MFe^{hi} from chow mice; there was a significant decrease in expression of *Tfrc* and increased expression of *Hmox, Fth1, Ftl1,* and *Slc40a1* (Fig. 3.6, Fig. 4.6A - F). Of particular interest to this study, when comparing these same iron-handling genes in the HFD mice, all significant differences were lost (Fig. 4.6A - F). Lastly, while MFe^{hi} had higher levels of *Spic* in control groups, this difference was lost following both iron injection and HFD treatments (Fig. 4.6G).

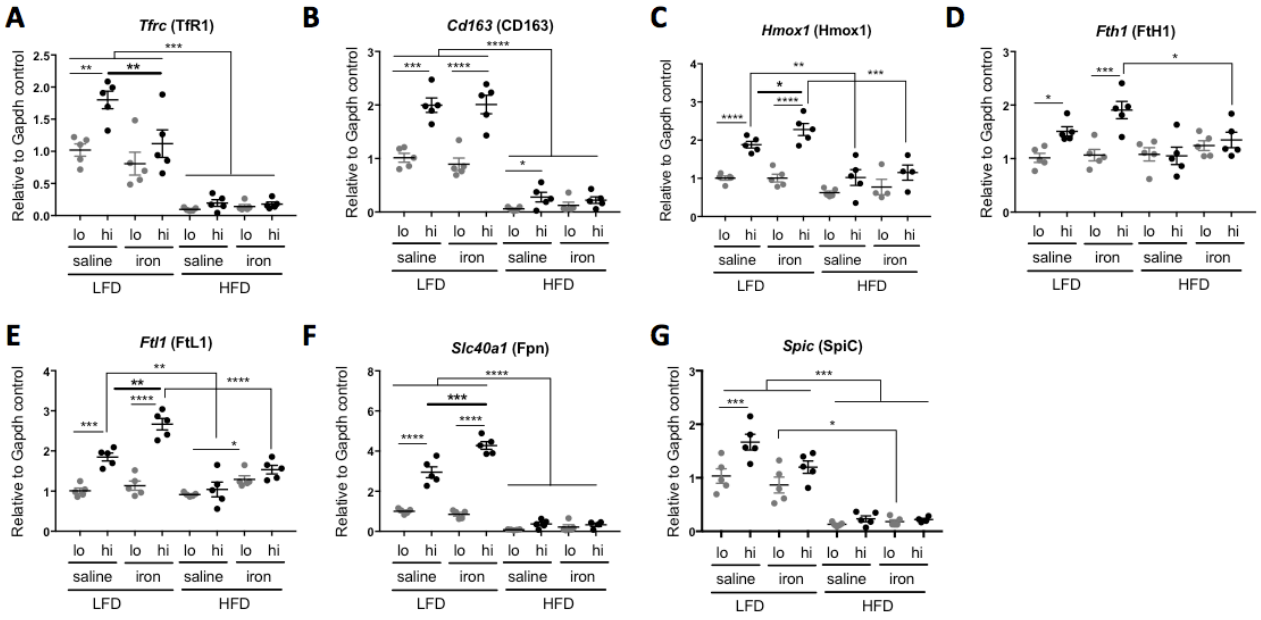

Fig. 4.6 Effect of iron injection on ATM expression of iron-handling genes. C57BL/6J mice on 16 weeks of LFD or HFD were given a IP injection of 5mg/kg iron-100 1 week prior to sacrifice. Iron-handling genes were quantified by RT-PCR for MFe^{lo} and MFe^{hi} ATMs (N=5). For all studies, significant differences were identified using ANOVA and t-test, with the following p-value indicators: *p<0.05, **p<0.01, ***p<0.001, ***p<0.0001.

Polarization, oxidative stress, and arginase metabolism responses to iron injection and HFD

Baseline differences in the M1-marker *Itgax* (CD11c) and M2-marker *Retnla* were observed between MFe^{lo} and MFe^{hi} in lean mice (Fig. 4.7A & B), in agreement with previously described polarization differences between the cell types (Fig. 1.3C). In response to HFD, *Itgax* transcript levels increased in all groups, and *Retnla* decreased (Fig. 4.7A & B). This inflammatory response to HFD was not unexpected, and reflects the M1-skewing of MFe^{hi} in obesity, as well as the influx of M1 ATMs to the MFe^{lo} population in obesity[71]. In these studies, there was no M2-skewing of MFe^{hi}, previously observed as a response to iron injection (Fig. 3.8C - E). HFD nearly ameliorated significant differences in polarization between MFe^{hi} and MFe^{lo}.

Nrf2 (*Nfe2l2*) is a master regulator of the antioxidant response, and it is rendered nonfunctional by Keap1 (*Keap1*). In ATMs, we observed an increase in *Nfe2l2* and *Keap1* in MFe^{hi} compared to MFe^{lo}, although these differences were lost on HFD (Fig. 4.7C & D). In general, HFD lead to an upward trend in *Nfe2l2*, and a significant reduction in *Keap1* in all groups (Fig. 4.7C & D). Excess iron did not appear to impact either gene (Fig. 4.7C & D).

Upregulation of arginase (*Arg1*) is linked to M2-polarization and reduced production of ROS (Fig. 4.3A). There were no significant differences in the gene expression for the arginase-uptake protein, *Slc7a2* (CAT2), except in MFe^{lo} with HFD (Fig. 4.7E). Even though MFe^{hi} are more M2-polarized, in lean mice, *Arg1* was decreased in MFe^{hi} relative to MFe^{lo} (Fig. 4.7F) This difference was lost in HFD, as MFe^{lo} reduced their expression of *Arg1*. iNOS (*Nos2*) is the enzymatic competitor to

arginase in arginine catabolism. In lean mice, *Nos2* was upregulated in MFe^{hi} relative to MFe^{lo} (Fig. 4.7G). While this is unexpected considering strong M2-polarization of MFe^{hi}, it corresponds with reduced *Arg1* expression in this cell. However, with iron injections, MFe^{hi} demonstrated both low *Arg1* and *Nos2*, while maintaining *Slc7a2*. This occurred in MFe^{hi} of both saline and iron-injected mice on HFD.

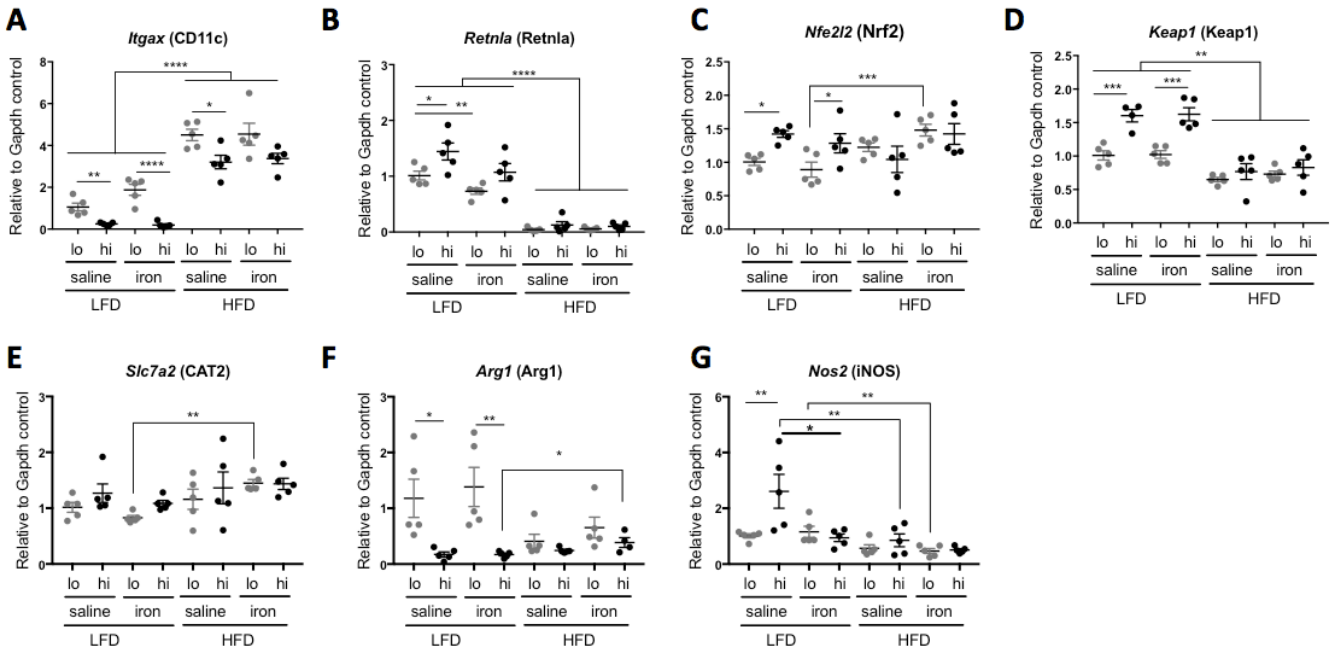

Figure 4.7. **Effect of iron injection on ATM polarization and inflammation genes.** C57BL/6J mice on 16 weeks of LFD or HFD were given a IP injection of 5mg/kg iron-100 1 week prior to sacrifice. Iron-handling genes were quantified by RT-PCR for MFe^{lo} and MFe^{hi} ATMs (N=5). Genes of interest can be grouped into (A,B) Polarization-associated genes, (C,D) antioxidant-pathway regulatory genes, and (E-G) arginase catabolism pathway genes. For all studies, significant differences were identified using ANOVA and t-test, with the following p-value indicators: *p<0.05, **p<0.01, ***p<0.001, ***p<0.0001.

Adipocyte response to iron injection in HFD

Previous studies demonstrated that in obesity MFe^{hi} had decreased iron content and adipocytes had a four-fold increase in iron (Fig. 4.2A). However, in these studies, we observed no significant changes in iron content in adipocytes in obese mice (Fig. 4.8A). Furthermore, we observed an increase in iron content in the liver in response to iron injections in LFD, but no difference in iron content between LFD and HFD (Fig. 4.8B).

Looking at adipocyte gene expression, there was no response in *Tfrc* in HFD, or iron injections (Fig. 4.9A). This correlates with unaltered cellular iron content (Fig. 4.9A). However, there was a significant increase in *Hmox1* in HFD (Fig. 4.9B), a previously described trend (Fig. 4.2C). Unchanged *Ftl1* and decreased *Fth1* (Fig. 4.9C & D) also contradicted the very significant increase in *Fth1* and *Ftl1* observed in previous studies in HFD (Fig. 4.2C). Again, these findings would correspond with low adipocyte iron storage. The other very significant responses seen in these studies were in *Slc40a1*, the iron-exporter Fpn (Fig. 4.9E), contrasting the downward trend previously described (Fig. 4.2C). While *Tnfa* and *Adipoq* responded to the HFD stimulus as would be expected in obese mice, their expression was not impacted by excess iron (Fig. 4.9G & H).

In general, these adipocyte results did not align with the premise of our studies and spurred further inquiry into adipocyte and liver iron content over the course of HFD studies. These studies are detailed in the next sections.

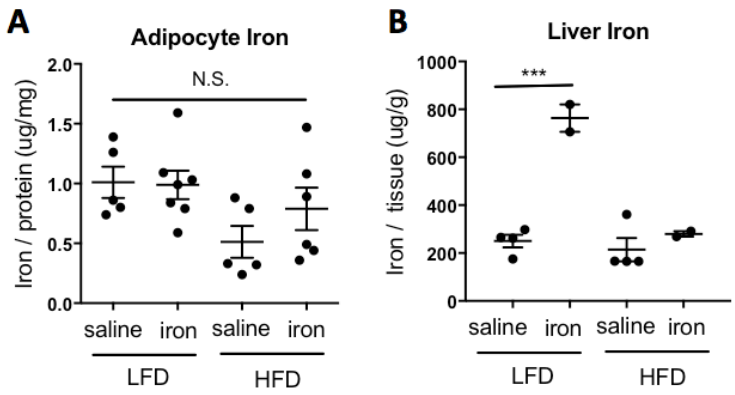

Figure 4.8. **Tissue iron content after iron injections in HFD-fed obesity model**. C57BL/6J mice on 16 weeks of LFD or HFD were given a IP injection of 5mg/kg iron-100 1 week prior to sacrifice. Tissue iron content was quantified by atomic absorption spectrometry in (**A**) adipocytes, standardized to protein concentration, and (**B**) liver, standardized to tissue weight. For all studies, significant differences were identified using ANOVA and t-test, with the following p-value indicator: ***p<0.001

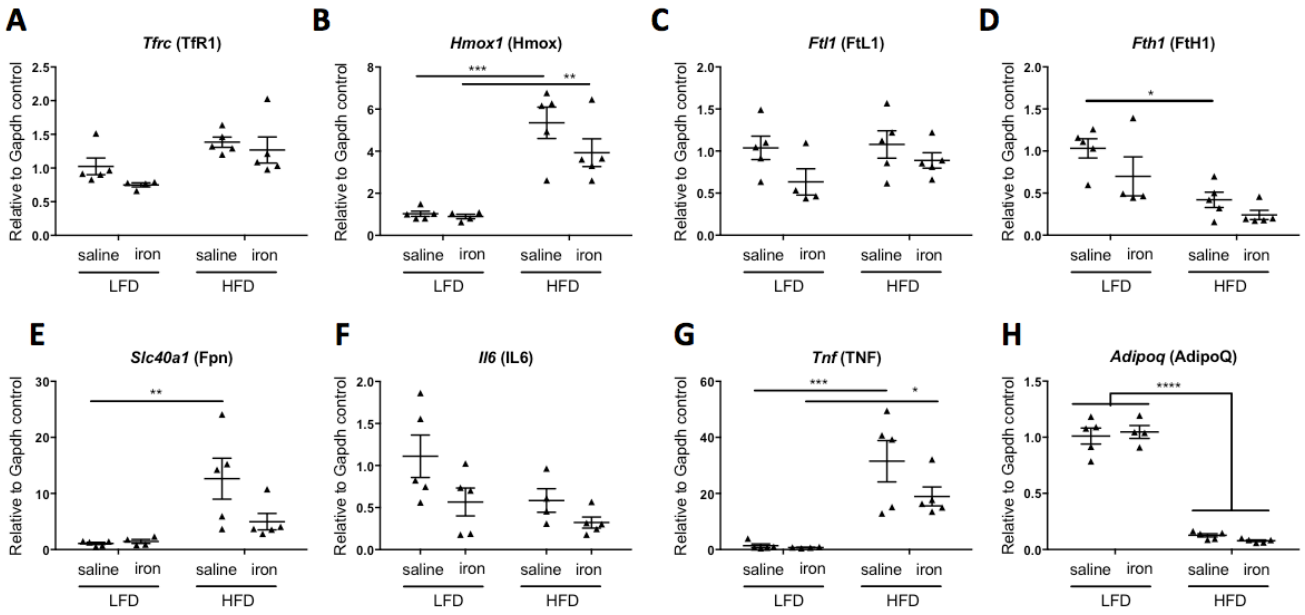

Figure 4.9. **Effect of iron injection on adipocyte gene expression.** C57BL/6J mice on 16 weeks of LFD or HFD were given a IP injection of 5mg/kg iron-100 1 week prior to sacrifice. Iron-handling genes were quantified by RT-PCR for adipocytes (N=5). Genes of interest can be grouped into (A-E) Iron-associated genes, (F,G) inflammatory cytokines, and (H) the adipokine, adiponectin. For all studies, significant differences were identified using ANOVA and t-test, with the following p-value indicators: *p<0.05, **p<0.01, ***p<0.001, ***p<0.0001.

Liver lipids and iron in a HFD feeding time course

C57BL/6J mice were on HFD for 14, 16, 18, or 20 weeks. There was no significant difference in liver weight between these time points (Fig. 4.10A). Furthermore, liver fat accumulation was not significantly changed, whether it was quantified by live-animal hydrogen MR spectroscopy (Fig. 4.10B) or by post-mortem liver TG assay (Fig. 4.10C). While there was an upward trend in liver iron, there were no significant differences between the 14-20 week time points (Fig. 4.10D). When all data points were combined, no significant correlation was found between liver TG and liver iron content (Fig. 4.10E).

AT lipids and iron in a HFD feeding time course

AT results were similar to liver results; no significant differences were seen in AT weight relative to body weight from 14 to 20 weeks of HFD (Fig. 4.11A). Specifically, we did no observe a drop in eAT fat pad weight at 16 weeks, a critical time point for AT remodeling, as reported by Strissel *et al*. (Fig. 4.1)[28]. While there was an upward trend in adipocyte iron at 20 weeks, there were no significant changes over the time course (Fig. 4.11B). The only linear correlation observed in these studies occurred between liver iron and adipocyte iron, likely reflecting systemic iron stores (Fig. 4.11C). When the data points were separated out by time point, the correlation between liver and adipocyte iron had a non-significant slope from zero (data not shown).

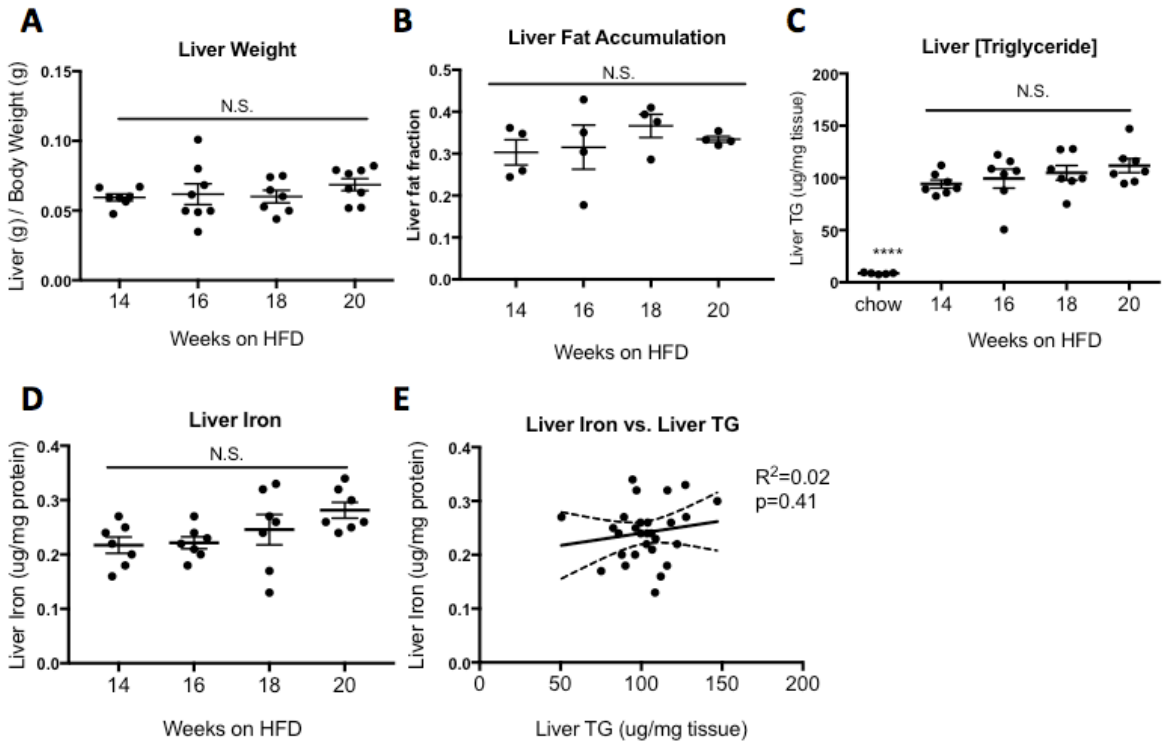

Figure 4.10. **Liver iron and lipid accumulation over 14- to 16-weeks of HFD.** C57BL/6J mice were sacrifice at either 14, 16, 18, or 20 weeks of HFD. (**A**) Total liver weight was collected at sacrifice. (**B**) Liver fat accumulation *in vivo* was quantified by hydrogen MS spectroscopy. (**C**) Liver TG were quantified by a colorimetric assay. (**D**) Liver iron was quantified by atomic absorption spectrometry. (**E**) Linear correlation between liver iron and liver TG with a non-significant slope from zero. For all studies, significant differences were identified using ANOVA and t-test.

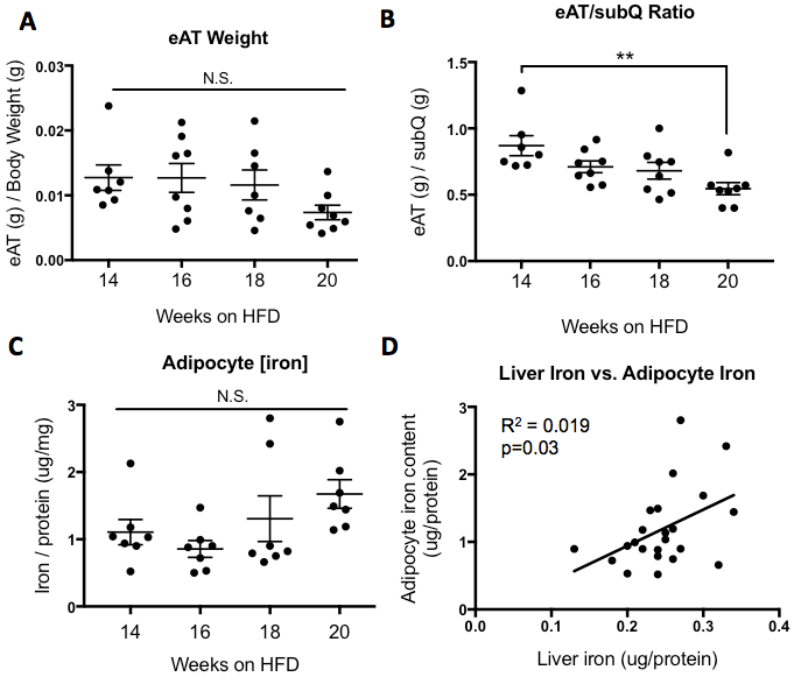

Figure 4.11. **Adipocyte weight and iron over 14- to 16-weeks of HFD.** C57BL/6J mice were sacrifice at either 14, 16, 18, or 20 weeks of HFD. (**A**) Total epididymal fat pad weight was collected at sacrifice. (**B**) eAT weight relative to subcutaneous (subQ) fat pad weight, (**C**) Adipocyte iron quantified by atomic absorption spectrometry. (**D**) Linear correlation between liver iron and adipocyte iron with a significantly non-zero slope (p=0.03). For all studies, significant differences were identified using ANOVA and t-test, with the following p-value indicators: **p<0.01.

Discussion

We initially hypothesized that MFe^{hi} would have attenuated iron-uptake in obese AT. This hypothesis was based on the observation that MFe^{hi} have decrease intracellular iron in obesity, and adipocytes have a four-fold increase in iron content. Furthermore, in lean AT, MFe^{hi} have strong M2-polarization and high expression of all iron-handling genes. In obesity, both M2-polarization genes and iron-uptake/iron-release genes were reduced. The studies outlined in this chapter combined the high iron model from Chapter III with a HFD-induced obesity model in order to "test" MFe^{hi} iron-handling in obesity. Surprisingly, we found that MFe^{hi} were still able to take up iron in HFD. However, their iron-handling phenotype was blunted in obesity, even with excess iron uptake. Their inflammatory polarization may alter their ability to be as flexible in their iron-handling genes. This presents an interesting follow up question: does altered flexibility in iron handling by MFe^{hi} in obesity impact their ability to provide iron for adipogenesis during AT remodeling?

Previous studies from our lab had shown that obesity is associated with a four-fold increase in adipocyte iron content (Fig. 4.2A)[71]. However, in these studies we did not observe this increase in adipocyte iron, nor the decrease in liver iron, at 16 weeks of HFD. Studies by other laboratories have demonstrated that 16 weeks of HFD in C57BL/6J mice is a critical time point of tissue remodeling. We considered that the contradictory findings between our studies and those of earlier work in our laboratory may have occurred due to differences in timing around this tissue remodeling. Therefore, we designed a study to correlate eAT and liver iron with lipid handling, and a way to assess this inflection point *in vivo* prior to mouse sacrifice. We used hydrogen

MS spectroscopy to quantify liver lipid content, as well liver TG content post-mortem. However, no differences were observed over the 14- to 20-week time course. Furthermore, we saw no differences in eAT weight or adipocyte iron content. While these negative findings are useful, they were unable to explain the contradictory findings in adipocyte and liver iron between the studies describe herein and those published by Orr *et al*. Future studies may benefit from adipocyte iron quantitation by ICP-MS, as well as sample standardization by metals, such as sulfur, rather than tissue weight.

CHAPTER V

TARGETING MFe^{hi} ATMS *IN VIVO*

Introduction

Potential methods for targeting cells

The studies outlined in previous chapters suggest that MFe^{hi} have an iron-handling role in AT. However, in order to mechanistically address the necessity of MFe^{hi} and their role in tissue homeostasis, our lab sought to target MFe^{hi} ATMs for depletion or functional alteration. Some common methods for cell targeting include: germline knockout of a developmentally-required gene specific to the cell type, conditional knockout of a gene specific to the cell type (i.e. with the Cre-Lox system), and nanoparticle delivery of toxins or siRNA targeted to that cell.

Germline knockout: Developmental knockout of macrophages has been accomplished. Examples include the *op/op* mouse, which is deficient in colony stimulating factor-1[139]. However, *op/op* mice have extensive developmental malformations. For this reason, developmental macrophage knockdown methods are primarily useful to address hypotheses concerning the developmental role of macrophages, not the functional role of macrophages in normal tissues. These malformations could possibly be avoided by knocking down a less generic macrophage gene, but no genes required specifically for the development of MFe^{hi} ATMs have been found. However, we have described elevated SpiC in MFe^{hi} ATMs (Fig. 3.3J & 4.6J). However, SpiC shares the same limitations as other developmental genes: it would not

target the knockdown to macrophages only in AT, and would include splenic red pulp macrophages.

Conditional knockout: In order to avoid developmental defects, conditional macrophage knockouts has been achieved with the Cre-Lox system under control of macrophage-specific gene expression. For example, mice with a lysozyme M (LysM) promoter-driven Cre with an excisable STOP codon in the diphtheria toxin receptor can be given diphtheria to induce a temporary knockout of LysM[140]. However, macrophages are known for the wide range of functions they play in nearly all tissues, and this type of global macrophage knockout study is confounded by the dysfunction of tissues in the whole organism. In our case, we are interested in understanding the specific function of one type of macrophage - and only in AT.

Liposomes and nanoparticles: The limitations of genetic knockdowns outlined so far have motivated investigators to develop small particles that can target macrophages especially well because they are both highly phagocytic and endocytic. The ideal design is a small particle that is taken up into the tissue of interest and can target a type of cell identifiable through a cell-surface protein. Ideally, such small particles would carry cytotoxins for cell depletion, or siRNA to alter the cell's function. A secondary benefit of a well-designed small particle method is the potential for translation into medical applications in humans. Currently, small particles fall into three main groups: lipid-bilayer particles (liposomes), lipid-monolayer particles (micelles), and beta-glucan particles.

Liposome characteristics and targeting

Liposomes are small vesicles composed of a lipid bilayer that have a 20-year history of medical applications, including the delivery of nutrients or pharmaceutical drugs[141]. They are most commonly composed of phosphatidylcholine and can have surface alterations that allow for their targeting to specific tissues. Hydrophilic solutes dissolved in the core of liposomes do not diffuse across the hydrophobic lipid bilayer membrane. Hydrophobic substances intercalate into the hydrophobic bilayer. In either case, hydrophilic and hydrophobic solutes can be carried by the liposomes until the bilayer is disrupted – either by a detergent, fusion with a cell membrane, or by cellular phagocytosis.

Liposomes can be either multilamellar vesicles (multiple bilayers 1-5um) or unilamellar (single bilayer, 50-250nm); the latter is preferred for delivery of hydrophobic drugs because they have a large aqueous core[141]. Adding cholesterol to the liposomes stabilizes the membrane and prevents incorporation into high-density lipoprotein (HDL) or low-density lipoprotein (LDL)[142]. Liposomes can accumulate in the interstitial space in tumors, due to inefficient lymphatic drainage[143]. Thereby, they serve as a sustained drug-release system. In contrast, they do not exit the bloodstream where endothelial cells have tight junctions. Therefore, when given IV, unmodified “first-generation” liposomes are primarily cleared through Kupffer cell of the liver or by splenic macrophages[144].

Cholesterol also allows for the attachment of PEG or other molecules to the surface of the liposomes to increase their blood circulation time and reduce their phagocytosis by the reticuloendothelial system (RES) – these are known as “second

generation" or "stealth" liposomes[145]. Specifically, PEG provides a space around the liposomes that buffers its interaction with other molecules (like opsonins and complement), and the van der Waals forces clumping liposomes together[146]. However, even with these alterations, liposomes are not inert; for example, PEGylated liposomal doxorubicin (DOXIL®, USA) has been shown to strongly activate the complement system[147]. Lastly, the size of the liposome determines its uptake by the RES. PEGylated liposomes that have a diameter of 250nm have a circulation time that is half of those with 100nm diameter or less[148].

Similar to PEGylation, liposomes can also be designed to target specific cells by coupling moieties to their surface to induce preferential internalization. For example, doxorubicin-loaded liposomes have been manipulated with surface moieties, such as antibodies[149] and receptor ligands[150], that allow for their interaction with specific cancer cells. An interesting area of current development in the field of targeted liposomes are stimuli-responsive liposomes; for example, ThermoDox® liposomes can be triggered to release their drug by localized heat treatment[151].

Liposomes for macrophage depletion

Cytotoxic liposomes are considered a standard method for depleting macrophages *in vivo* in rodents. Specifically, clodronate liposomes have been used by researchers since their development in the 1980s (ClodronateLiposome.org)[152, 153]. However, whether given IV or IP, these liposomes cannot cross vascular membranes; rather their uptake leads to the accumulation of clodronate in vascular macrophages, Kupffer cells, or splenic macrophages. At a certain threshold, clodronate induces

apoptosis and depletes macrophages, while released clodronate is non-toxic in low concentrations and simply cleared by the kidneys[154].

For the reason described, clodronate liposomes are not a method conducive to selectively depleting macrophages in AT. In order to target ATMs, liposomes would need to be injected into the peritoneal cavity, where much of the absorption occurs through direct capillary absorption[155]. This is advantageous because eAT is an unencapsulated organ, in contrast to liver, kidney and spleen. Furthermore, ATM selectivity in lean mice would be best achieved with PEGylated liposomes with a surface moiety that would support selective uptake by M2-polarized macrophages.

While all M2-polarized macrophages are known to express the hemoglobin-haptoglobin receptor CD163, our previous studies showed that this receptor is expressed higher on MFe^{hi} than MFe^{lo} [71]. For these reasons, anti-CD163 liposomes (CD163lipos), published by the Moestrup lab (Aarhus University, Denmark), were methodologically promising to us. Dr. Moestrup and Dr. Etzerodt developed PEGylated liposomes made of hydrogenated soy L-alpha-phosphatidylcholine, cholesterol, and PEG at a ratio of 55:40:5 (please refer to their publication for technical biochemical details)[110]. They produced liposomes loaded with either calcein (Fig. 5.1A) or the toxin doxorubicin (Fig. 5.2A), and the liposomes were dialyzed to remove any extra-liposomal material.

Calcein-loaded CD163lipos (CD163lipo/calcein) allow for the visualization of liposome accumulation but does not interfere with normal cell function. Doxorubicin is a chemotherapeutic agent that increases free radical production, activates apoptosis pathways, and intercalates into DNA, stalling replication[156]. While there was no specific

advantage for our studies to use doxorubicin over clodronate, doxorubicin-loaded liposomes were readily available through the collaboration with the Moestrup lab. Furthermore, initial studies with non-targeted clodronate liposomes in the Hasty lab led to rapid and consistent morbidity (data not shown), and no adverse effects were observed with the CD163lipos with doxorubicin.

Etzerodt *et al*. modified CD163lipos with a rat anti-mouse antibody against CD163 (E10B10) or human CD163 antibody. They demonstrated that CD163lipos/calcein were preferentially taken up through the endocytic pathway in macrophages and their anti-CD163 modification increases the efficiency of uptake by CHO cells expressing murine CD163 *in vitro* nearly ten-fold[110]. Furthermore, the peak level of uptake occurred at 32 hours after exposure, but was maintained up to their last time point, at 48 hours. *In vivo* experiments were performed in BALB/c mice IP injected with 200ul of 0.67mM liposome solutions and demonstrated increased uptake of CD163lipos/calcein over untargeted calcein-loaded liposomes by 30 min. When human monocytes were incubated with untargeted dox liposomes (lipo/dox, Doxil®) versus CD163lipos/dox, viability decreased from 96% to 53%. This is because the targeted delivery of dox through the CD163lipos allowed for sufficient dox accumulation intracellularly to induce apoptosis.

Ultimately, the advantages of targeted stealth liposomes outlined in this section, and the previous utility of CD163lipos by Etzerodt *et al.* lead to the application of CD163lipos as a tool to target MFe^{hi} in this chapter.

Micelle nanoparticles

Micelles are simply an aggregation of amphoteric lipids. In aqueous solutions, they can spontaneously form spheres with hydrophilic head groups outward, and lipid tails inward. They are detergents because they can carry insoluble materials within their hydrophilic center. Micelles caught the attention of researchers and the pharmaceutical industry because they are also able to "carry" siRNA through an aqueous environment, like blood, protected from degradation by RNAses. Like liposomes, combining micelles' siRNA carrying capacity with targeting moieties could be a powerful way of delivering siRNA *in vivo* to a subtype of cells.

Functional delivery of siRNA to a specific cell require that: (1) the carrier has a cell targeting moiety, (2) siRNAs are protected from RNAses in transit, and (3) the siRNAs are delivered in a way that maintains their capacity to bind mRNA in the cytoplasm, inhibiting translation of the target gene. In 2013, the Giorgio lab (Vanderbilt University, USA) developed tri-block mannosylated polymer nanoparticles (MnNPs) that fulfill the specifications listed above in the following ways[111]: (1) These MnNPs use copper (I) "click" chemistry to attach mannose to the polymer surface, thereby targeting cells with high expression of the mannose-receptor CD206; (2) MnNPs have a poly(DMAEMA) polymer with a polycationic charge that can condense siRNA, protecting it from degradation; (3) MnNPs have a very unique hydrophobic, pH responsive core that allows the siRNA to escape endosomal degradation to reach the cytoplasm (Fig. 5.6A).

MnNPs have been used *in vivo* to target CD206^{hi} TAMs[111]. Mannosylation of the NPs increased delivery to primary macrophages 4-fold, and achieved 87% knockdown of their gene of interest. MnNPs also delivered 13-fold more siRNA to TAMs than cancer cells. Repeated treatment with MnNPs *in vivo* did not lead to liver or kidney dysfunction in mice, but delivered siRNA to mammary tumors and lung metasteses[157].

Modulating specific signaling pathways is a more refined method of delineating the function of a cell in a system – rather than just eliminating the cell entirely. Therefore, siRNA technology opens up many more options for characterizing the importance of M2-like cells, like MFe^{hi} in the context of iron-handling. Using Dr. Giorgio's MnNPs could allow for the delivery of siRNA of interest to CD206^{hi} ATMs, like MFe^{hi}, in a way that avoids the endosomal degradation pathway. This chapter includes preliminary studies concerning MnNP targeting for use *in vivo* in the context of AT.

Beta-glucan nanoparticles

Beta-glucan particles are polymeric carbohydrates sourced from microbes that have also been used to target macrophages specifically. Due to their source, these nanoparticles are recognized by the pathogen-recognizing dectin-1 receptor on macrophages. Beta-glucan particles have been formulated to carry drugs to macrophages for tuberculosis therapy[158], and to carry siRNA to silence inflammatory genes in macrophages, reducing obesity-associated glucose intolerance[159]. Because beta-glucan nanoparticles are intended to target M1-polarized macrophages, they were not used in these studies but were included here for a complete representation of the breadth of methods available for targeting macrophages.

Results

Calcein-loaded CD163 liposome injections

CD163lipo studies were initiated using CD163lipo/calcein injections in order to quantify their relative uptake by MFe^{lo} and MFe^{hi} ATMs, and to grossly assess the uptake of these liposomes into specific peritoneal tissues. Mice were injected with saline, 0.1mM CD163lipo/calcein, or 1.0mM CD163lipo/calcein. 24 hours later, ATMs were magnetically sorted and analyzed by flow cytometry. Results indicated that they were taken up by both MFe^{hi} and MFe^{lo}, with preferential uptake by MFe^{hi} in the lower dose, but a consistent high uptake of 80% in the high dose in both cell types (Fig. 5.1B). Based on these results, all further CD163lipo injections were performed at an intermediate concentration of 0.67mM lipid. In another experiment, whole tissues were collected for fluorescent imaging. After background fluorescence was subtracted, it was visually apparent that calcein fluorescence was only present in the various peritoneal AT samples – not in liver, kidney, spleen, or lung (Fig. 5.1C).

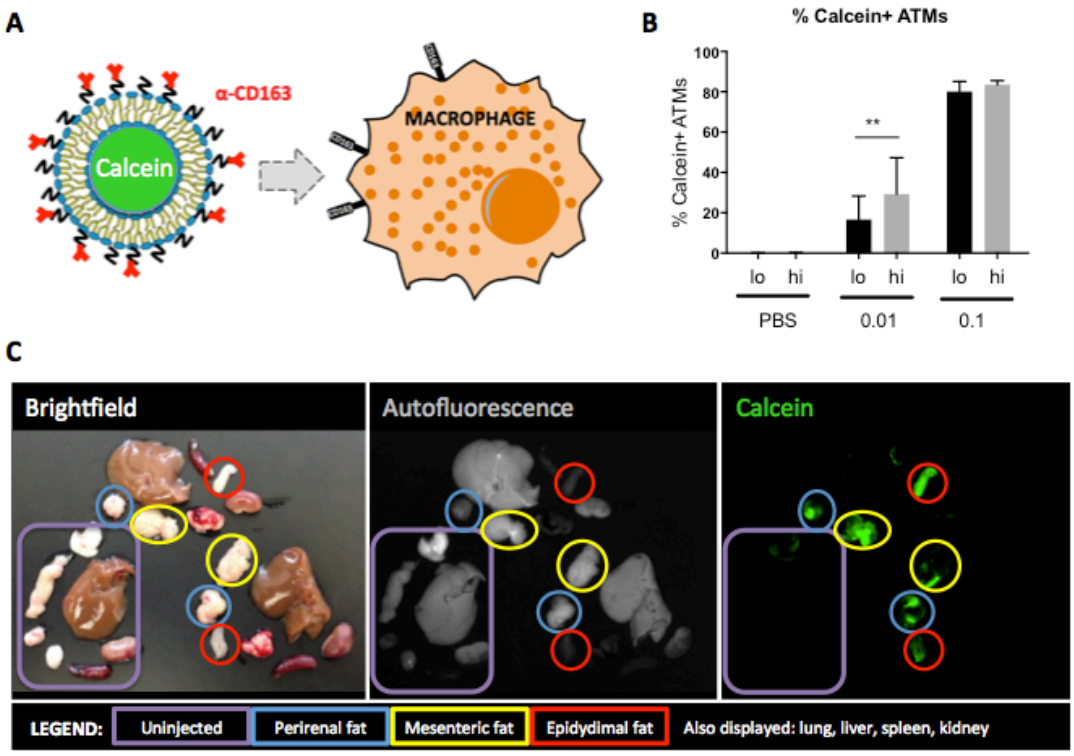

Figure 5.1. **Quantifying targeting of CD163lipos to ATMs using a fluorescent marker.** (**A**) A schematic of PEG-coated lipid bilayer liposomes coated with anti-CD163 antibody and loaded with calcein that were used to assess the targeting of $CD163^{hi}$ macrophage. (**B**) Calcein fluorescence in ATMs from mice injected with either PBS, low-dose CD163lipo/calcein, or high-dose CD163lipo/calcein. (**C**) Whole-tissue imaging for calcein fluorescence from mice injected with 0.03uM of CD163lipo/calcein. Results visually demonstrate preferential uptake by AT following IP injection of CD163lipo/calcein, rather than liver, lung, spleen or kidney. Significant differences were identified using ANOVA and t-test, with the following p-value indicators: **p<0.01.

CD163 liposome-mediated ATM depletion with iron injections

The goal of this study was to understand how adipocytes respond to excess iron when MFe^{hi} ATMs have been depleted. In order to address this question, CD163lipo/empty and CD163lipo/dox study groups were combined with saline and iron injections in a 2 x 2 study design. Preliminary studies were performed to assess the efficacy of CD163lipo/dox-mediated depletion. Supporting our ability to target $CD163^{hi}$ cells, whole eAT gene expression of *Cd163* was reduced in both groups receiving CD163lipo/dox compared to CD163lipo/empty controls (Fig. 5.2B) Reflecting the preferential uptake into AT we noted in our calcein studies, *Cd163* expression was not reduced in the liver (Fig. 5.2C). Similarly, by flow cytometry, there was significant reduction in $CD163^{+}$ ATMs in the eAT samples from mice with cytotoxic liposomes, which was not seen in liver (Fig. 5.2D). In a replicate experiment, the ATMs were magnetically sorted prior to flow cytometry. As previously described, iron injection was associated with a significant increase in the count of MFe^{hi} but not MFe^{lo} (Fig. 5.2E). Superimposed on this iron-injection effect, there was a significant reduction in the count of MFe^{hi} in mice that received cytotoxic CD163lipos (Fig. 5.2E).

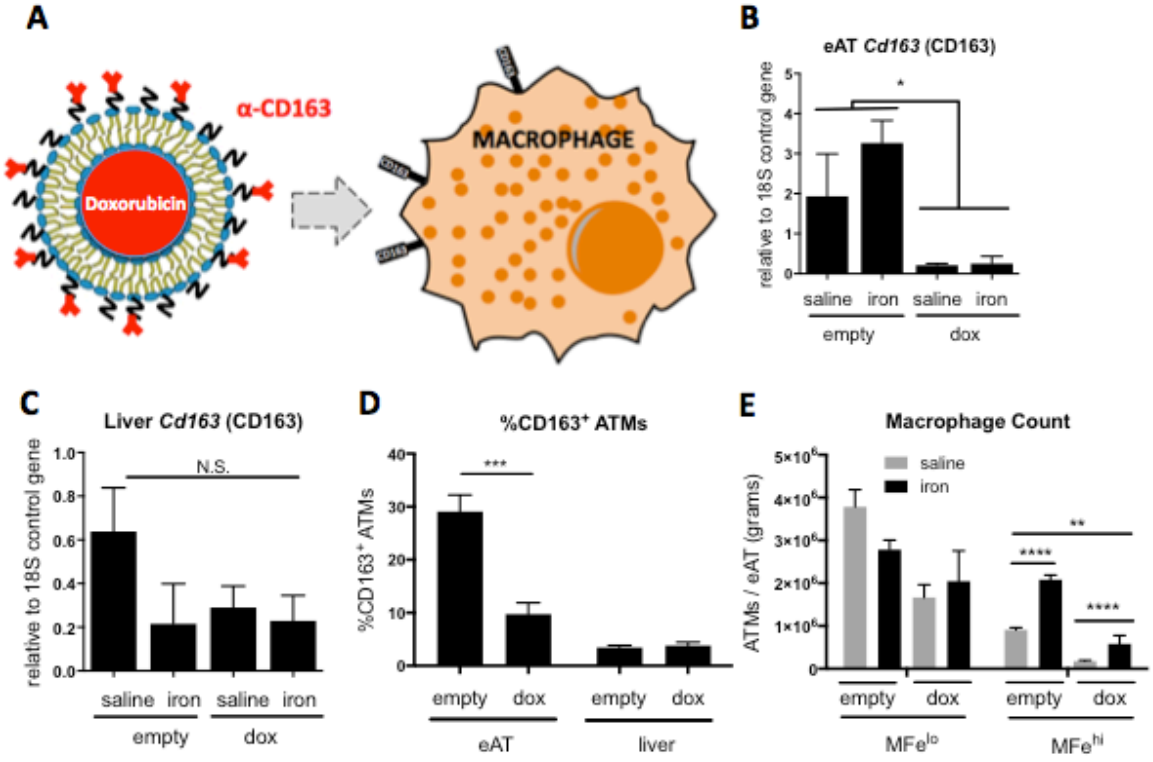

Figure 5.2. **Targeted uptake of CD163lipos by ATMs.** (**A**) A schematic of PEG-coated lipid bilayer liposomes coated with anti-CD163 antibody and loaded with the cytotoxin doxorubicin (CD163lipo/dox) to deplete CD163^{hi} ATMs. (**B**) Epididymal AT and (**C**) liver expression of *Cd163* demonstrates knockdown in only the eAT. (**D**) Flow cytometry of macrophages in eAT and liver demonstrate a significant reduction in CD163^{+} ATMs. (E) Magnetically-sorted ATMs demonstrate a preferential reduction in MFe^{hi}, not MFe^{lo}, with cytotoxic CD163lipos. For all studies, significant differences were identified using ANOVA and t-test, with the following p-value indicators: *p<0.05, **p<0.01, ***p<0.001, ****p<0.0001.

AT response to iron-injections with MFe^{hi} depletion

After we had established that MFe^{hi} were depleted in the CD163lipo/dox study with iron-injection, insulin action in AT was assessed by Western-blot quantification of pAkt. Specifically, each study group was divided to receive either PBS or insulin injection 15 minutes prior to sacrifice. Tissue was collected and assessed for expression of pAkt relative to total Akt in eAT, liver and muscle. In eAT, there was the expected increase in pAkt/Akt in response to insulin injection (Fig. 5.3A & B). However, in the group that had ATM depletion *and* iron-injections, this increase in pAkt/Akt was lost (Fig. 5.3A & B). In contrast, in liver and muscle, the fold-increase in pAkt in insulin-injected mice was robustly present in all study groups (Fig. 5.3A, C & D).

Based on previous studies, we expected that adipocytes would have no difference in iron content in response to iron injections (Fig. 3.5D). Furthermore, in this study specifically, we expected an increase in adipocyte iron content only with ATM depletion and high iron. However, AAS iron quantification showed an increase in adipocyte iron in all iron injection groups (Fig. 5.4A). Furthermore, this effect was actually blunted in mice with ATM depletion (Fig. 5.4A). Adipocytes also had an increase in the expression of *Tnfα* in both saline and iron CD163lipo/dox groups (Fig. 5.4B), and an increase in *Il1β* in the CD163lipo/dox iron group (Fig. 5.4C). However, there was no significant change in *Adipoq* between groups (Fig. 5.4D). Similarly, there were no significant differences in plasma adiponectin between the groups (Fig. 5.4E). In general, CD163lipo/dox lead to increased serum Tf (Fig. 5.4F), and iron injections and CD163lipo/dox had an additive effect in increasing serum Ft (Fig. 5.4G).

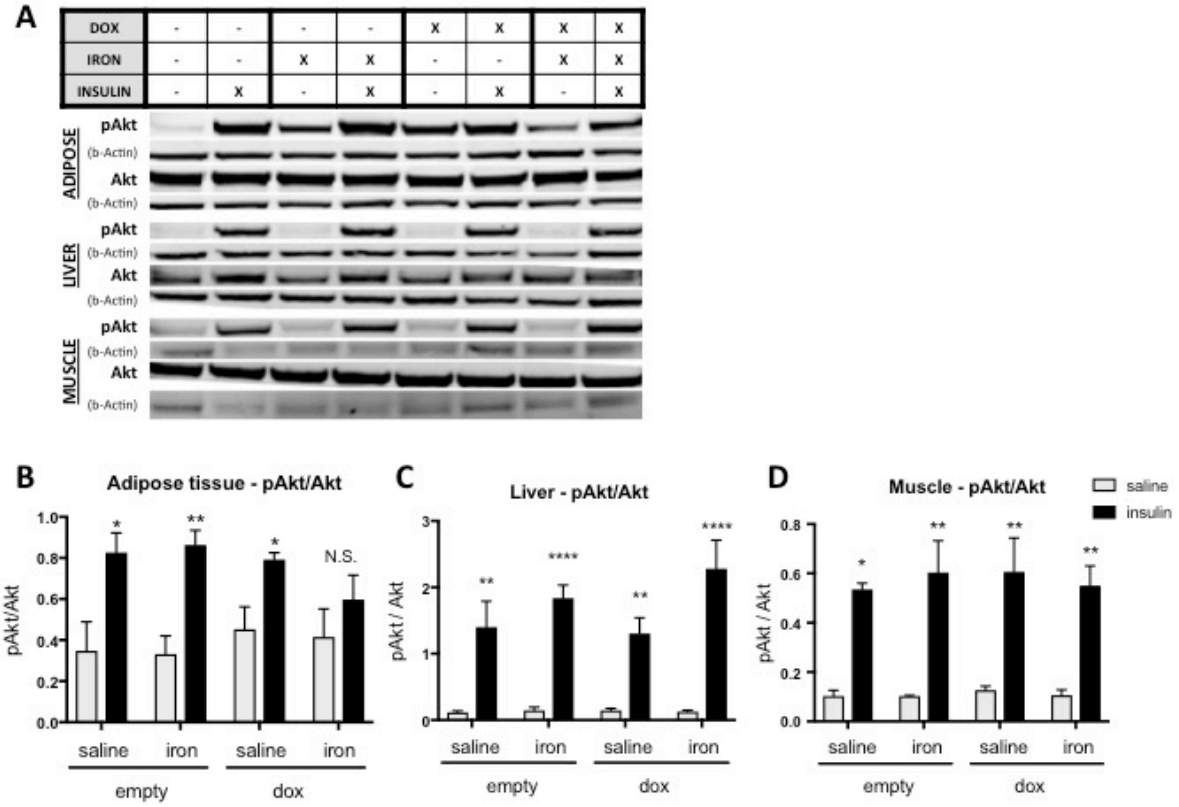

Figure 5.3. **Insulin signaling following CD163^{hi} ATM depletion and iron injection.** Experimental groups (CD163lipo/dox with saline or iron) and control groups (CD163lipo/empty with saline or iron) were injected with either saline or insulin. (**A**) The insulin signaling response was quantified by Western blot of pAkt and Akt. From these blots, the relative ratio of pAkt/Akt was calculated in (**B**) adipose tissue, (**C**) liver, and (**D**) muscle. Significant differences were identified using ANOVA and t-test, with the following p-value indicators: *p<0.05, **p<0.01, ****p<0.0001.

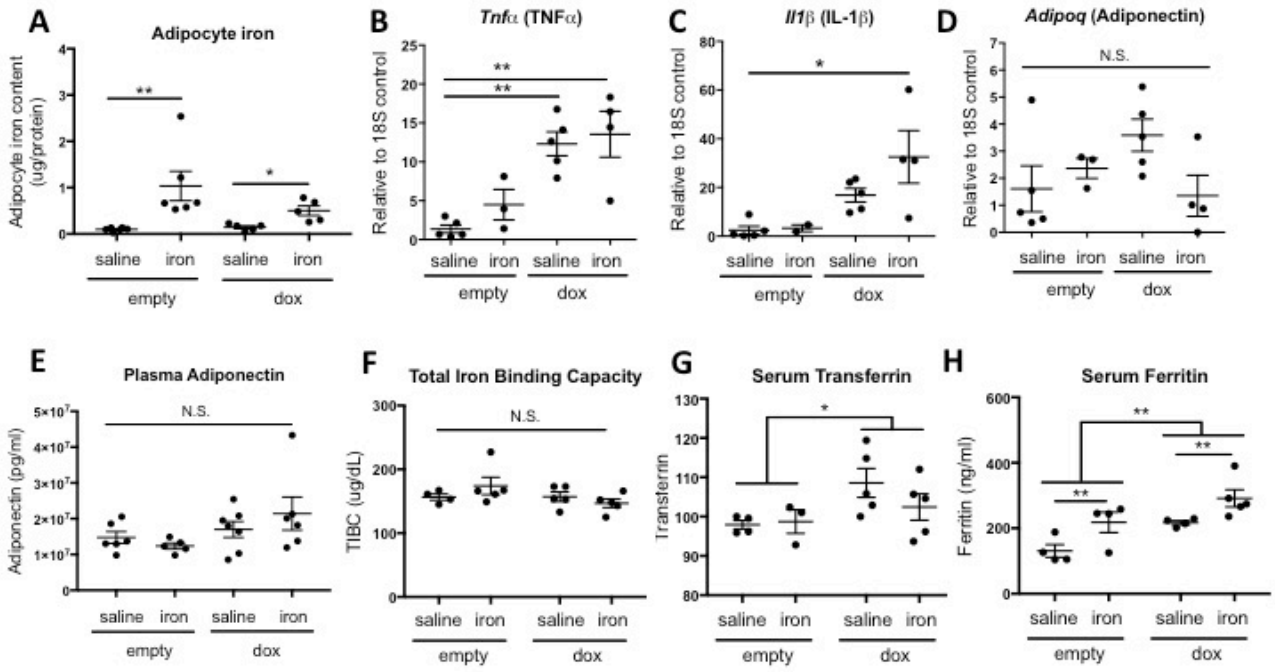

Figure 5.4. **AT and plasma parameters after CD163^{hi} ATM depletion and iron injection.** (**A**) Iron was quantified by AAS in the adipocyte fraction. Gene expression in whole AT was assessed for (**B**) *Tnfα*, (**C**) *Il1β*, and (**D**) *Adipoq*. Plasma was collected to quantify (**E**) plasma adiponectin, (**F**) total iron binding capacity, (**G**) serum transferrin, and (**H**) serum ferritin. For all studies, significant differences were identified using ANOVA and t-test, with the following p-value indicators: *p<0.05, **p<0.01.

Adipose tissue treated ex vivo with cytotoxic liposomes

To circumvent possible off-targets effects from exposing the whole peritoneum to CD163lipos, we also treated eAT fat pads with CD163lipo/dox *ex vivo*. First, the *ex vivo* model had to be established; fat pads were collected at different time points in order to assess their physiological state in culture over 48 hours. RT-PCR analysis on whole fat pads that had been *ex vivo* demonstrated a drop in *Adipoq* starting at the first time point, and maintained for 48 hours (Fig. 5.5A). While there was an initial increase in the inflammatory gene *Tnfa* at 12 hours, this returned to normal after 24 hours (Fig. 5.5B). However, *Nos2* expression was increased at 48 hours (Fig. 5.5C); possibly indicating that explants undergo oxidative stress when they have been 48 hours in culture. Lastly, we demonstrated that *Xiap*, a inhibitor of apoptosis, was down-regulated starting at 12 hours (Fig. 5.5D). When we assessed for macrophage knockdown in these explants by flow cytometry, there were no significant differences in MFe^{lo}, and only a small reduction in MFe^{hi} at 1.27mM dose of doxorubicin for 24 hours. However, at 48 hours there was a downward trend in MFe^{hi} which did no occur in MFe^{lo}. While this further supports the specificity of CD163lipo targeting to MFe^{hi} with high expression of CD163, the trends in *Adipoq, Nos2,* and *Xiap* suggested that this *ex vivo* methodology was too confounded by physiologic dysfunction of the eAT for further applications.

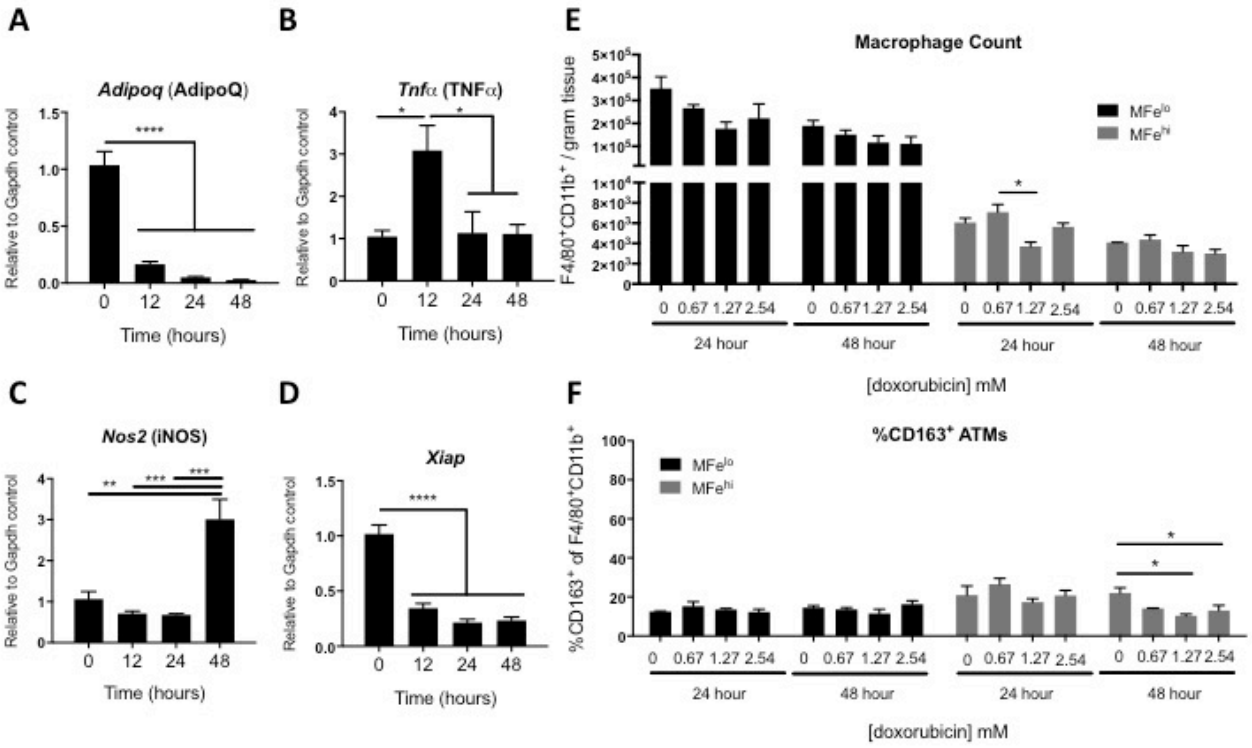

Figure 5.5. **CD163lipo treatments in AT explants.** The physiologic health of AT explants was analyzed over 0-48 hours by quantification of certain genes, including(**A**) Iron was quantified by AAS in the adipocyte fraction. Gene expression in whole AT was assessed for (**B**) *Tnfα*, (**C**) *Il1β*, and (**D**) *Adipoq*. Plasma was collected to quantify (**E**) plasma adiponectin, (**F**) total iron binding capacity, (**G**) serum transferrin, and (**H**) serum ferritin. For all studies, significant differences were identified using ANOVA and t-test, with the following p-value indicators: *p<0.05, **p<0.01, ***p<0.001, ****p<0.0001.

Mannosylated nanoparticle delivery of siRNA

MnNPs allow for the delivery of siRNA, with the intention of altering a specific cell's physiology. In these studies, MnNPs were loaded with different combinations of three siRNA molecules against the iron-exporter *Slc40a1* (Fpn) and used for *in vitro* treatments of M2- and Mme-polarized bone marrow-derived macrophages (BMDMs). These MnNPs were expected to preferentially target cells with high expression of the mannose receptor, CD206. In preliminary studies with BMDMs, we observed a 50% knockdown of *Slc40a1* in M2-polarized BMDMs using the "B" combination of three siRNAs (Fig. 5.6B). There was no significant reduction in *Slc40a1* with any treatments in Mme-polarized BMDMs (Fig. 5.6B). We intended to apply this combination of siRNAs for *in* vivo injections. However, due to the cost associated with high doses of siRNA required for *in vivo* experiments, we chose to secondarily verify the preferential uptake of MnNPs by $CD206^{hi}$ ATMs. For this purpose, MnNPs loaded with fluorescent $Cy5^+$ double-stranded DNA ($Cy5^+$dsDNA) were incubated with polarized BMDMs. After 48 hours, BMDMs were assessed by flow cytometry using macrophage markers (F4/80 and CD11b), as well as CD206. Saline was used as a control for autofluorescence, and free $Cy5^+$dsDNA served as a control to assess for nonspecific uptake of the dsDNA. As would be expected by our polarization stimulus, M2-polarized BMDMs had a two-fold increase in CD206, while Mme- and M1-polarized BMDMs had reduced CD206 (Fig. 5.6C). When we assessed $Cy5^+$ fluorescence, comparing the negative control (NC) to either $Cy5^+$dsDNA treatment or $Cy5^+$dsDNA MnNPs, it was clear that the $Cy5^+$ signal was a true signal, not background autofluorescence. However, in these differentially polarized BMDMs, there was no preferential delivery of $Cy5^+$ dsDNA to M2-polarized

CD206^{hi} BMDMs (Fig. 5.6D). In fact, unpolarized and M1-polarized BMDMs had the highest levels of fluorescence associated with MnNP uptake. Furthermore, this uptake of Cy5^{+}dsDNA occurred even in the absence of MnNP (Fig. 5.6D). These findings suggest to us that the MnNPs at this stage in development did not provide an efficient method of delivering siRNA to M2-polarized macrophages.

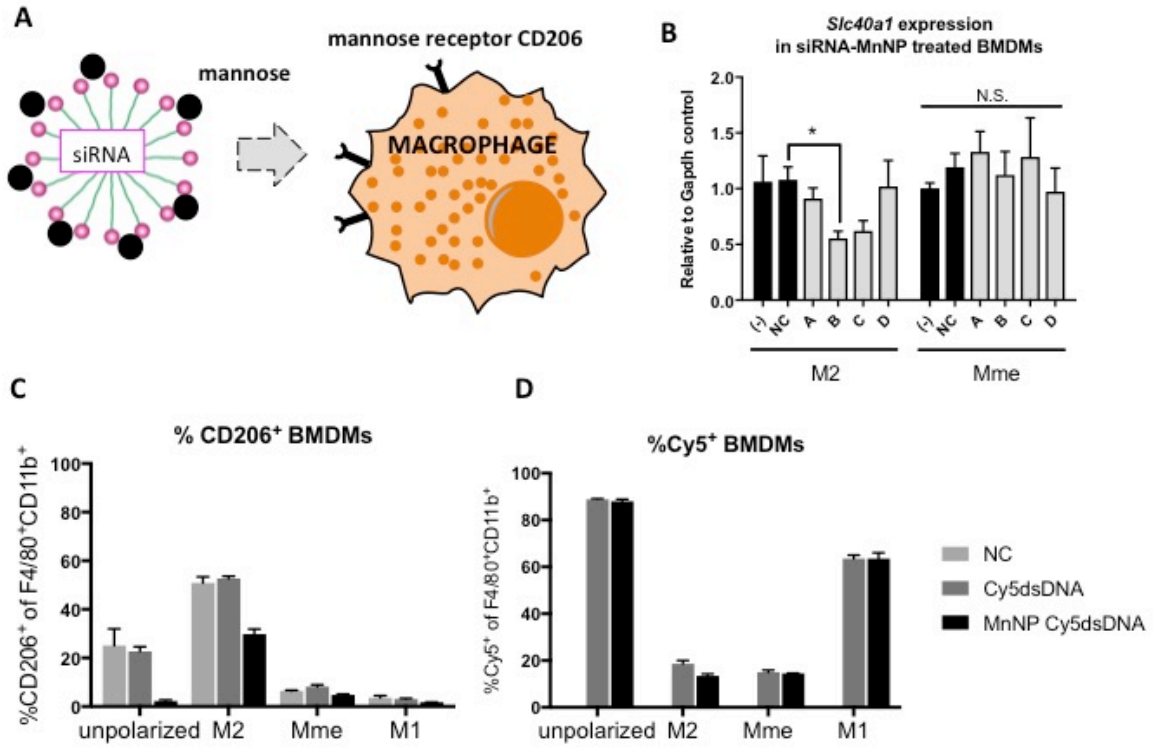

Figure 5.6. **Testing mannosylated nanoparticle specificity.** (**A**) A model of mannosylated nanoparticle (MnNP) delivery of siRNA to macrophages. (**B**) Preliminary testing of different iterations of three siRNA combinations loaded onto MnNPs and provided to either M2- or Mme-polarized bone marrow derived macrophages (BMDMs). (**C**) CD206 expression was quantified by flow cytometry in BMDMs of different polarization statuses. (**D**) Polarized BMDMs were treated with a negative control (NC), free Cy5-conjugated dsDNA (Cy5dsDNA), or Cy5dsDNA loaded onto MnNPs. Cy5 fluorescence was quantified in cells positive for F4/80 and CD11b. For all studies, significant differences were identified using ANOVA and t-test, with the following p-value indicator: *$p<0.05$.

Discussion

The ubiquitous presence of macrophages in most tissues of the body makes them difficult to target with specificity. Simultaneously, the unique adaptations and role macrophages play in resident tissues makes them appealing to study in a targeted way. The field of immunometabolism has been seeking a way to target ATMs, and other tissue-associated macrophages, in order to understand the implications they have for whole-body physiology.

This chapter gives insight into preliminary studies, attempts, and limitations of two methods of targeting ATMs. In this case, targeting of MFe^{hi} instigated both of the collaborations that lead to our use of CD163lipos and MnNPs. In the studies with CD163lipo/calcein *in vivo*, it was apparent that these liposomes were taken up primarily into the AT of the peritoneal cavity, rather than other organs. Not only does the PEG coating of the CD163lipos support their ingestion by macrophages, but it is possible that the organ capsules on liver, spleen, and kidney prevent their ready uptake. The preferential uptake of CD163lipos into AT was also reflected in reduced expression of *Cd163* in AT relative to liver, following the injection of cytotoxic CD163lipos. Furthermore, sorting MFe^{hi} and MFe^{lo} following CD163lipo injection show that their uptake could be somewhat targeted toward the MFe^{hi} - "$CD163^{hi}$" - ATMs with the correct dosage. These were all encouraging results and bode well for future studies using CD163lipos to target $CD163^{hi}$ macrophages in AT.

The intent of using CD163lipos was to determine if $CD163^{hi}$ ATMs were necessary for iron homeostasis in AT. To this end, CD163lipo ATM depletion was combined with iron injections. The results of these studies opened up more questions;

we were especially intrigued if these results may indicate that the empty CD163lipos could induce adipocyte iron uptake. To address this finding, we would need to use a non-liposome (saline) control group in future studies. Lastly, iron quantification in adipocytes in these studies could be performed with ICP-MS and AAS to verify that the quantification was consistent. However, the targeted uptake of CD163lipo that was seen in these studies suggests that this methodology could still prove to be useful in addressing these or other questions.

Preliminary studies were performed with CD163lipos *ex vivo* in order to avoid off-target effects and narrow in on eAT physiology. However, analysis of AT explants from these studies suggested that the explant methodology itself was confounded by the health of the tissue. Once it was identified that CD163lipos are preferentially taken up into AT *in vivo*, explants studies were not further pursued.

MnNPs were assessed as a method of altering the function of macrophages using siRNA against specific genes. In this context, the intention was to knock down either iron-uptake or iron-release genes in ATMs to assess the role of ATMs in iron handling and their impact on adipocyte or AT health. The studies outlined in this chapter were preliminary studies to confirm that mannosylation of the NPs did actually lead to preferential uptake by cells with high expression of CD206 – a protein highly expressed on M2-like macrophages, including MFe^{hi}. While we were able to induce a 50% knockdown of *Slc40a1,* further studies using a fluorescent marker dsDNA did not demonstrate the preferential uptake by $CD206^{hi}$ macrophages that had previously been described[157]. What was particularly concerning to us was that uptake was enhanced in M1-polarized macrophages in this system, and that uptake occurred whether the

dsDNA was provided with or without the MnNPs. After discussing these findings with the collaborating lab (Dr. Giorgio, Vanderbilt), it was decided to not pursue this technology for *in vivo* applications until modifications had been made to the MnNPs.

While the field of immunometabolism commonly focuses on the influx of monocyte-derived inflammatory macrophages in obesity, it is also commonly accepted that resident M2-polarized ATMs play a role in maintaining homeostasis of lean AT. However, studies of resident ATMs have been limited by our inability to target them. It has not been possible to demonstrate that they are, by definition, “necessary”, and to tie their presence to a specific type of physiological homeostasis. The two technologies outlined in this chapter – CD163lipos and MnNPs – were pursued for exactly this reason. While the CD163lipo/iron studies had unexpected results, and the MnNPs we used need to be further optimized, both of these methods have unique qualities that demonstrate great potential for future applications.

CHAPTER VI

SUMMARY AND CONCLUSIONS

Immunometabolism is a field that was born from the discovery of immune cells in metabolic tissues, such as AT[26]. In fact, the field is part of a broader scientific understanding that dysregulation of the immune system may underlie many of the modern, chronic "uncured" diseases – such as vascular hypertension, pulmonary hypertension, non-alcoholic steatohepatitis, cancer, autoimmune diseases, and type 2 diabetes[160-164].

Immune cells evolved to contend with infectious microbes by functioning as a system with flexibility and complexity from both cellular diversity and intricate intercellular interactions. This also gives the immune system the ability for acute accommodation and chronic adaptation to environmental cues, spatially and temporally. It can be surmised that these qualities explain why immune cells have been evolutionarily coopted to respond to environmental cues and maintain other types of homeostasis – such as metabolism.

Classic metabolism-associated cells – like hepatocytes, beta cells, muscle cells, and adipocytes – are very specialized, making them sensitive to perturbation. This has limited the successful medical therapies available to treat metabolic dysfunction of these cell types, leaving some metabolic diseases "incurable". For this reason, there is a growing appreciation for therapies that target the immune cells in the tissues instead[165].

As the technology to modulate tissue-associated immune cells progresses rapidly, so must our understanding of the natural function of these cells.

Immune cells use nutrient partitioning as a way to limit the growth of invasive microbes[166, 167]. For example, monocytes have developed methods to sequester metals in plasma during an infection, while microbes respond with complex ways to steal away these same metals. A very similar interaction plays out between cancerous cells and TAMs[168]. These examples highlight the importance of metals to all living cells. As discussed in the Introduction, fine-tuned metal availability is likewise important in the function of metabolic cells, like adipocytes[17]. For this reason, it was fortuitous, but not altogether surprising, when our lab discovered that macrophages are involved in iron-handling in AT[71].

DIOS – or dysmetabolic iron overload syndrome – is a syndrome that describes aberrant iron storage in certain cell types in association with the metabolic syndrome[169]. This syndrome was based on a growing set of human and rodent studies that correlate systemic iron stores and metabolic dysfunction, independent of inflammation[51, 54, 56, 170-172]. Further studies have shown that many cells aside from macrophages require iron to function and replicate, but they can be sensitive to oxidative stress from excess iron. This supported the findings by our laboratory that MFe^{hi} may be responsible for iron-handling in adipose tissue. While the previous studies by Orr *et al*. described the phenotype of MFe^{hi} ATMs in lean and obese AT, and proposed interesting hypotheses, no functional studies were performed to ascertain their iron-handling capacity. The experiments described in Chapters II-V of this dissertation were designed to probe the function and necessity of ATMs for iron homeostasis in lean and obese AT (Fig. 5.7).

In Chapter III, iron-diet and iron-injection were introduced as two models of iron excess in the mouse. The advantage of the iron-diet model was its chronicity and physiologic relevance. The iron-injection model offered a more acute and direct approach to providing excess iron in AT. Both studies demonstrated gene-level responses to excess iron only in MFe^{hi}, not MFe^{lo}. In addition, changes in the count of MFe^{hi} were attributed primarily to MFe^{lo} "conversion" to MFe^{hi}. This finding draws into question the identity of MFe^{hi} as a unique subtype of resident ATMs. The original discovery of MFe^{hi} defined them based on their intracellular iron content and then further associated an iron-handling gene profile with those cells. However, if MFe^{lo} can also take up iron in a high-iron context, then high-iron ATMs may simply represent the percent of ATMs that are accommodating the most iron when needed, rather than a unique phenotype or ATM subtype. These ideas will be further parsed out in Future Directions (Chapter VII).

In both models of excess iron in lean mice, MFe^{hi} were able to take up excess iron, and adipocytes showed no uptake of iron. This was particularly unexpected in the iron-injection model, as this was an extreme model of iron excess. However, it served well as a proof-of-concept that MFe^{hi} ATMs could function as an iron sink. It also further supports the ability of MFe^{hi} to accommodate excess iron and compensate for the relative sensitivity of other metabolic cells, like adipocytes. Furthermore, the small percent of monocyte recruitment we observed demonstrates chronic adaptation of these resident macrophages to the iron-excess stimulus. For this reason, the iron-injection model was also applied in Chapter IV to assess the impact of obesity on MFe^{hi} iron uptake.

The experiments outlined in Chapter IV intended to address how ATMs respond to excess iron in the obese setting. The studies were designed around previous findings that adipocytes have a 4-fold increase in iron content in obesity, while MFe^{hi} have decreased iron content. Orr *et al*. hypothesized that this demonstrated a "dysfunction" of MFe^{hi} in obesity. However, the data in this chapter did not directly address this hypothesis. While the experiments intended to test adipocyte response to excess iron in obesity, it ultimately demonstrated decreased iron content in control groups in obesity – contradicting previous findings[71]. To reconcile these conflicting findings we designed studies to understand the timing of HFD weight gain in the context of AT and liver iron content with lipid storage. Unfortunately, the negative results of these studies did not help to clarify our initial findings. As with all conflicting results, the data outlined in this chapter offer an opportunity for further studies regarding adipocyte iron content in obesity, as discussed in Future Directions (Chapter VII).

Chapter V outlined two methods used to target M2-polarized ATMs. While both technologies were developed with the intention of targeting M2-like macrophages, their application to ATMs is promising. CD163lipos are mainly useful for cellular depletion. This means that their experimental and pharmaceutical utility is contingent on their ability to target specific tissues; depleting the same cell type, like M2-like macrophages, in many tissues could lead to unacceptable adverse effects. Therefore, it is important to note the specific uptake of CD163lipo/calcein in only AT of the peritoneum is extremely promising. Furthermore, selective depletion of $CD163^{hi}$ MFe^{hi} ATMs demonstrated even greater potential applications for CD163lipo/dox. However, when we applied CD163lipo/dox to our high-iron model we observed confounding results – iron uptake by

adipocytes even in empty liposome control groups. It is interesting to consider if CD163lipos are able to activate complement, and that this may impact adipocytes,[173] possibly influencing iron uptake. The potential utility of C163-targeting liposomes as a method for further research studies is outlined in Future Directions (Chapter VII).

In contrast to cytotoxic liposomes, MnNPs are made to target cellular function via siRNA against specific mRNA. So, tissue-specific uptake may be less critical than for cytotoxic liposomes. i.e. Altering *only* iron-handling by M2-like macrophages in different tissues may not have as dramatic adverse effects as abolishing those cells completely. However, for research and pharmaceutical applications, it is absolutely required that MnNPs deliver their cargo consistently, because siRNA is expensive and functionally limited by its protected status within the micelle. Based on the results of our preliminary studies, we determined that the MnNPs provided to us did not fulfill these criteria. For this reason, we chose not to move forward with *in vivo* studies with these MnNPs. However, should the technology evolve, they could very experimentally useful, as described in Future Directions (Chapter VII).

Generally, the studies in these chapters address how ATMs may respond to conditions of iron excess, possibly protecting adipocytes. By understanding the normal roles of macrophages in tissues, we lay the groundwork for future methods that may intervene to alter the physiology of AT – such as liposomes or nanoparticles.

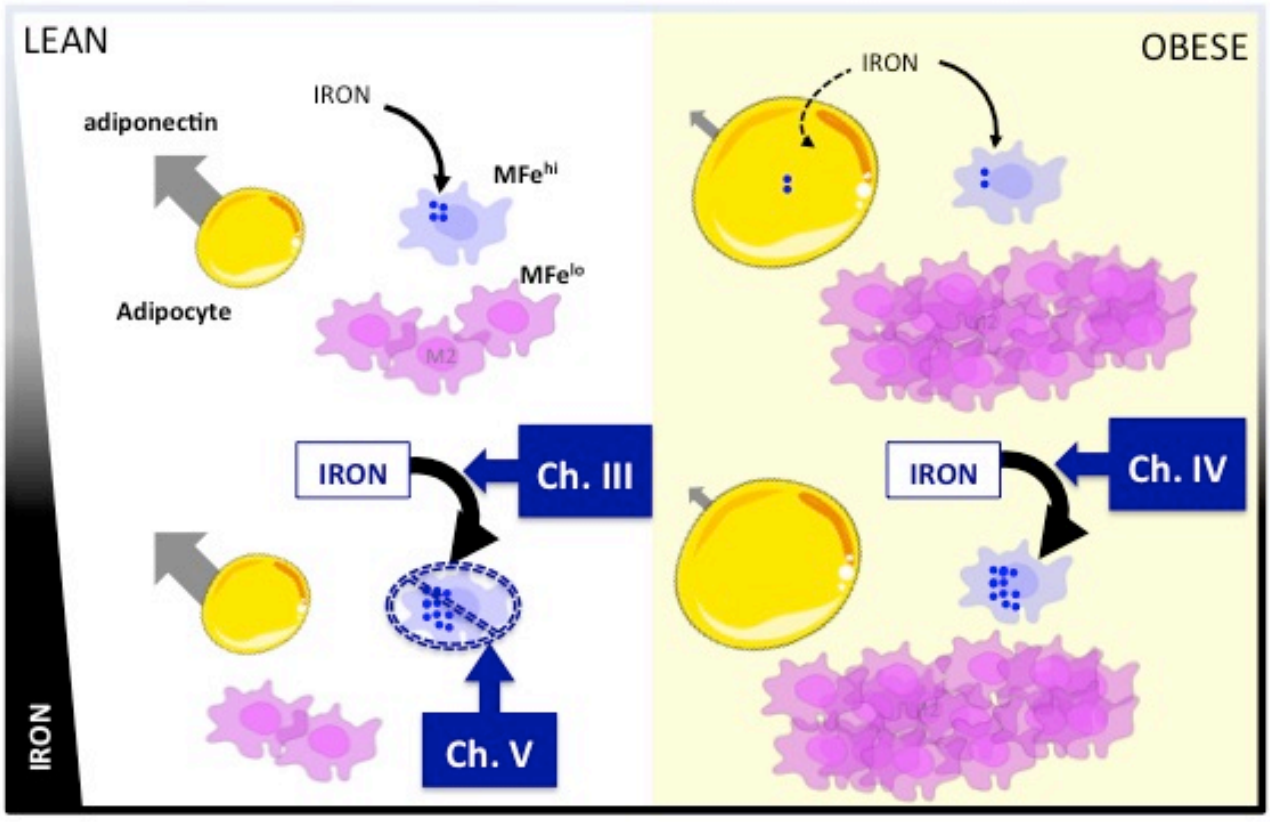

Figure 5.7. **Model representing a summary of dissertation scope and findings.** Previous studies by our lab demonstrated that MFe^{hi} ATMs have increased intracellular iron content. In obesity, the iron content of MFe^{hi} is decreased but adipocyte iron increases. The findings described in Chapter III demonstrated the proof-of-concept that MFe^{hi} act as an iron-sink in models of excess iron. Chapter IV outlined studies showing that MFe^{hi} can still take up excess iron in obesity. In Chapter V we explored methods of interfering with MFe^{hi} uptake of iron.

CHAPTER VII

FUTURE DIRECTIONS

The studies detailed in this dissertation provide insights into the function of ATMs in regards to iron-handling. However, these same results led to more questions, providing a rich resource for further research in the area of ATM-associated iron handling. In the following sections, these future directions have been structured as a specific set of questions, along with potential experimental plans.

Do MFe^{hi} have an increased labile iron pool (LIP)?

The MFe^{hi} population was defined as the 80-90% of the paramagnetic fraction that stains positive for macrophage markers. Using this same definition, MFe^{hi} can be sorted by FACS, in order to assess their gene expression. To the surprise of Orr *et al.,* MFe^{hi} did not have a gene profile that reflected iron-storage, but had higher expression of *all* iron-handling genes, relative to MFe^{lo}. This is especially surprising considering the IRP-associated regulation of iron-associated genes. In the classic understanding, when a cell has an increase in free intracellular iron (the LIP), it increases its expression of iron-storage proteins (like Ft) and iron-releasing proteins (like Fpn), while down-regulating iron-uptake proteins (like TfR1). All of this regulation is mediated through IRPs and exists to avoid the threat of oxidative stress posed by a high LIP. However, the gene-expression seen in MFe^{hi} seems to contradict this classic regulatory

mechanism because iron-uptake, -storage, and -export genes are all upregulated. This may be explained in two ways:

(1) MFe^{hi} have a very unique phenotype in regards to iron handling that does not follow the classic IRP-IRE response, differentiating them from other macrophages. In order to demonstrate this, the LIP of MFe^{hi} would need to be quantified relative to gene expression. LIP can be quantified directly using calcein-AM quenching assays[174, 175]. These studies would be supported by using IRP-IRE-binding bandshift assays to quantify the binding of IRP in these cells[176, 177]. These studies would allow us to place MFe^{hi} in the broader context of known mechanism of iron-handling by macrophages.

(2) The iron-cycling gene profile describe herein may actually be a reflection of MFe^{hi} ATMs existing at temporally different responses to iron uptake. For example: Cell 1 may have been exposed to high iron one day ago, so it has had time to respond through IRPs, increasing Fpn and Ft expression and decreasing TfR1. Cell 1 would have a lower LIP but high intracellular iron. In contrast, Cell 2 may be actively taking up iron from the local microenvironment, with a growing LIP that is giving it the same paramagnetic qualities as Cell 1. However, Cell 2 still has high *Tfrc*, and low *Slc40a1* and *Ft* expression. When both cells sort as paramagnetic in the AutoMACS and as macrophages via FACS, their pooled gene expression would appear to have upregulation in all genes, relative to MFe^{lo}. This hypothesis is supported by the response of MFe^{hi} to high-iron studies; in both models of iron excess, the baseline MFe^{hi} gene profiles is reflective an IRP-regulated response. Ultimately, considering that iron-handling proteins are regulated by IRPs that actively impact the stability of

mRNA[178], the gene expression profiles described may not reflect the state of the cells. The studies by Orr *et al.*, and those in this dissertation, used a gene expression readout because they were limited by low counts of MFe^{hi}. There are multiple methodological options available to clarify this question. In both cases, it would be beneficial to compare ATMs from untreated and iron-treated mice in order to determine the impact of microenvironmental iron availability. One option is to use flow cytometry[120] or plated fluorescent antibody-mediated cell imaging to quantify protein levels of all the iron-handling proteins and see if they are expressed by the same cells. Another option is to use carefully optimized Western Blotting techniques for low protein levels, or proteomics[179], in order to accurately determine the iron-handling state of the MFe^{hi} and MFe^{lo} on a protein level.

Are MFe^{hi} a unique subpopulation?

In our studies investigating MFe^{hi} in iron-excess conditions, we noted an unexpected increase in the count of MFe^{hi}. For iron-injection studies, this increase could primarily be attributed to MFe^{lo} "switching" to MFe^{hi}. These findings may suggest that MFe^{hi} are not, in fact, a unique subpopulation of ATMs, but simply those ATMs in lean tissue that happen to take up iron where it is present in the microenvironment. This in no way mitigates the importance of iron-handling by M2-polarized ATMs. Future studies concerning MFe^{hi} could address this question in the following ways:

(1) The entire ATM population from a lean AT could be sorted and plated *in vitro.* They would then be exposed to either M2- or Mme-polarization stimulus as well as high-

iron in order to determine how they alter their iron uptake or iron-handling. The cell-specific response would be best quantified by cell fixation and fluorescent antibody-mediated imaging. Furthermore, comparison of M2- and Mme-polarized to a control un-polarized group would demonstrate how heterogeneous the ATMs were initially. This experimental setup effectively removes the micro-environmental differences in iron availability that may be underlying heterogeneity observed *in vivo*.

(2) The studies described could be taken a step further by performing a cross-over experiment, where the polarization stimulus is switched in the context of high iron. This type of experiment would begin to address the impact that an obesity-associated inflammatory state may have on ATM iron handling. This is especially interesting because in Chapter IV we described that in the obese AT, MFe^{hi} still took up excess iron but their iron-cycling phenotype was blunted. Lastly, BMDMs or macrophages from other sources – like red pulp macrophages – could be used in parallel experiments to demonstrate how ATMs respond to these stimuli relative to other macrophages.

Are MFe^{hi} (or ATMs) also responsive to, or required, in low-iron conditions?

Some results from low iron diet studies suggest that MFe^{hi} are homeostatically responsive to iron; after 8 weeks of low iron, there are reduced counts of MFe^{hi} and lower MFe^{hi} iron concentrations (Fig. 3.2A - C). "Iron-cycling" is used as a descriptor of the MFe^{hi} gene profile. However, the studies included in Chapters III-V were more heavily weighted towards high iron, not low iron. Future studies could incorporate the

following experimental designs with iron-demand conditions to establish that MFe^{hi} partake in bidirectional homeostatic responses.

(1) Iron chelation can be applied in the same contexts as iron-excess, both *in vitro* and *in vivo*. *In vitro* studies would be similar to those previously described: whole ATM population would be plated, exposed to polarization stimulus, and then treated with a chelator, like deferoxamine. The advantage of *in vivo* studies is that they could directly complement iron-injection studies. However, *in vitro* studies circumvent the whole-body physiologic adaptation that may buffer efforts to chelate iron in the peritoneum (the liver may simply release iron or more iron may be absorbed from the GI tract, such that a true state of iron depletion would not be achieved *in vivo*).

(2) Physiologic relevance could be attained *in vivo* by investigating the role of ATMs during a natural state of AT iron demand – AT hyperplasia. All replicating cells require iron to produce iron-containing genes, especially for mitochondrial replication. In fact, iron chelation has been shown to inhibit replication and differentiation in adipocyte cell lines[77]. Therefore, the expanding tip of a fat pad likely represents an iron-demanding microenvironment. Previous studies have shown that macrophages are intimately involved, even required, for AT development and expansion[180]. Iron provision could be one of the functions that they perform in this context. This idea could be approached by separating the tip of a fat pad undergoing hyperplasia – like in early stages of development or HFD – and comparing relative ratios of MFe^{hi} to MFe^{lo} to

other parts of the fat pad, either by flow or iron staining. The cells could also be analyzed for iron-handling proteins by flow cytometry.

(3) Once optimized, CD163lipos or MnNPs carrying anti-Fpn siRNA could be injected during early stages of AT hyperplasia. These studies would demonstrate whether ATMs, or specific iron-handling functions, are required for healthy hyperplasia.

Is *SpiC* an important developmental gene for iron-handling ATMs?

Spic is a protein required for the development of iron-handling red pulp macrophages of the spleen. Its expression has also been found to be elevated in MFe^{hi} compared to MFe^{lo} (4.6G). However, this difference was lost following iron-injections or HFD. This may indicate two things – either the elevation in SpiC in MFe^{hi} at baseline is subtle and insignificant, or it demonstrates that MFe^{hi} are in fact a unique subpopulation with unique developmental genes. These questions could be addressed in two mains ways:

(1) *In vivo* changes in *SpiC* are confounded by shifts of MFe^{lo} to paramagnetic fractions, as has been previously discussed. To avoid this confounding effect, SpiC could be quantified in unsorted ATMs sourced after multiple iron injections, or long-term iron diet. A long exposure to iron is suggested for these studies in order to allow for detectable responses in developmental gene expression in ATMs. Alternatively, plated ATMs could be exposed to iron *in vitro.* This would demonstrate if only some, or all, ATMs alter SpiC levels in response to iron.

(2) These questions could be further addressed with inducible SpiC knockout mice. In this case, it would be interesting to induce the knockout prior to iron injections or prior to the initiation of AT hyperplasia (like HFD, an iron-demand scenario), and compare the adipocyte response between knockout and control mice. ATMs from conditional knockout mice could also be used *in vitro* under conditions of high or low iron to investigate if knockout of SpiC impacts the availability of ATMs that regulate iron.

During the last months with the Hasty lab, I intend to delve into some of the studies described – particularly, the application of CD163lipos *in vivo*, and MFe^{hi} during adipogenesis. However, most of these Future Directions remain as potential studies of interest for students of the Hasty lab to explore. Not only will understanding ATM iron handling satisfy our curiosity on the role of immune cells in AT, but these studies may lead to therapeutic targets for situations of AT dysfunction down the line.

REFERENCES

1. Hesse M, Modolell M, La Flamme AC, Schito M, Fuentes JM, Cheever AW, Pearce EJ and Wynn TA. Differential regulation of nitric oxide synthase-2 and arginase-1 by type 1/type 2 cytokines in vivo: granulomatous pathology is shaped by the pattern of L-arginine metabolism. *J Immunol*. 2001;167:6533-44.

2. Hubler MJ, Peterson KR and Hasty AH. Iron homeostasis: a new job for macrophages in adipose tissue? *Trends in endocrinology and metabolism: TEM*. 2015;26:101-9.

3. CDC. Adult Obesity Facts. 2018;2018.

4. Singh VP, Bali A, Singh N and Jaggi AS. Advanced glycation end products and diabetic complications. *Korean J Physiol Pharmacol*. 2014;18:1-14.

5. van Belle TL, Coppieters KT and von Herrath MG. Type 1 diabetes: etiology, immunology, and therapeutic strategies. *Physiol Rev*. 2011;91:79-118.

6. Kahn SE, Cooper ME and Del Prato S. Pathophysiology and treatment of type 2 diabetes: perspectives on the past, present, and future. *Lancet*. 2014;383:1068-83.

7. Samuel VT and Shulman GI. Mechanisms for insulin resistance: common threads and missing links. *Cell*. 2012;148:852-71.

8. Trujillo ME and Scherer PE. Adipose tissue-derived factors: impact on health and disease. *Endocr Rev*. 2006;27:762-78.

9. Winer S and Winer DA. The adaptive immune system as a fundamental regulator of adipose tissue inflammation and insulin resistance. *Immunol Cell Biol*. 2012;90:755-62.

10. Hotamisligil GS, Shargill NS and Spiegelman BM. Adipose expression of tumor necrosis factor-alpha: direct role in obesity-linked insulin resistance. *Science*. 1993;259:87-91.

11. Wallenius V, Wallenius K, Ahren B, Rudling M, Carlsten H, Dickson SL, Ohlsson C and Jansson JO. Interleukin-6-deficient mice develop mature-onset obesity. *Nat Med*. 2002;8:75-9.

12. Tourniaire F, Romier-Crouzet B, Lee JH, Marcotorchino J, Gouranton E, Salles J, Malezet C, Astier J, Darmon P, Blouin E, Walrand S, Ye J and Landrier JF. Chemokine Expression in Inflamed Adipose Tissue Is Mainly Mediated by NF-kappaB. *PLoS One*. 2013;8:e66515.

13. Zhang Y, Proenca R, Maffei M, Barone M, Leopold L and Friedman JM. Positional cloning of the mouse obese gene and its human homologue. *Nature*. 1994;372:425-32.

14. Friedman JM and Halaas JL. Leptin and the regulation of body weight in mammals. *Nature*. 1998;395:763-70.

15. Gainsford T, Willson TA, Metcalf D, Handman E, McFarlane C, Ng A, Nicola NA, Alexander WS and Hilton DJ. Leptin can induce proliferation, differentiation, and functional activation of hemopoietic cells. *Proc Natl Acad Sci U S A*. 1996;93:14564-8.

16. Li S, Shin HJ, Ding EL and van Dam RM. Adiponectin levels and risk of type 2 diabetes: a systematic review and meta-analysis. *JAMA : the journal of the American Medical Association*. 2009;302:179-88.

17. Gabrielsen JS, Gao Y, Simcox JA, Huang J, Thorup D, Jones D, Cooksey RC, Gabrielsen D, Adams TD, Hunt SC, Hopkins PN, Cefalu WT and McClain DA. Adipocyte iron regulates adiponectin and insulin sensitivity. *J Clin Invest*. 2012;122:3529-40.

18. Yamauchi T, Kamon J, Minokoshi Y, Ito Y, Waki H, Uchida S, Yamashita S, Noda M, Kita S, Ueki K, Eto K, Akanuma Y, Froguel P, Foufelle F, Ferre P, Carling D, Kimura S, Nagai R, Kahn BB and Kadowaki T. Adiponectin stimulates glucose utilization and fatty-acid oxidation by activating AMP-activated protein kinase. *Nat Med*. 2002;8:1288-95.

19. Maeda N, Shimomura I, Kishida K, Nishizawa H, Matsuda M, Nagaretani H, Furuyama N, Kondo H, Takahashi M, Arita Y, Komuro R, Ouchi N, Kihara S, Tochino Y, Okutomi K, Horie M, Takeda S, Aoyama T, Funahashi T and Matsuzawa Y. Diet-induced insulin resistance in mice lacking adiponectin/ACRP30. *Nat Med*. 2002;8:731-7.

20. Kim JY, van de Wall E, Laplante M, Azzara A, Trujillo ME, Hofmann SM, Schraw T, Durand JL, Li H, Li G, Jelicks LA, Mehler MF, Hui DY, Deshaies Y, Shulman GI, Schwartz GJ and Scherer PE. Obesity-associated improvements in metabolic profile through expansion of adipose tissue. *J Clin Invest*. 2007;117:2621-37.

21. Hill AA, Reid Bolus W and Hasty AH. A decade of progress in adipose tissue macrophage biology. *Immunol Rev*. 2014;262:134-52.

22. Cho CH, Koh YJ, Han J, Sung HK, Jong Lee H, Morisada T, Schwendener RA, Brekken RA, Kang G, Oike Y, Choi TS, Suda T, Yoo OJ and Koh GY. Angiogenic role of LYVE-1-positive macrophages in adipose tissue. *Circulation research*. 2007;100:e47-57.

23. Nishimura S, Manabe I, Nagasaki M, Hosoya Y, Yamashita H, Fujita H, Ohsugi M, Tobe K, Kadowaki T, Nagai R and Sugiura S. Adipogenesis in obesity

requires close interplay between differentiating adipocytes, stromal cells, and blood vessels. *Diabetes*. 2007;56:1517-26.

24. Morris DL, Cho KW, Delproposto JL, Oatmen KE, Geletka LM, Martinez-Santibanez G, Singer K and Lumeng CN. Adipose tissue macrophages function as antigen-presenting cells and regulate adipose tissue CD4+ T cells in mice. *Diabetes*. 2013;62:2762-72.

25. Nguyen KD, Qiu Y, Cui X, Goh YP, Mwangi J, David T, Mukundan L, Brombacher F, Locksley RM and Chawla A. Alternatively activated macrophages produce catecholamines to sustain adaptive thermogenesis. *Nature*. 2011;480:104-8.

26. Weisberg SP, McCann D, Desai M, Rosenbaum M, Leibel RL and Ferrante AW, Jr. Obesity is associated with macrophage accumulation in adipose tissue. *J Clin Invest*. 2003;112:1796-808.

27. Cinti S, Mitchell G, Barbatelli G, Murano I, Ceresi E, Faloia E, Wang S, Fortier M, Greenberg AS and Obin MS. Adipocyte death defines macrophage localization and function in adipose tissue of obese mice and humans. *Journal of lipid research*. 2005;46:2347-55.

28. Strissel KJ, Stancheva Z, Miyoshi H, Perfield JW, 2nd, DeFuria J, Jick Z, Greenberg AS and Obin MS. Adipocyte death, adipose tissue remodeling, and obesity complications. *Diabetes*. 2007;56:2910-8.

29. Nakae J, Kitamura T, Kitamura Y, Biggs WH, 3rd, Arden KC and Accili D. The forkhead transcription factor Foxo1 regulates adipocyte differentiation. *Dev Cell*. 2003;4:119-29.

30. Kratz M, Coats BR, Hisert KB, Hagman D, Mutskov V, Peris E, Schoenfelt KQ, Kuzma JN, Larson I, Billing PS, Landerholm RW, Crouthamel M, Gozal D, Hwang S, Singh PK and Becker L. Metabolic dysfunction drives a mechanistically distinct proinflammatory phenotype in adipose tissue macrophages. *Cell Metab*. 2014;20:614-25.

31. Cho KW, Zamarron BF, Muir LA, Singer K, Porsche CE, DelProposto JB, Geletka L, Meyer KA, O'Rourke RW and Lumeng CN. Adipose Tissue Dendritic Cells Are Independent Contributors to Obesity-Induced Inflammation and Insulin Resistance. *J Immunol*. 2016;197:3650-3661.

32. Elgazar-Carmon V, Rudich A, Hadad N and Levy R. Neutrophils transiently infiltrate intra-abdominal fat early in the course of high-fat feeding. *Journal of lipid research*. 2008;49:1894-903.

33. Wu D, Molofsky AB, Liang HE, Ricardo-Gonzalez RR, Jouihan HA, Bando JK, Chawla A and Locksley RM. Eosinophils sustain adipose alternatively activated macrophages associated with glucose homeostasis. *Science*. 2011;332:243-7.

34. Bolus WR, Peterson KR, Hubler MJ, Kennedy AJ, Gruen ML and Hasty AH. Elevating adipose eosinophils in obese mice to physiologically normal levels does not rescue metabolic impairments. *Molecular metabolism*. 2018;8:86-95.

35. Liu J, Divoux A, Sun J, Zhang J, Clement K, Glickman JN, Sukhova GK, Wolters PJ, Du J, Gorgun CZ, Doria A, Libby P, Blumberg RS, Kahn BB, Hotamisligil GS and Shi GP. Genetic deficiency and pharmacological stabilization of mast cells reduce diet-induced obesity and diabetes in mice. *Nat Med*. 2009;15:940-5.

36. Poglio S, De Toni-Costes F, Arnaud E, Laharrague P, Espinosa E, Casteilla L and Cousin B. Adipose tissue as a dedicated reservoir of functional mast cell progenitors. *Stem Cells*. 2010;28:2065-72.

37. Feuerer M, Herrero L, Cipolletta D, Naaz A, Wong J, Nayer A, Lee J, Goldfine AB, Benoist C, Shoelson S and Mathis D. Lean, but not obese, fat is enriched for a unique population of regulatory T cells that affect metabolic parameters. *Nat Med*. 2009;15:930-9.

38. Winer S, Chan Y, Paltser G, Truong D, Tsui H, Bahrami J, Dorfman R, Wang Y, Zielenski J, Mastronardi F, Maezawa Y, Drucker DJ, Engleman E, Winer D and Dosch HM. Normalization of obesity-associated insulin resistance through immunotherapy. *Nat Med*. 2009;15:921-9.

39. Rocha VZ, Folco EJ, Sukhova G, Shimizu K, Gotsman I, Vernon AH and Libby P. Interferon-gamma, a Th1 cytokine, regulates fat inflammation: a role for adaptive immunity in obesity. *Circulation research*. 2008;103:467-76.

40. Yang H, Youm YH, Vandanmagsar B, Ravussin A, Gimble JM, Greenway F, Stephens JM, Mynatt RL and Dixit VD. Obesity increases the production of proinflammatory mediators from adipose tissue T cells and compromises TCR repertoire diversity: implications for systemic inflammation and insulin resistance. *J Immunol*. 2010;185:1836-45.

41. Bozzini C, Girelli D, Olivieri O, Martinelli N, Bassi A, De Matteis G, Tenuti I, Lotto V, Friso S, Pizzolo F and Corrocher R. Prevalence of body iron excess in the metabolic syndrome. *Diabetes care*. 2005;28:2061-3.

42. Gonzalez AS, Guerrero DB, Soto MB, Diaz SP, Martinez-Olmos M and Vidal O. Metabolic syndrome, insulin resistance and the inflammation markers C-reactive protein and ferritin. *European journal of clinical nutrition*. 2006;60:802-9.

43. Chang JS, Lin SM, Huang TC, Chao JC, Chen YC, Pan WH and Bai CH. Serum ferritin and risk of the metabolic syndrome: a population-based study. *Asia Pacific journal of clinical nutrition*. 2013;22:400-7.

44. Jehn M, Clark JM and Guallar E. Serum ferritin and risk of the metabolic syndrome in U.S. adults. *Diabetes care*. 2004;27:2422-8.

45. Iwasaki T, Nakajima A, Yoneda M, Yamada Y, Mukasa K, Fujita K, Fujisawa N, Wada K and Terauchi Y. Serum ferritin is associated with visceral fat area and subcutaneous fat area. *Diabetes care*. 2005;28:2486-91.

46. Simcox JA and McClain DA. Iron and diabetes risk. *Cell Metab*. 2013;17:329-41.

47. Dongiovanni P, Fracanzani AL, Fargion S and Valenti L. Iron in fatty liver and in the metabolic syndrome: a promising therapeutic target. *Journal of hepatology*. 2011;55:920-32.

48. Basuli D, Stevens RG, Torti FM and Torti SV. Epidemiological associations between iron and cardiovascular disease and diabetes. *Frontiers in pharmacology*. 2014;5:117.

49. Jiang R, Manson JE, Meigs JB, Ma J, Rifai N and Hu FB. Body iron stores in relation to risk of type 2 diabetes in apparently healthy women. *JAMA : the journal of the American Medical Association*. 2004;291:711-7.

50. Dongiovanni P, Ruscica M, Rametta R, Recalcati S, Steffani L, Gatti S, Girelli D, Cairo G, Magni P, Fargion S and Valenti L. Dietary iron overload induces visceral adipose tissue insulin resistance. *The American journal of pathology*. 2013;182:2254-63.

51. Fernandez-Real JM, Ricart-Engel W, Arroyo E, Balanca R, Casamitjana-Abella R, Cabrero D, Fernandez-Castaner M and Soler J. Serum ferritin as a component of the insulin resistance syndrome. *Diabetes care*. 1998;21:62-8.

52. Menzie CM, Yanoff LB, Denkinger BI, McHugh T, Sebring NG, Calis KA and Yanovski JA. Obesity-related hypoferremia is not explained by differences in reported intake of heme and nonheme iron or intake of dietary factors that can affect iron absorption. *Journal of the American Dietetic Association*. 2008;108:145-8.

53. Haap M, Fritsche A, Mensing HJ, Haring HU and Stumvoll M. Association of high serum ferritin concentration with glucose intolerance and insulin resistance in healthy people. *Annals of internal medicine*. 2003;139:869-71.

54. Wlazlo N, van Greevenbroek MM, Ferreira I, Jansen EH, Feskens EJ, van der Kallen CJ, Schalkwijk CG, Bravenboer B and Stehouwer CD. Iron metabolism is associated with adipocyte insulin resistance and plasma adiponectin: the Cohort on Diabetes and Atherosclerosis Maastricht (CODAM) study. *Diabetes care*. 2013;36:309-15.

55. Moreno-Navarrete JM, Novelle MG, Catalan V, Ortega F, Moreno M, Gomez-Ambrosi J, Xifra G, Serrano M, Guerra E, Ricart W, Fruhbeck G, Dieguez C and Fernandez-Real JM. Insulin resistance modulates iron-related proteins in adipose tissue. *Diabetes care*. 2014;37:1092-100.

56. Fernandez-Real JM, Lopez-Bermejo A and Ricart W. Iron stores, blood donation, and insulin sensitivity and secretion. *Clinical chemistry*. 2005;51:1201-5.

57. Tussing-Humphreys LM, Nemeth E, Fantuzzi G, Freels S, Guzman G, Holterman AX and Braunschweig C. Elevated systemic hepcidin and iron depletion in obese premenopausal females. *Obesity*. 2010;18:1449-56.

58. Kohyama M, Ise W, Edelson BT, Wilker PR, Hildner K, Mejia C, Frazier WA, Murphy TL and Murphy KM. Role for Spi-C in the development of red pulp macrophages and splenic iron homeostasis. *Nature*. 2009;457:318-21.

59. Ganz T. Macrophages and systemic iron homeostasis. *J Innate Immun*. 2012;4:446-53.

60. Haldar M, Kohyama M, So AY, Kc W, Wu X, Briseno CG, Satpathy AT, Kretzer NM, Arase H, Rajasekaran NS, Wang L, Egawa T, Igarashi K, Baltimore D, Murphy TL and Murphy KM. Heme-mediated SPI-C induction promotes monocyte differentiation into iron-recycling macrophages. *Cell*. 2014;156:1223-1234.

61. Shoden A and Sturgeon P. Iron storage, IV. Cellular distribution of excess liver iron. *The American journal of pathology*. 1962;40:671-83.

62. Corhay JL, Weber G, Bury T, Mariz S, Roelandts I and Radermecker MF. Iron content in human alveolar macrophages. *Eur Respir J*. 1992;5:804-9.

63. Nemeth E, Tuttle MS, Powelson J, Vaughn MB, Donovan A, Ward DM, Ganz T and Kaplan J. Hepcidin regulates cellular iron efflux by binding to ferroportin and inducing its internalization. *Science*. 2004;306:2090-3.

64. Frazer DM, Wilkins SJ, Becker EM, Vulpe CD, McKie AT, Trinder D and Anderson GJ. Hepcidin expression inversely correlates with the expression of duodenal iron transporters and iron absorption in rats. *Gastroenterology*. 2002;123:835-44.

65. Bekri S, Gual P, Anty R, Luciani N, Dahman M, Ramesh B, Iannelli A, Staccini-Myx A, Casanova D, Ben Amor I, Saint-Paul MC, Huet PM, Sadoul JL, Gugenheim J, Srai SK, Tran A and Le Marchand-Brustel Y. Increased adipose tissue expression of hepcidin in severe obesity is independent from diabetes and NASH. *Gastroenterology*. 2006;131:788-96.

66. Wu X, Yung LM, Cheng WH, Yu PB, Babitt JL, Lin HY and Xia Y. Hepcidin regulation by BMP signaling in macrophages is lipopolysaccharide dependent. *PLoS One*. 2012;7:e44622.

67. Nemeth E and Ganz T. The role of hepcidin in iron metabolism. *Acta haematologica*. 2009;122:78-86.

68. Donovan A, Lima CA, Pinkus JL, Pinkus GS, Zon LI, Robine S and Andrews NC. The iron exporter ferroportin/Slc40a1 is essential for iron homeostasis. *Cell Metab*. 2005;1:191-200.

69. Tsuchiya H, Ebata Y, Sakabe T, Hama S, Kogure K and Shiota G. High-fat, high-fructose diet induces hepatic iron overload via a hepcidin-independent mechanism prior to the onset of liver steatosis and insulin resistance in mice. *Metabolism: clinical and experimental*. 2013;62:62-9.

70. Chung J, Kim MS and Han SN. Diet-induced obesity leads to decreased hepatic iron storage in mice. *Nutrition research*. 2011;31:915-21.

71. Orr JS, Kennedy A, Anderson-Baucum EK, Webb CD, Fordahl SC, Erikson KM, Zhang Y, Etzerodt A, Moestrup SK and Hasty AH. Obesity Alters Adipose Tissue Macrophage Iron Content and Tissue Iron Distribution. *Diabetes*. 2013.

72. Wang J and Pantopoulos K. Regulation of cellular iron metabolism. *The Biochemical journal*. 2011;434:365-81.

73. Salgia RJ and Brown K. Diagnosis and management of hereditary hemochromatosis. *Clin Liver Dis*. 2015;19:187-98.

74. Drakesmith H, Sweetland E, Schimanski L, Edwards J, Cowley D, Ashraf M, Bastin J and Townsend AR. The hemochromatosis protein HFE inhibits iron export from macrophages. *Proc Natl Acad Sci U S A*. 2002;99:15602-7.

75. Bugianesi E, Manzini P, D'Antico S, Vanni E, Longo F, Leone N, Massarenti P, Piga A, Marchesini G and Rizzetto M. Relative contribution of iron burden, HFE mutations, and insulin resistance to fibrosis in nonalcoholic fatty liver. *Hepatology*. 2004;39:179-87.

76. Valenti L, Canavesi E, Galmozzi E, Dongiovanni P, Rametta R, Maggioni P, Maggioni M, Fracanzani AL and Fargion S. Beta-globin mutations are associated with parenchymal siderosis and fibrosis in patients with non-alcoholic fatty liver disease. *Journal of hepatology*. 2010;53:927-33.

77. Moreno-Navarrete JM, Ortega F, Moreno M, Ricart W and Fernandez-Real JM. Fine-tuned iron availability is essential to achieve optimal adipocyte differentiation and mitochondrial biogenesis. *Diabetologia*. 2014;57:1957-67.

78. Rumberger JM, Peters T, Jr., Burrington C and Green A. Transferrin and iron contribute to the lipolytic effect of serum in isolated adipocytes. *Diabetes*. 2004;53:2535-41.

79. Green A, Basile R and Rumberger JM. Transferrin and iron induce insulin resistance of glucose transport in adipocytes. *Metabolism: clinical and experimental*. 2006;55:1042-5.

80. Murdolo G, Piroddi M, Luchetti F, Tortoioli C, Canonico B, Zerbinati C, Galli F and Iuliano L. Oxidative stress and lipid peroxidation by-products at the crossroad between adipose organ dysregulation and obesity-linked insulin resistance. *Biochimie*. 2013;95:585-94.

81. Levi S and Rovida E. The role of iron in mitochondrial function. *Biochimica et biophysica acta*. 2009;1790:629-36.

82. Wilson-Fritch L, Nicoloro S, Chouinard M, Lazar MA, Chui PC, Leszyk J, Straubhaar J, Czech MP and Corvera S. Mitochondrial remodeling in adipose tissue associated with obesity and treatment with rosiglitazone. *J Clin Invest*. 2004;114:1281-9.

83. Cooksey RC, Jones D, Gabrielsen S, Huang J, Simcox JA, Luo B, Soesanto Y, Rienhoff H, Abel ED and McClain DA. Dietary iron restriction or iron chelation protects from diabetes and loss of beta-cell function in the obese (ob/ob lep-/-) mouse. *American journal of physiology Endocrinology and metabolism*. 2010;298:E1236-43.

84. Britton L, Jaskowski LA, Bridle K, Secondes E, Wallace D, Santrampurwala N, Reiling J, Miller G, Mangiafico S, Andrikopoulos S, Subramaniam VN and Crawford D. Ferroportin Expression in Adipocytes Does Not Contribute to Iron Homeostasis or Metabolic Responses to a High Calorie Diet. *Cell Mol Gastroenterol Hepatol*. 2018;5:319-331.

85. Ku BJ, Kim SY, Lee TY and Park KS. Serum ferritin is inversely correlated with serum adiponectin level: population-based cross-sectional study. *Disease markers*. 2009;27:303-10.

86. Kusminski CM and Scherer PE. Mitochondrial dysfunction in white adipose tissue. *Trends in endocrinology and metabolism: TEM*. 2012;23:435-43.

87. Ponugoti B, Dong G and Graves DT. Role of forkhead transcription factors in diabetes-induced oxidative stress. *Experimental diabetes research*. 2012;2012:939751.

88. Boyle JJ, Harrington HA, Piper E, Elderfield K, Stark J, Landis RC and Haskard DO. Coronary intraplaque hemorrhage evokes a novel atheroprotective macrophage phenotype. *The American journal of pathology*. 2009;174:1097-108.

89. Finn AV, Nakano M, Polavarapu R, Karmali V, Saeed O, Zhao X, Yazdani S, Otsuka F, Davis T, Habib A, Narula J, Kolodgie FD and Virmani R. Hemoglobin directs macrophage differentiation and prevents foam cell formation in human atherosclerotic plaques. *J Am Coll Cardiol*. 2012;59:166-77.

90. Bories G, Colin S, Vanhoutte J, Derudas B, Copin C, Fanchon M, Daoudi M, Belloy L, Haulon S, Zawadzki C, Jude B, Staels B and Chinetti-Gbaguidi G. Liver

X receptor activation stimulates iron export in human alternative macrophages. *Circulation research*. 2013;113:1196-205.

91. Sindrilaru A, Peters T, Wieschalka S, Baican C, Baican A, Peter H, Hainzl A, Schatz S, Qi Y, Schlecht A, Weiss JM, Wlaschek M, Sunderkotter C and Scharffetter-Kochanek K. An unrestrained proinflammatory M1 macrophage population induced by iron impairs wound healing in humans and mice. *J Clin Invest*. 2011;121:985-97.

92. Biswas SK and Mantovani A. Macrophage plasticity and interaction with lymphocyte subsets: cancer as a paradigm. *Nat Immunol*. 2010;11:889-96.

93. Mehta V, Pei W, Yang G, Li S, Swamy E, Boster A, Schmalbrock P and Pitt D. Iron is a sensitive biomarker for inflammation in multiple sclerosis lesions. *PLoS One*. 2013;8:e57573.

94. Lumeng CN, Bodzin JL and Saltiel AR. Obesity induces a phenotypic switch in adipose tissue macrophage polarization. *J Clin Invest*. 2007;117:175-84.

95. Cairo G, Bernuzzi F and Recalcati S. A precious metal: Iron, an essential nutrient for all cells. *Genes Nutr*. 2006;1:25-39.

96. Corna G, Campana L, Pignatti E, Castiglioni A, Tagliafico E, Bosurgi L, Campanella A, Brunelli S, Manfredi AA, Apostoli P, Silvestri L, Camaschella C and Rovere-Querini P. Polarization dictates iron handling by inflammatory and alternatively activated macrophages. *Haematologica*. 2010;95:1814-22.

97. Recalcati S, Locati M, Marini A, Santambrogio P, Zaninotto F, De Pizzol M, Zammataro L, Girelli D and Cairo G. Differential regulation of iron homeostasis during human macrophage polarized activation. *Eur J Immunol*. 2010;40:824-35.

98. Kroner A, Greenhalgh AD, Zarruk JG, Passos Dos Santos R, Gaestel M and David S. TNF and increased intracellular iron alter macrophage polarization to a detrimental M1 phenotype in the injured spinal cord. *Neuron*. 2014;83:1098-116.

99. Fried SK, Bunkin DA and Greenberg AS. Omental and subcutaneous adipose tissues of obese subjects release interleukin-6: depot difference and regulation by glucocorticoid. *J Clin Endocrinol Metab*. 1998;83:847-50.

100. Wrighting DM and Andrews NC. Interleukin-6 induces hepcidin expression through STAT3. *Blood*. 2006;108:3204-9.

101. Gotardo EM, dos Santos AN, Miyashiro RA, Gambero S, Rocha T, Ribeiro ML and Gambero A. Mice that are fed a high-fat diet display increased hepcidin expression in adipose tissue. *Journal of nutritional science and vitaminology*. 2013;59:454-61.

102. Kim S and Ponka P. Effects of interferon-gamma and lipopolysaccharide on macrophage iron metabolism are mediated by nitric oxide-induced degradation of iron regulatory protein 2. *J Biol Chem*. 2000;275:6220-6.

103. Orozco LD, Kapturczak MH, Barajas B, Wang X, Weinstein MM, Wong J, Deshane J, Bolisetty S, Shaposhnik Z, Shih DM, Agarwal A, Lusis AJ and Araujo JA. Heme oxygenase-1 expression in macrophages plays a beneficial role in atherosclerosis. *Circulation research*. 2007;100:1703-11.

104. Jais A, Einwallner E, Sharif O, Gossens K, Lu TT, Soyal SM, Medgyesi D, Neureiter D, Paier-Pourani J, Dalgaard K, Duvigneau JC, Lindroos-Christensen J, Zapf TC, Amann S, Saluzzo S, Jantscher F, Stiedl P, Todoric J, Martins R, Oberkofler H, Muller S, Hauser-Kronberger C, Kenner L, Casanova E, Sutterluty-Fall H, Bilban M, Miller K, Kozlov AV, Krempler F, Knapp S, Lumeng CN, Patsch W, Wagner O, Pospisilik JA and Esterbauer H. Heme oxygenase-1 drives metaflammation and insulin resistance in mouse and man. *Cell*. 2014;158:25-40.

105. Kovtunovych G, Eckhaus MA, Ghosh MC, Ollivierre-Wilson H and Rouault TA. Dysfunction of the heme recycling system in heme oxygenase 1-deficient mice: effects on macrophage viability and tissue iron distribution. *Blood*. 2010;116:6054-62.

106. Sierra-Filardi E, Vega MA, Sanchez-Mateos P, Corbi AL and Puig-Kroger A. Heme Oxygenase-1 expression in M-CSF-polarized M2 macrophages contributes to LPS-induced IL-10 release. *Immunobiology*. 2010;215:788-95.

107. Sorbie J and Valberg LS. Iron balance in the mouse. *Lab Anim Sci*. 1974;24:900-4.

108. Knapka JJ, Smith KP and Judge FJ. Effect of open and closed formula rations on the performance of three strains of laboratory mice. *Lab Anim Sci*. 1974;24:480-7.

109. Orr JS, Kennedy AJ and Hasty AH. Isolation of adipose tissue immune cells. *J Vis Exp*. 2013:e50707.

110. Etzerodt A, Maniecki MB, Graversen JH, Moller HJ, Torchilin VP and Moestrup SK. Efficient intracellular drug-targeting of macrophages using stealth liposomes directed to the hemoglobin scavenger receptor CD163. *Journal of controlled release : official journal of the Controlled Release Society*. 2012;160:72-80.

111. Yu SS, Lau CM, Barham WJ, Onishko HM, Nelson CE, Li H, Smith CA, Yull FE, Duvall CL and Giorgio TD. Macrophage-specific RNA interference targeting via "click", mannosylated polymeric micelles. *Mol Pharm*. 2013;10:975-87.

112. Merla J Hubler KME, Arion J Kennedy, Alyssa H Hasty. MFehi adipose tissue macrophages compensate for tissue iron perturbations in mice. *American Journal of Physiology - Cell Physiology*. 2018;accepted.

113. Xu H, Barnes GT, Yang Q, Tan G, Yang D, Chou CJ, Sole J, Nichols A, Ross JS, Tartaglia LA and Chen H. Chronic inflammation in fat plays a crucial role in the development of obesity-related insulin resistance. *J Clin Invest*. 2003;112:1821-30.

114. Coffey R and Ganz T. Iron homeostasis: An anthropocentric perspective. *J Biol Chem*. 2017;292:12727-12734.

115. Corna G, Caserta I, Monno A, Apostoli P, Manfredi AA, Camaschella C and Rovere-Querini P. The Repair of Skeletal Muscle Requires Iron Recycling through Macrophage Ferroportin. *J Immunol*. 2016;197:1914-25.

116. Syrovatka P, Kraml P, Potockova J, Fialova L, Vejrazka M, Crkovska J and Andel M. Relationship between increased body iron stores, oxidative stress and insulin resistance in healthy men. *Ann Nutr Metab*. 2009;54:268-74.

117. Zheng J, Chen M, Liu G, Xu E and Chen H. Ablation of hephaestin and ceruloplasmin results in iron accumulation in adipocytes and type 2 diabetes. *FEBS letters*. 2018;592:394-401.

118. Morris DL, Singer K and Lumeng CN. Adipose tissue macrophages: phenotypic plasticity and diversity in lean and obese states. *Curr Opin Clin Nutr Metab Care*. 2011;14:341-6.

119. Murray PJ. Macrophage Polarization. *Annual review of physiology*. 2017;79:541-566.

120. Mertens C, Akam EA, Rehwald C, Brune B, Tomat E and Jung M. Intracellular Iron Chelation Modulates the Macrophage Iron Phenotype with Consequences on Tumor Progression. *PLoS One*. 2016;11:e0166164.

121. Fillebeen C, Gkouvatsos K, Fragoso G, Calve A, Garcia-Santos D, Buffler M, Becker C, Schumann K, Ponka P, Santos MM and Pantopoulos K. Mice are poor heme absorbers and do not require intestinal Hmox1 for dietary heme iron assimilation. *Haematologica*. 2015;100:e334-7.

122. Mamula P, Piccoli DA, Peck SN, Markowitz JE and Baldassano RN. Total dose intravenous infusion of iron dextran for iron-deficiency anemia in children with inflammatory bowel disease. *J Pediatr Gastroenterol Nutr*. 2002;34:286-90.

123. Pham BTT, Colvin EK, Pham NTH, Kim BJ, Fuller ES, Moon EA, Barbey R, Yuen S, Rickman BH, Bryce NS, Bickley S, Tanudji M, Jones SK, Howell VM and Hawkett BS. Biodistribution and Clearance of Stable Superparamagnetic Maghemite Iron Oxide Nanoparticles in Mice Following Intraperitoneal Administration. *Int J Mol Sci*. 2018;19.

124. Musumeci M, Maccari S, Massimi A, Stati T, Sestili P, Corritore E, Pastorelli A, Stacchini P, Marano G and Catalano L. Iron excretion in iron dextran-overloaded mice. *Blood Transfus*. 2014;12:485-90.

125. Cairo G, Recalcati S, Mantovani A and Locati M. Iron trafficking and metabolism in macrophages: contribution to the polarized phenotype. *Trends in immunology*. 2011;32:241-7.

126. Boyle JJ, Johns M, Kampfer T, Nguyen AT, Game L, Schaer DJ, Mason JC and Haskard DO. Activating transcription factor 1 directs Mhem atheroprotective macrophages through coordinated iron handling and foam cell protection. *Circulation research*. 2012;110:20-33.

127. Zhang Z, Zhang F, An P, Guo X, Shen Y, Tao Y, Wu Q, Zhang Y, Yu Y, Ning B, Nie G, Knutson MD, Anderson GJ and Wang F. Ferroportin1 deficiency in mouse macrophages impairs iron homeostasis and inflammatory responses. *Blood*. 2011;118:1912-22.

128. Tsukamoto H. Iron regulation of hepatic macrophage TNFalpha expression. *Free radical biology & medicine*. 2002;32:309-13.

129. Surwit RS, Kuhn CM, Cochrane C, McCubbin JA and Feinglos MN. Diet-induced type II diabetes in C57BL/6J mice. *Diabetes*. 1988;37:1163-7.

130. Ahmed U, Latham PS and Oates PS. Interactions between hepatic iron and lipid metabolism with possible relevance to steatohepatitis. *World J Gastroenterol*. 2012;18:4651-8.

131. Sherman AR. Lipogenesis in iron-deficient adult rats. *Lipids*. 1978;13:473-8.

132. Yeramian A, Martin L, Serrat N, Arpa L, Soler C, Bertran J, McLeod C, Palacin M, Modolell M, Lloberas J and Celada A. Arginine transport via cationic amino acid transporter 2 plays a critical regulatory role in classical or alternative activation of macrophages. *J Immunol*. 2006;176:5918-24.

133. Pou S, Pou WS, Bredt DS, Snyder SH and Rosen GM. Generation of superoxide by purified brain nitric oxide synthase. *J Biol Chem*. 1992;267:24173-6.

134. Xia Y, Tsai AL, Berka V and Zweier JL. Superoxide generation from endothelial nitric-oxide synthase. A Ca2+/calmodulin-dependent and tetrahydrobiopterin regulatory process. *J Biol Chem*. 1998;273:25804-8.

135. Tan HY, Wang N, Li S, Hong M, Wang X and Feng Y. The Reactive Oxygen Species in Macrophage Polarization: Reflecting Its Dual Role in Progression and Treatment of Human Diseases. *Oxid Med Cell Longev*. 2016;2016:2795090.

136. Miao H, Ou J, Ma Y, Guo F, Yang Z, Wiggins M, Liu C, Song W, Han X, Wang M, Cao Q, Chung BH, Yang D, Liang H, Xue B, Shi H, Gan L and Yu L. Macrophage

CGI-58 deficiency activates ROS-inflammasome pathway to promote insulin resistance in mice. *Cell Rep*. 2014;7:223-35.

137. Kobayashi A, Kang MI, Okawa H, Ohtsuji M, Zenke Y, Chiba T, Igarashi K and Yamamoto M. Oxidative stress sensor Keap1 functions as an adaptor for Cul3-based E3 ligase to regulate proteasomal degradation of Nrf2. *Molecular and cellular biology*. 2004;24:7130-9.

138. Tian W, Rojo de la Vega M, Schmidlin CJ, Ooi A and Zhang DD. Kelch-like ECH-associated protein 1 (KEAP1) differentially regulates nuclear factor erythroid-2-related factors 1 and 2 (NRF1 and NRF2). *J Biol Chem*. 2018;293:2029-2040.

139. Wiktor-Jedrzejczak W, Bartocci A, Ferrante AW, Jr., Ahmed-Ansari A, Sell KW, Pollard JW and Stanley ER. Total absence of colony-stimulating factor 1 in the macrophage-deficient osteopetrotic (op/op) mouse. *Proc Natl Acad Sci U S A*. 1990;87:4828-32.

140. Goren I, Allmann N, Yogev N, Schurmann C, Linke A, Holdener M, Waisman A, Pfeilschifter J and Frank S. A transgenic mouse model of inducible macrophage depletion: effects of diphtheria toxin-driven lysozyme M-specific cell lineage ablation on wound inflammatory, angiogenic, and contractive processes. *The American journal of pathology*. 2009;175:132-47.

141. Bozzuto G and Molinari A. Liposomes as nanomedical devices. *Int J Nanomedicine*. 2015;10:975-99.

142. Damen J, Regts J and Scherphof G. Transfer and exchange of phospholipid between small unilamellar liposomes and rat plasma high density lipoproteins. Dependence on cholesterol content and phospholipid composition. *Biochimica et biophysica acta*. 1981;665:538-45.

143. Maeda H, Sawa T and Konno T. Mechanism of tumor-targeted delivery of macromolecular drugs, including the EPR effect in solid tumor and clinical overview of the prototype polymeric drug SMANCS. *Journal of controlled release : official journal of the Controlled Release Society*. 2001;74:47-61.

144. Zamboni WC. Concept and clinical evaluation of carrier-mediated anticancer agents. *Oncologist*. 2008;13:248-260.

145. Devine DV, Wong K, Serrano K, Chonn A and Cullis PR. Liposome-complement interactions in rat serum: implications for liposome survival studies. *Biochimica et biophysica acta*. 1994;1191:43-51.

146. Needham D, McIntosh TJ and Lasic DD. Repulsive interactions and mechanical stability of polymer-grafted lipid membranes. *Biochimica et biophysica acta*. 1992;1108:40-8.

147. Chanan-Khan A, Szebeni J, Savay S, Liebes L, Rafique NM, Alving CR and Muggia FM. Complement activation following first exposure to pegylated liposomal doxorubicin (Doxil): possible role in hypersensitivity reactions. *Ann Oncol*. 2003;14:1430-7.

148. Woodle MC, Matthay KK, Newman MS, Hidayat JE, Collins LR, Redemann C, Martin FJ and Papahadjopoulos D. Versatility in Lipid Compositions Showing Prolonged Circulation with Sterically Stabilized Liposomes. *Biochimica et biophysica acta*. 1992;1105:193-200.

149. Ishida T, Kirchmeier MJ, Moase EH, Zalipsky S and Allen TM. Targeted delivery and triggered release of liposomal doxorubicin enhances cytotoxicity against human B lymphoma cells. *Biochimica et biophysica acta*. 2001;1515:144-58.

150. Ringhieri P, Diaferia C, Galdiero S, Palumbo R, Morelli G and Accardo A. Liposomal doxorubicin doubly functionalized with CCK8 and R8 peptide sequences for selective intracellular drug delivery. *J Pept Sci*. 2015;21:415-25.

151. Kheirolomoom A, Lai CY, Tam SM, Mahakian LM, Ingham ES, Watson KD and Ferrara KW. Complete regression of local cancer using temperature-sensitive liposomes combined with ultrasound-mediated hyperthermia. *Journal of controlled release : official journal of the Controlled Release Society*. 2013;172:266-73.

152. van Rooijen N and van Nieuwmegen R. Elimination of phagocytic cells in the spleen after intravenous injection of liposome-encapsulated dichloromethylene diphosphonate. An enzyme-histochemical study. *Cell Tissue Res*. 1984;238:355-8.

153. van Rooijen N and Hendrikx E. Liposomes for specific depletion of macrophages from organs and tissues. *Methods in molecular biology*. 2010;605:189-203.

154. Van Rooijen N and Sanders A. Kupffer cell depletion by liposome-delivered drugs: comparative activity of intracellular clodronate, propamidine, and ethylenediaminetetraacetic acid. *Hepatology*. 1996;23:1239-43.

155. Rippe B and Zakaria ER. Lymphatic versus nonlymphatic fluid absorption from the peritoneal cavity as related to the peritoneal ultrafiltration capacity and sieving properties. *Blood Purif*. 1992;10:189-202.

156. Tacar O, Sriamornsak P and Dass CR. Doxorubicin: an update on anticancer molecular action, toxicity and novel drug delivery systems. *J Pharm Pharmacol*. 2013;65:157-70.

157. Ortega RA, Barham WJ, Kumar B, Tikhomirov O, McFadden ID, Yull FE and Giorgio TD. Biocompatible mannosylated endosomal-escape nanoparticles enhance selective delivery of short nucleotide sequences to tumor associated macrophages. *Nanoscale*. 2015;7:500-10.

158. Upadhyay TK, Fatima N, Sharma D, Saravanakumar V and Sharma R. Preparation and characterization of beta-glucan particles containing a payload of nanoembedded rifabutin for enhanced targeted delivery to macrophages. *EXCLI J*. 2017;16:210-228.

159. Cohen JL, Shen Y, Aouadi M, Vangala P, Tencerova M, Amano SU, Nicoloro SM, Yawe JC and Czech MP. Peptide- and Amine-Modified Glucan Particles for the Delivery of Therapeutic siRNA. *Mol Pharm*. 2016;13:964-978.

160. Cader MZ and Kaser A. Recent advances in inflammatory bowel disease: mucosal immune cells in intestinal inflammation. *Gut*. 2013;62:1653-64.

161. Singh MV, Chapleau MW, Harwani SC and Abboud FM. The immune system and hypertension. *Immunol Res*. 2014;59:243-53.

162. Rabinovitch M, Guignabert C, Humbert M and Nicolls MR. Inflammation and immunity in the pathogenesis of pulmonary arterial hypertension. *Circulation research*. 2014;115:165-75.

163. Ganz M and Szabo G. Immune and inflammatory pathways in NASH. *Hepatol Int*. 2013;7 Suppl 2:771-81.

164. Aamodt KI and Powers AC. Signals in the pancreatic islet microenvironment influence beta-cell proliferation. *Diabetes Obes Metab*. 2017;19 Suppl 1:124-136.

165. Neurimmune. Lab Insights: Immunotherapy fot Type-2 Diabetes. 2018;2018.

166. Kehl-Fie TE and Skaar EP. Nutritional immunity beyond iron: a role for manganese and zinc. *Curr Opin Chem Biol*. 2010;14:218-24.

167. Hood MI and Skaar EP. Nutritional immunity: transition metals at the pathogen-host interface. *Nat Rev Microbiol*. 2012;10:525-37.

168. Jung M, Weigert A, Mertens C, Rehwald C and Brune B. Iron Handling in Tumor-Associated Macrophages-Is There a New Role for Lipocalin-2? *Front Immunol*. 2017;8:1171.

169. Deugnier Y, Bardou-Jacquet E and Laine F. Dysmetabolic iron overload syndrome (DIOS). *Presse Med*. 2017;46:e306-e311.

170. Yan HF, Liu ZY, Guan ZA and Guo C. Deferoxamine ameliorates adipocyte dysfunction by modulating iron metabolism in ob/ob mice. *Endocr Connect*. 2018;7:604-616.

171. Fernandez-Real JM, Penarroja G, Castro A, Garcia-Bragado F, Hernandez-Aguado I and Ricart W. Blood letting in high-ferritin type 2 diabetes: effects on insulin sensitivity and beta-cell function. *Diabetes*. 2002;51:1000-4.

172. Fernandez-Real JM, Lopez-Bermejo A and Ricart W. Cross-talk between iron metabolism and diabetes. *Diabetes*. 2002;51:2348-54.

173. Vlaicu SI, Tatomir A, Boodhoo D, Vesa S, Mircea PA and Rus H. The role of complement system in adipose tissue-related inflammation. *Immunol Res*. 2016;64:653-64.

174. Thomas F, Serratrice G, Beguin C, Aman ES, Pierre JL, Fontecave M and Laulhere JP. Calcein as a fluorescent probe for ferric iron. Application to iron nutrition in plant cells. *J Biol Chem*. 1999;274:13375-83.

175. Prus E and Fibach E. Flow cytometry measurement of the labile iron pool in human hematopoietic cells. *Cytometry A*. 2008;73:22-7.

176. Hu J and Connor JR. Demonstration and characterization of the iron regulatory protein in human brain. *J Neurochem*. 1996;67:838-44.

177. Yu Y, Radisky E and Leibold EA. The iron-responsive element binding protein. Purification, cloning, and regulation in rat liver. *J Biol Chem*. 1992;267:19005-10.

178. Thomson AM, Rogers JT and Leedman PJ. Iron-regulatory proteins, iron-responsive elements and ferritin mRNA translation. *Int J Biochem Cell Biol*. 1999;31:1139-52.

179. Li X, Li S, Lu M, Yang G, Shen Y and Zhou X. Proteomic Profiling of Iron Overload-Induced Human Hepatic Cells Reveals Activation of TLR2-Mediated Inflammatory Response. *Molecules*. 2016;21:322.

180. Han J, Lee JE, Jin J, Lim JS, Oh N, Kim K, Chang SI, Shibuya M, Kim H and Koh GY. The spatiotemporal development of adipose tissue. *Development*. 2011;138:5027-37.